Siltation Mitigation In A Data Poor Environment

Assessing The Influence Of A Sluice On Siltation Rates In The Nga Moe Yeik Creek, Yangon

TU Delft Delft University of Technology

On the cover

The cover shows an image of the significant mud deposit near the Nga Moe Yeik Sluice Gates in a tributary of the Yangon River in Myanmar, which takes up the mayor part of the river cross-section leaving only a shallow channel during low water. The picture was taken in May 2017 during the instalment of a water level station.

Siltation Mitigation In A Data Poor Environment

Assessing The Influence Of A Sluice On Siltation Rates In The Nga Moe Yeik Creek, Yangon

by

Bob Keulers

to obtain the degree of Master of Science
at the Delft University of Technology,
to be defended publicly on 13 June 2018 at 02:00 PM

Student number:	4015436	
Thesis committee:	Prof. dr. ir. S.G.J. Aarninkhof,	TU Delft, Coastal Engineering
	Dr. ir. M. M. Rutten,	TU Delft, Water Resource Management
	Dr. D.S. Maren van,	TU Delft, Environmental Fluid Mechanics
	Ir. A.S. Commandeur,	TU Delft, Valorisation Centre
	Ir. H.C.M. Hendriks,	TU Delft, Environmental Fluid Mechanics

Contents

Preface

This thesis is the product of several month of research in the final stage of the master Hydraulic Engineering at Delft University of Technology. The topic of the thesis was initiated by local authorities in collaboration with one of my supervisors Alwin Commandeur. The diversity of the suggested research; from preparing and conducting fieldwork abroad, visiting Yangon and meeting local actors, to post-processing gathered data, setting up a numerical model to assess the mitigating effect of the Nga Moe Yeik Sluice Gates on siltation rates, strongly appealed to me. As part of my thesis research, I lived for 3 months in Yangon, Myanmar aiming to understand the local siltation problem in the Nga Moe Yeik Creek. I gratefully acknowledge a grant from Stichting Het Lamminga Fonds, technical research and development work and Treub-Maatschappij, the Society for the Advancement of Research in the Tropics that supported my local research in Yangon. By conducting fieldwork and personal communication with local authorities, I attempted to increase my insight in the problem. I committed my time and efforts with pleasure and I'm feeling lucky to have had the opportunity to visit Myanmar.

Furthermore, I would like to thank my committee, consisting of Stefan Aarninkhof, Martine Rutten, Bas van Maren, Erik Hendriks and Alwin Commandeur. Due to your guidance and valuable feedback during our meetings, I could improve my work significantly. Stefan Aarninkhof, I would like to thank you for the constructive guidance of the committee meetings and your enthusiasm. I would like to express my gratitude to Alwin Commandeur, for your advice and ideas especially during my stay in Yangon. Furthermore, Martine Rutten, thank you for sharing your ideas and feedback. Erik Hendriks, thank you very much for your critical look at my report and guidance. Bas van Maren, special thanks to you for being my daily supervisor. I really appreciated our plentiful meetings to verify my new findings.

Next to my committee, I would like to express my gratitude to Thom Bogaard, who helped me prepare my fieldwork and introduced me to several measuring devices. Furthermore, I would like to thank all the locals I met in Myanmar. Special thanks to Aung Kyaw Hmuu (Director DWIR) and staff for your help in organizing and realising the fieldwork in the Nga Moe Yeik Creek and to introduce me to boatman Ko Myint Thein. Thank you, for the plentiful days navigating and helping me with all the fieldwork in the Nga Moe Yeik Creek. I would like to thank U Toe Nyein (Assistant Director Irrigation Department), for the helpful discussions we had and sharing data and knowledge about the Nga Moe Yeik Sluice Gates. Besides, I would like to thank Alwin Commandeur and colleagues of Royal HaskoningDHV Yangon for your practical help and providing a workspace at your office. Furthermore, I would like to thank the staff of Myanmar Maritime University. Thank you, Htike Htike and Khin Kyu Kyu for your hospitality and help. Also thanks to the students Pyae Phyo Sein Wan, Pan Ei Phyu and WaiYan MoeAye for your helping hands in the fieldwork and showing me around your university.

Finally I would like to thank my friends and family for always supporting me during my study time in Delft. Special thanks go to Jasper Verschuur and Teije van der Horst for the great times we had while living in and exporing Yangon.

Bob Keulers
Delft, 30th May, 2018

Abstract

The typically mild slopes of the muddy coastline in the south of Myanmar, enable the tide to propagate deep into the mainland, carrying muddy and saline water. The Nga Moe Yeik Creek (a tributary of the Yangon River) is closed off at the upstream end during the dry season and is subject to high siltation rates. Extensive dredging is necessary to ensure navigability. However, dredging activities stopped in 2015 because dredging appeared to be insufficient.

Flushing the creek, by opening the Nga Moe Yeik Creek Sluice Gates more often could contribute to a solution to minimise the siltation rates, leading to lowered dredging volumes and an improved navigability of the creek. However, it may decrease the availability of irrigation and drinking water behind the sluice in the dry season. The responsible authorities are looking for an optimal solution. The current insight in the siltation problem is limited due to a lack of measured data collected in the Nga Moe Yeik Creek. The general consensus is that siltation rates can be decreased by an improved operating scheme of the Nga Moe Yeik Sluice Gates.

Since data resources are scarce or not available at all, data on bathymetry, water levels and suspended sediment concentration is collected from the field between May and July 2017. The observed water levels show a flood-dominant tidal wave with a tidal range in the order of 4 - 6 meters. Depths are measured in a zigzag pattern in the creek stretch between mouth and sluice. Suspended sediment concentrations are measured between 0.3 and 1 gram/L. Tidally and depth averaged concentrations in the order of 0.5 gram/L and 0.4 gram/L are observed at respectively 2 and 17 km from the mouth of the creek.

Part of this data is used to set up a Delft3D-flow model of the system that simulates the main sediment transport processes in the Nga Moe Yeik Creek. The initial hydrodynamic model is calibrated against observed water levels. In the next phase, the sediment transport model is used in a qualitative analysis to determine best suitable sediment parameters. Using a combination of model and collected data it is aimed to increase the insight in the siltation problem.

Both model and data showed similar hydrodynamic and sediment transport processes. The water level observations showed that the tidal wave deforms asymmetrically and becomes more flood-dominant as it propagates into the creek. A similar phenomenon is observed in the model results. Forced with a constant 2 gram/L the model generated tidally and depth averaged sediment concentrations in the same order of magnitude as the observations. From field observations and personal communication with local authorities, it is known that the siltation is most severe in the upstream end of the creek. This is also confirmed by the model results. In the scope of this work it is assumed that the model gives reliable results on the assessment of water levels and siltation

The final model was used to assess several flushing scenarios (continuously or pulsatile flushing). Although all scenarios reduced thalweg siltation in the upper domain, pulsatile flushing reduced siltation slightly better. The scenario with 3 pulses gives best results followed by the scenario with 6 pulses. Less effective is the current flushing scheme with a continuous discharge. However to be able to give an quantitative answer on the extend of mitigation, more specific values of river discharge and critical bed shear stress are necessary.

List of Figures

Chapter 1

Introduction

Developing countries all over the world, but especially countries in Southeast Asia have had some of the fastest growing economies in the world (Wilson, 2014). The coastal regions in these countries, usually consisting of complex muddy deltas, induce a lot of economic activities. However, dynamic mud characteristics in these deltas, such as high turbidity levels and siltation (accumulation of mud) often hinder economic development. As a consequence, human interventions and activities develop continuously, often leading to unforeseen and unwanted changes in the environment. To prevent or mitigate these unwanted changes in the future, it is important to understand and monitor the dynamics of mud in delta regions. But in these rapidly developing countries, it is often the case that data needed for assessing local problems is limited or not available at all. An example of such a rapidly developing country in Southeast Asia is Myanmar.

1.1 Background case study

1.1.1 Myanmar

Formerly known as Burma, Myanmar shares borders with Bangladesh, India, China, Laos and Thailand. Due to recent political reforms Myanmar is undergoing rapid changes in many sectors, such as industry, agriculture and infrastructure. Large investments are being made on infrastructural projects to boost the economy (OBG, 2017). In the delta regions, typical challenges to overcome are related to high siltation rates and saline intrusion. Both processes are influenced by tidal and seasonal conditions. The lowlands of Myanmar have a low gradient, which enable the tide, carrying saline water with high turbidity levels, to propagate deep into the mainland. Myanmar knows three different seasons (Aung et al., 2017); a Southwest Monsoon season, with heavy rainfall from mid-May to October (also referred to as rainy or wet season), a Northeast Monsoon season, cool and dry from November to February (also referred to as winter or post-monsoon season) and a hot weather season, hot and dry from February to early or mid-May (also referred to as summer or Pre-Monsoon period). Figure 1.2 illustrates the different seasons in Myanmar.

1.1.2 Ayeyarwady Delta

The Ayeyarwady Delta, located in the Ayeyarwady Region in the south of Myanmar, is shaped by the Ayeyarwady River and its numerous meandering tributaries and creeks, which discharge into the Andaman Sea. The Ayeyarwady continental shelf receives a large sediment influx (annually more than 360 million tons) from the Ayeyarwady, Sittaung and Salween River combined. In terms of suspended sediment discharge, the Ayeyarwady River is the fifth largest river in the world (Meade, 1996). Rao et al. (2005) conclude that the bulk of sediment from the Ayeyarwady River is displaced eastward by a combination of tidal currents and a clockwise flowing Southwest monsoon current. Hereby, mud is deposited in the Gulf of Martaban, resulting in a near-shore mud belt.

1.1.3 Yangon Region

The Yangon Region is located in the south of Myanmar, eastward of the Ayeyarwady Region, see the left-hand side of Figure 1.1. The Yangon Region includes the most populous city of Myanmar, Yangon, which was formerly known as Rangoon. Yangon is situated at the confluence of the Bago River and Yangon River. River slopes are very mild in this region. The lower 80 km reach of the Bago River has a concave slope between 1/15000 and 1/7000 (JICA, 2014). Two main actors managing the river system in the Yangon Region are two governmental departments. Firstly, the Department of Water resources and Improvement of River Systems (DWIR) as part of The Ministry of Transport and Communication (MoT) is responsible for dredging activities to ensure the navigability in waterways. Secondly, Irrigation Department as part of The Ministry of Agriculture, Livestock and Irrigation (MoALI)is responsible for the provision of irrigation and drinking water and is engaged in flood protection.

1.1.4 Nga Moe Yeik Creek

The Nga Moe Yeik Creek, see the right-hand side of Figure 1.1, partly meanders through the city of Yangon and discharges into the Yangon River and Bago River. In England and in many countries of the Commonwealth a (tidal) creek is the lower section of a river that is affected by the seawater. The bottom slope of the Nga Moe Yeik Creek is not known, but based on the slope of the Bago River it is estimated to be smaller than 1/15000. The Nga Moe Yeik Creek is subject to extensive siltation. The lower part of the Nga Moe Yeik Creek is referred to as the Pazundaung Creek. A case study about the siltation in this creek forms the motivation for this thesis. At 45 km upstream from the mouth of the Pazundang Creek, the creek is closed off by the Nga Moe Yeik Sluice Gates. This hydraulic structure is commissioned into service in 2012 and controls the water level and flow rate downstream with 27 vertical rising gates. The Nga Moe Yeik Sluice Gates are operated by the Irrigation Department, Construction circle 6. During the monsoon period, the sluice gates are opened to release excess water from its catchment area, with a design discharge of 319 $m^3 s^{-1}$. In the dry season (mid-November to mid-May) the sluice gate is closed to store fresh water and prevent saline intrusion and silt deposition behind the sluice gate. The stored fresh water mainly provides irrigation water for cultivation of rice and distributes drinking water to the Yangon region (Kitnan, 2012). To provide enough irrigation water to a benefited area of about 4050 ha (see yellow area in the right-hand side of Figure 1.1), the operation scheme of the sluice gate aims to keep the water level at the upstream side of the sluice gates at 12 feet (about 3.66 m) above mean sea level (U Toe Nyein, Construction 6 Assistant Director, personal communication May 2017).

1.2 Problem description

Known problems in the rivers and adjacent creeks in the Yangon Region are high siltation rates (Aung et al., 2013) and saline intrusion (Nelson, 2001). This research focuses on mitigation of high siltation rates in the Nga Moe Yeik Creek. The present-day high siltation rates lead to increased water levels, reducing the navigability of the creek in two ways. Firstly, during extreme low water levels in the dry season, the combination of low water levels and increased bed levels reduces the water depth in the creek leading to a decreased navigability in this situation. Secondly, with the combination of a tidal range of in the order of 5 meters and increased bed levels, existing bridges form a risk for vessels, during the wet season. In this situation there is only a short tidal window to navigate under the various existing bridges in the Nga Moe Yeik Creek. Incidents between vessels and bridges are a serious risk (Thonnya, 2013) and have been observed during the fieldwork (see Figure D.2). These incidents indicate that the current situation has changed drastically.

1.3 Research motivation

Because of the high siltation rates extensive dredging is necessary to ensure navigability. However, in 2015 the responsible authorities stopped dredging operations in the Nga Moe Yeik Creek since it was not sufficient any more. Dredging is no longer an effective option (Aung Kyaw Hmuu, Director DWIR, personal communication May 2017). The Ministry of Transport (MoT) desires to open the sluice gates more often in the dry season to flush the creek in order to export sediment by strengthening the ebb current. This could reduce the siltation rates in the Nga Moe Yeik Creek, leading to lower dredging volumes and an improved navigability of the creek. However, it may decrease the availability of fresh water for irrigation and drink water purposes. The

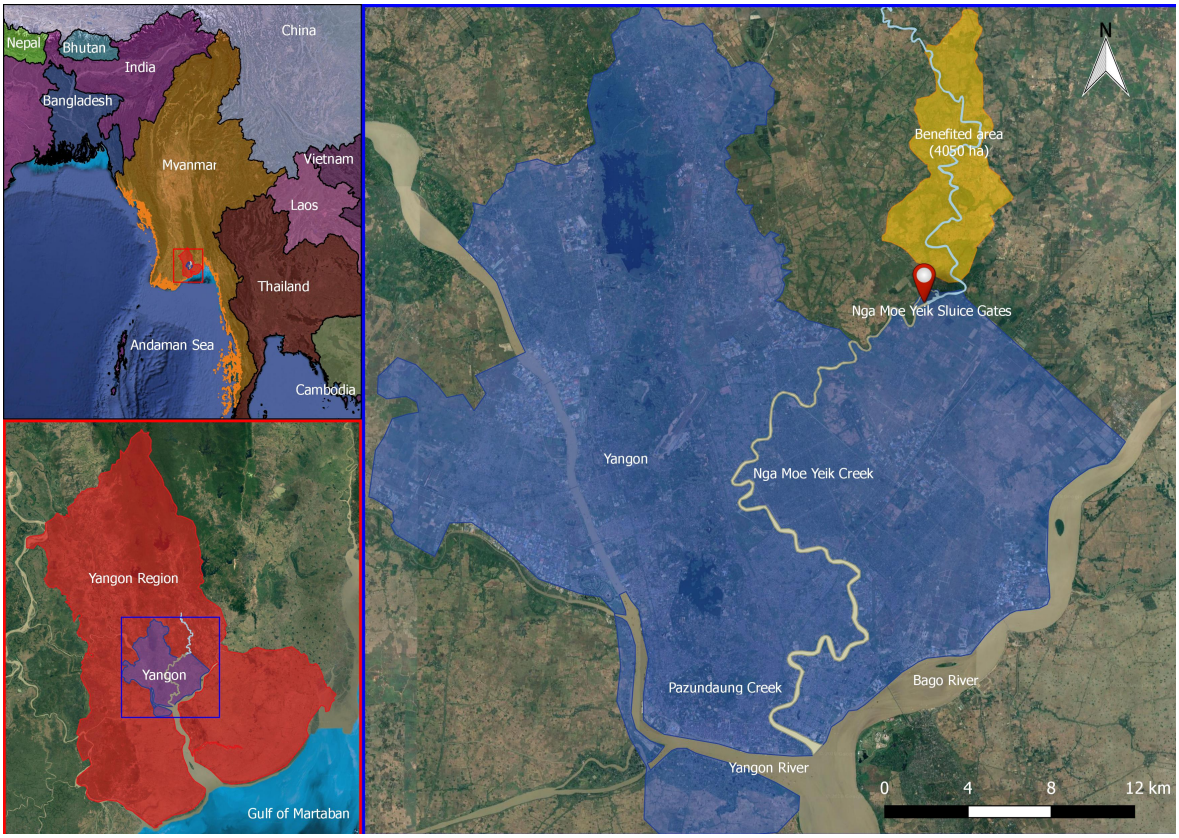

Figure 1.1: Overview of study area in Yangon, Myanmar. Subject of the case study is the Pazungdaung/Nga Moe Yeik Creek between the mouth (0 km) and the Nga Moe Yeik Sluice Gate (45 km). The yellow area (right figure) is the region where 4050 ha rice is cultivated and benefits from the closed sluice gates.

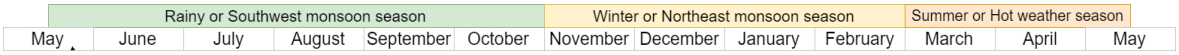

Figure 1.2: Overview of yearly seasons in Myanmar based on Aung et al. (2017)

Ministry of Agriculture, Livestock and Irrigation (MoALI) and MoT are looking for an optimal solution. Figure 1.3 illustrates the opposing interests between two local ministries.

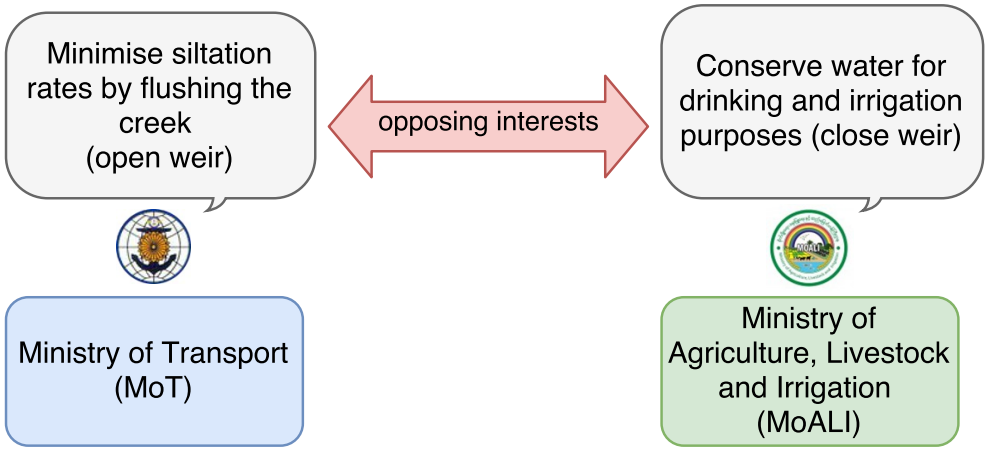

Figure 1.3: Opposing interests between MoT and MoALI. The general consensus is that siltation rates can be minimised by an improved operation scheme of the Nga Moe Yeik sluice gate

Considerations in present and future policy regarding the use of the Nga Moe Yeik Sluice Gates for siltation

mitigation by means of flushing the Nga Moe Yeik Creek are important as there are currently no dredging activities and navigability in the creek is likely to decrease in the near future. The current insight in the siltation problem is limited due to a lack of data on the depth profile, tidal propagation and sediment concentrations in the Nga Moe Yeik Creek. There are limited studies in literature which adequately describe the situation in the creek. Data on bathymetry, water levels and turbidity is required to gain insight in the system.

1.4 Aim of this research

In this research, the aim is to improve the current insight in the siltation problem in the Nga Moe Yeik Creek. The following objectives have been formulated to contribute to the current insight in siltation problems in the Nga Moe Yeik Creek:

- To quantify and increase insight in processes that determine siltation in the Pazundaung/Nga Moe Yeik Creek.
- To evaluate the effect of flushing the Nga Moe Yeik Creek in order to minimise siltation rates.
- To provide generic guidance for the use of limited data in combination with a model in data poor environments

1.5 Research questions

The following research questions have been formulated based on the previously identified problems and objectives;

Insight in processes

- What are the main processes that influence siltation in the Nga Moe Yeik Creek?
- How does the tidal wave propagate and deform in the Nga Moe Yeik Creek ?
- What are typical suspended sediment concentrations in the Nga Moe Yeik Creek?
- When and where do highest concentrations occur?
- What is the distribution of siltation in the Nga Moe Yeik Creek?
- What is the effect of varying tidal range on siltation ?

Effect flushing

- What is the effect of fresh water discharge (flushing) on siltation?
- To what extent can an improved operating scheme of the Nga Moe Yeik Sluice Gates mitigate siltation?

Data poor environment

- What are the minimum necessary parameters to assess siltation rates in a data poor environment?
- To what extent are model and field data dependent on each other in a data poor environment?

1.6 Hypothesis

It is hypothesised that a flood-dominant tidal asymmetry imports large amounts of mud into the Nga Moe Yeik Creek. Flushing the creek with an improved operating scheme of the Nga Moe Yeik Sluice Gates may mitigate siltation in the creek.

1.7 Methodology

Since data resources are scarce or not available at all, data on bathymetry, water levels and turbidity is collected from the field between May and July 2017. Furthermore, personal communication with local actors (authorities and university) helped to increase insight in the system. The main sediment transport processes in the Nga Moe Yeik Creek are simulated by a numerical D3D-Flow model, for which a part of the collected field data is used to set up the model. In an interactive process between model and field data, uncertainties induced during field data acquisition and by imposed model input parameters, are diminished. By combining information from local actors, the collected field data and the model, it is aimed to increase insight in the siltation problems of the Nga Moe Yeik Creek and answer the research questions. Figure 1.4 gives an visual representation of this methodology.

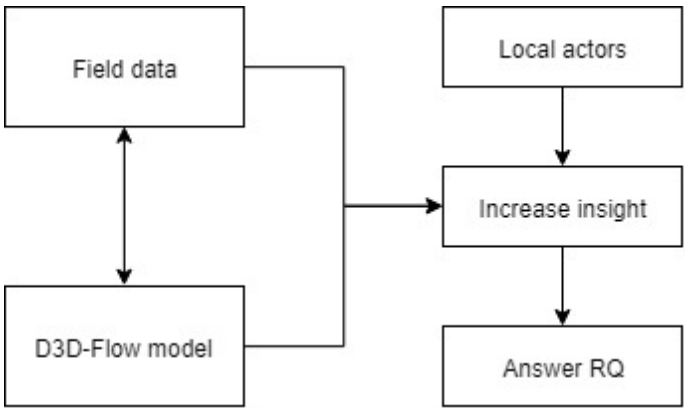

Figure 1.4: Methodology

Chapter 2

Theoretical background

This chapter gives a general introduction to the theoretical concepts of the main processes that influence the siltation rates in an estuarine environment (Section 2.1 and 2.2) and a numerical model which is able to simulate these processes (Section 2.3). The final section (Section 2.4) discusses the current knowledge about the sediment dynamics in the Nga Moe Yeik Creek.

2.1 Tidal dynamics

The hydrodynamics of shallow tidal creeks such as the Nga Moe Yeik Creek are dominantly influenced by the tide. In these relatively sheltered environments wind waves are small and their effects on sediment processes can therefore be neglected. The explanation of tidal dynamics in this section is largely based on Bosboom & Stive (2015) and corresponding lectures of the course Coastal Dynamics at the TU Delft.

2.1.1 Definitions

A tidal wave is a long, shallow water wave with a length in the order of hundreds of kilometres. The periodic rise and fall of water levels is referred to as the vertical tide. High and low tide, or high water (HW) and low water (LW) refer to the crest and trough of the wave. The time it takes the tidal wave to get from the lowest water level to the highest water level is referred to as rising tide. And similarly, falling tide is the time between highest and lowest water level. The related tidal currents, flood and ebb, are referred to as horizontal tide. During flood, an estuary shows (landward directed) inflow of water and during ebb outflow (seaward directed). Slack water period is the time during which reversal of tidal currents takes place. High water slack is the period of flow reversal between flood and ebb and low water slack is the period of flow reversal between ebb and flood.

2.1.2 Tidal generation

The tides in ocean basins, seas and estuaries are generated by the combined effect of the earth's rotation and gravitational forces of the moon and the sun. The time it takes earth to reach the same position with respect to the moon takes on average 24 hours and 50 minutes. In this period, known as a lunar day, two tidal cycles occur with a period of roughly half a day (12 hours and 25 minutes). Because it occurs almost twice per day, this type of tide is called semi-diurnal. The tidal force of the moon is stronger than the sun; therefore the tides follow a lunar day and not a solar day (24 hours). Semi-diurnal tides show a periodic increasing and decreasing range in amplitude in a period of two weeks. These are known as spring (maximum range) and neap tides (minimum range). Spring tides occur a few days after both full and new moon. This happens when the earth, moon and sun are aligned (this orientation is referred to as syzygy). Neap tides occur shortly after first and last quarters of the moon (referred to as lunar quadrature). This happens when the moon and sun are orientated in a 90 degree angle, as seen from the earth. At syzygy, the sun reinforces the lunar tide, but reduces it at quadrature. Often, there is a difference between the two daily high and low waters. The diurnal inequality refers to this difference in water levels (or the difference in velocity in two daily flood or two ebb tidal currents).

2.1.3 Tidal characteristics

Tides are reliable phenomena and are predicted relatively easily. A measured tidal signal (observed varying water levels at one location) can be decomposed into various constituents (or tidal components) that refer to specific phenomena that have an influence on the tidal motion with a certain frequency. The amplitudes and phases of these constituents depend on the location on the earth. When the constituents are known at one location, they can be used to characterise the tidal signal and predict the tides in the future.

Tidal constituents

Tidal constituents can be divided into primary constituents, which appear in the equilibrium tide (in a model of the earth with no landmasses; only one big ocean) and compound constituents, a linear combination of primary constituents (Deltares, 2014). M2 and S2 are the two main constituents in the equilibrium tide. The influences of the moon (main lunar tide) or sun (main solar tide) are characterised by the letter M or S and the index 2 refers to semi-diurnal phenomena. Two main diurnal components are K1 and O1, representing the effect of moons declination, K1 with P1 the suns. K1, P1 and O1 account for the diurnal inequality. The K2 constituent influences the frequency and amplitude of M2 and S2 for the declination effect of the moon and sun. Constituents N2 and Q1 are introduced by the varying distance between moon and earth because of the elliptical orbit of the moon. Other effects will generate other tidal constituents defined by their own amplitudes and phases with respect to each other. The explanation of all tidal constituents is pretty complex due to all the interactions between different frequencies involved. Doodson (1921) showed that all tidal constituents have frequencies that are linear combinations of six astronomical variables and distinguished 388 tidal frequencies.

Form factor

The semi-diurnal or diurnal characteristic of a tidal signal can be determined by comparing the sum of amplitudes of the main diurnal components over the sum of amplitudes of the main semi-diurnal components using the form factor F:

$$F = \frac{K1 + O1}{M2 + S2} \tag{2.1}$$

Four tidal characters can be classified for a tidal signal based on the form factor, see Table 2.1.

Table 2.1: Tidal characteristics based on the form factor F

Category	value of F
Semi-diurnal	0-0.25
Mixed, mainly semi-diurnal	0.25-1.5
Mixed, mainly diurnal	1.5-3
Diurnal	> 3

Tidal asymmetry

Similar to wind waves, tidal waves propagating into estuaries become more and more asymmetric. Amplitudes increase due to shoaling and narrowing of the estuary also leads to a progressively shorter rising tide. Consider a prismatic tidal channel. If friction can be neglected the propagation speed of the tidal wave (c) in this channel is given by the square root of the gravitational constant (g) and the water depth (h) consisting of the mean water level (h_0) and the water level elevation (η) with tidal amplitude (a);

$$c = \sqrt{g * h} = \sqrt{g * (h_0 + \eta)} \tag{2.2}$$

So, the propagation velocity of the high tide ($\sqrt{g * (h_0 + a)}$) is larger than the propagation velocity of the low tide ($\sqrt{g * (h_0 - a)}$), thus the rising period is shorter than the falling period and the tidal wave becomes distorted with a steep vertical face. The bed shear stress due to current alone may be computed using various types of formulations like Chézy, Manning or White-Colebrook and can be written in the form:

$$\tau_b = \frac{g * \rho * U|U|}{C_{2D}^2} \tag{2.3}$$

In coastal areas where friction can not be neglected, the propagation velocity can be affected. Here the asymmetry can induce higher tidal velocities. In tidal rivers this effect can even be enlarged by the river discharge if the flow velocity and thus the bed shear stress is much larger at maximum ebb than at maximum flood. During ebb around low water, the damping of the amplitude caused by friction is stronger than during flood around high water, resulting in an asymmetry of the water level elevation about the horizontal axis (a positively skewed signal). As a consequence of tidal asymmetry, a tidal system shows ebb- or flood-dominance. Flood-dominant systems tend to import sediment and as a consequence bed levels increase. Ebb-dominant systems keep their channels deep and export sediment.

Peak flow asymmetry

Asymmetry in tidal peak velocity is characterised by a rapid increase in water level after low water and large flood velocity directly after low water slack or vice versa. Without other non-tidal forcing or river discharge, the averaged discharge over a tidal cycle should be zero, even if the current is asymmetric. This means that in the case of a shorter flood duration, the maximum flood velocity is higher compared to the maximum ebb velocity (flood-dominant). And vice versa, in case of a shorter ebb duration, higher ebb than flood velocities occur (ebb-dominant). Basin geometry controls the tidal distortion. Large tidal amplitudes and a shallow channel (or more precisely a large ratio of tidal amplitude over water depth a/h) enhance flood-dominance. In tidal creeks, flood-dominance can be counteracted by river discharge which enhances ebb-dominance.

Slack tide asymmetry

Slack tide asymmetry is characterised by a longer high water slack period compared to the low water slack period. In short tidal basins (where the length of the basin is smaller than 1/4 of the tidal wave length) this is the dominant form of asymmetry. For a short basin with shallow channels and little storage area (little or no tidal flats), the flow cross-section is larger around high water than at low water. As a result, the rate of velocity change is smaller at high water. In other words, the high water slack period is longer than low water slack period (flood-dominant). For a basin with deep channels and a vast storage area (big tidal flats) the basin area is larger around high water than low water. Consequently, around high water slack a greater flow variation occurs then around low water slack. In other words, the high water slack period is shorter than the low water slack period (ebb-dominant). Slack tide asymmetry is an important feature for the net transport of fine sediment. In flood-dominant system (with a longer high water slack period) fine sediment has more time to settle.

Role of river discharge

Without sources like river discharge, the discharge in a tidal system integrated over a tidal period equals zero. In other words, during ebb and flood an equal volume of water is moved. When river discharge is considered as a source in a tidal system, the total volumes of water during ebb or flow are not equal. River discharge can influence the flood- or ebb-dominance of a system as it strengthens the ebb flow and weakens the flood flow.

Relative phase difference between M2 and M4

M2 and its first harmonic, M4, can be used to illustrate the nature the of the tidal asymmetry depending on the relative phase difference between M4 and M2 ($2\phi_{m2} - \phi_{m4}$). If $2\phi_{m2} - \phi_{m4} = 0°$ (or 180°) the duration of low water (or high water) slack is larger. This tidal asymmetry is referred to as LW slack tide asymmetry (or HW slack tide asymmetry). If $2\phi_{m2} - \phi_{m4} = 90°$ (or 270°) the duration of flood (or ebb) is shorter. This tidal asymmetry is referred to as max flood flow asymmetry (or max ebb flow asymmetry).

2.2 Sediment dynamics

In order to understand the morphodynamic behaviour of a tidal creek in a muddy coast, this section describes some relevant sediment concepts. These concepts are mainly based on Winterwerp & Van Kesteren (2004) and corresponding lectures of the course Sediment Dynamics at the TU Delft.

2.2.1 Fine sediment characteristics

Sediments in an estuarine environment that are affected by tidal currents are clays, silts and sands. They can be classified based on cohesion; non-cohesive sediments (coarse sediment, e.g. sand) and cohesive sediments (fine sediment, e.g. mud). Cohesive sediment, or mud, as encountered in the marine environment, consists of a mixture of clay, silt, (fine) sand, organic material, water and sometimes gas (Winterwerp & Van Kesteren, 2004).

Flocculation

Cohesive sediments in suspension tend to flocculate, therefore the settling velocity of a floc is not constant. Flocs are formed as a result of collisions between particles. The water content of flocs is typically 80-95% making it loose structures. Turbulent (shear) forces can break up flocs again. The dynamic flocculation and breakup processes result in variety of occurring fractions determined by various factors such as: location, time, organic composition and salinity. It takes time for flocs to be in equilibrium.

Settling and deposition

Suspended sediment is subject to balance between turbulence and gravity. Turbulence keeps the particles in suspension and gravity enforces the particles to settle. The larger particles of non-cohesive sediments settle more rapidly out of suspension than the finer particles of cohesive sediments. But the finer cohesive sediment particles flocculated together have an increased settling rate than individual cohesive particles. The settling rates of non-cohesive sediments largely depends on their physical characteristics (Pugh, 1996). Fine sediment particles, settling on top of consolidated soil, form a loosely packed layer (referred to as fluffy layer) in the order of millimetres. These particles can easily be entrained by turbulent mixing of the tidal flow. Only at slack period, where velocities are small, fine sediment particles have enough time to settle again on the consolidated bed, reforming the fluffy layer. Stokes' law states that for Euclidean particles (such as sand grains) drag forces are balanced by gravity forces, with a constant settling velocity in a viscous fluid. This law does not apply for mud flocs as they are not massive Euclidean particles. Settling velocity for flocs increase with floc size. The settling velocity of flocs is increased by a higher concentration of suspended material by enhanced flocculation until a certain concentration threshold is exceeded beyond which the settling velocity is decreased by a hindered settling. Because of the increasingly higher near bottom suspended sediment concentrations (Rouse concentration profile), flocs higher in the water column are slowed down by the wake flow of flocs lower in the water column. Because of the high water content of the flocs (large volume/mass ratio) the resulting buoyancy effect is particularly relevant for flocs. Settling velocity is not constant for flocs because of flocculation and hindered settling. Particles deposited in a layer at the bed start to consolidate. During this process water is squeezed out of the soil by the weight of the growing layer. Density and strength of the soil are increased gradually during consolidation.

Erosion

The erosion rate parameters (M and τ_{cr}) depend on consolidating stage and sediment properties. In a consolidated muddy bed the availability of sediment is limited (starved bed condition). The erosion of such a bed is governed by the strength distribution within the bed. For soft cohesive sediments critical bed shear stress amounts 0.1 0-1 Pa, whereas typically the peak critical bed shear stress is 1-2 Pa for more consolidated soils. Three erosion modes can be distinguished for muddy soils: floc, mass and surface erosion. When the drained strength of unconsolidated flocs is exceeded by flow-induced stresses, individual sediment flocs or parts of it are disrupted from the bed. This process is called floc erosion. Mass erosion occurs when flow-induced stresses become even larger as they locally exceed the undrained bed strength in over-consolidated soils and a whole lump of material is eroded out of the bed. With surface erosion, layers of flocs are eroded from a consolidated bed. Turbulent flows change the stress state of a soil inducing small bed deformations in the bed and negative pore water pressure gradients. As a consequence, the over-consolidated soil induces a water inflow reducing the soil strength. During this process sediment particles are replaced by water.

2.2.2 Fine sediment transport

Fine sediments are eroded and mobilised from the bed in areas with high bed shear stresses (areas with large currents and or waves, such as the mouth of a tidal channel), where they are easily kept in suspension, to

places with low bed shear stresses (sheltered areas with reduced velocities, such as the landward side of a tidal channel).
Import of fine sediment is influenced by various flow inducing processes, such as tidal asymmetry and saline-driven gravitational circulation. Fine sediment transport by the latter is induced by a horizontal salinity gradient in a tidal channel. A starved bed is mainly influenced by slack water asymmetry and an alluvial bed is also influenced by peak flow asymmetry. For peak flow asymmetry, the residual sediment transport has the direction of the highest peak velocity. The sediment transport for cohesive sediment is related to the velocity to third power, U^3 and for non-cohesive sediment is related to U^4. For slack water asymmetry, the sediment transport is a result of the difference in acceleration or deceleration velocity gradients which is caused by the horizontal asymmetry related to the settling time (Gatto et al., 2017).
In general, a relative phase difference M2 and M4 (vertical tide) between 45 °and 225 °indicates import of fine sediment. Postma (1954) found that once cohesive fine sediments are eroded and suspended, they are difficult to settle down (settling lag). When cohesive fine sediments are deposited, they are not easily eroded due to cohesion of the sediments (scour lag). As a consequence of scour and settling lag, net transport of fine sediment is in flood direction. After a particle travelled landward with flood, it can rests on the bed longer than after ebb. This shows that finer sediments tend to settle further landward in a tidal channel and can not be eroded when as long as the flow-induced stresses are below the critical bed shear stresses.

2.3 Delft3D-Flow

Deltares has developed a fully integrated computer software suite for a multi-disciplinary approach and 3D computations for coastal, river and estuarine areas. It can carry out simulations of flows, sediment transports, waves, water quality, morphological developments and ecology. The Delft3D suite is composed of several modules, grouped around a mutual interface, while being capable to interact with one another. Delft3D-FLOW is a multi-dimensional (2D or 3D) hydrodynamic (and sediment transport) simulation program which calculates non-steady flow and transport phenomena that result from tidal and meteorological forcing (Deltares, 2014). The Delft3D-Flow module calculates erosion and deposition fluxes for cohesive sediment using the Partheniades-Krone formulations;

$$E = M(\frac{\tau_b}{\tau_{b,cr,e}} - 1) \tag{2.4}$$

In which; E is the erosion flux [$\mathrm{kg\,m^{-2}\,s^{-1}}$] for $\tau_b \geq \tau_{b,cr,e}$, M is the erosion parameter [$\mathrm{kg\,m^{-2}\,s}$], τ_b is the bed shear stress [$\mathrm{kg\,m^{-1}\,s^{-2}}$] and $\tau_{b,cr,e}$ the critical bed shear stress for erosion [$\mathrm{kg\,m^{-1}\,s^{-2}}$]

$$D = w_s * c_b \tag{2.5}$$

In which; D is the deposition flux [$\mathrm{kg\,m^{-2}\,s^{-1}}$], w_s is the settling velocity [$\mathrm{mm\,s^{-1}}$] and c_b the averaged near bottom sediment concentration [$\mathrm{kg\,m^{-3}}$].
The settling velocity, w_s can be user specified or calculated according to the formulation of Richardson & Zaki (1954) when hindered settling should be accounted for (Deltares, 2014).
The Delft3D-flow module requires the following parameters in order to compute cohesive sediment processes; reference density C_{soil} [$\mathrm{kg\,m^{-3}}$], specific density ρ_{soil} [$\mathrm{kg\,m^{-3}}$], dry bed density ρ_{dry} [$\mathrm{kg\,m^{-3}}$], settling velocity w_s [$\mathrm{mm\,s^{-1}}$], critical bed shear stress for sedimentation $\tau_{cr,s}$ [$\mathrm{kg\,m^{-1}\,s^{-2}}$], critical bed shear stress for erosion $\tau_{cr,e}$ [$\mathrm{kg\,m^{-1}\,s^{-2}}$], the erosion parameter M [$\mathrm{kg\,m^{-2}\,s}$] and the initial sediment layer thickness at the bed δz_0 (Deltares, 2014).

2.4 Sediment dynamics in the Pazundaung / Nga Moe Yeik Creek

As stated before, little is known in literature about the sediment dynamics in the Nga Moe Yeik Creek. Current insight in the situation is mainly based on measurements of Sir Alexander Gibb & Partners (1976) (Section 2.4.1), Google satellite imagery (Section 2.4.2) and field visits and personal communication with the local authorities (Section 2.4.3).

2.4.1 Measurements Sir Alexander Gibb & Partners (1976)

Nelson (2001) states that average sediment concentrations in the dry season are approximately 4 times that of the Monsoon season in the Yangon River (which connects to the mouth of the Nga Moe Yeik Creek), and that the depth-averaged dry season sediment concentrations vary between approximately 0.3 gL^{-1} during neaps and 5.5 gL^{-1} during springs. British firm of Consulting Civil Engineers Sir Alexander Gibb & Partners (1976) measured discharge and sediment transport in the Pazundaung Creek, see Figure A.1. The measurements were done in a cross section of the creek mouth during the Pre-Monsoon, Monsoon and Post-Monsoon. The Pre-Monsoon measurements show, especially during spring tide, a flood-dominant signal (with greater flood than ebb velocities) and a max flood discharge of about $3 * 10^3$ $m^3 s^{-1}$. This is twice the max ebb discharge which is about $1.5 * 10^3$ $m^3 s^{-1}$. Max sediment transport rates occur during spring tide and are in the order of $15 * 10^3$ kgs^{-1} during flood and in the order of $8 * 10^3$ kgs^{-1} during ebb. During the Monsoon period the measurements show an ebb-dominant signal. The ebb period increases significantly and max flood and ebb discharges are in the same order of about $2.0 * 10^3$ $m^3 s^{-1}$ during spring tide. The ebb discharge is strengthened by the increased river discharges during the Monsoon period. Max sediment transport rates are lower and are in the order of $1.5 * 10^3$ kgs^{-1} for both ebb and flood periods. In the Post-Monsoon season the max discharges increase to the order of $2.0 * 10^3$ $m^3 s^{-1}$. The measurements do not clearly show flood or ebb dominant and the max sediment transport rates are in the order of $1 * 10^3$ kgs^{-1} for both ebb and flood periods. The discharge and sediment transport measurements can give insight in the sediment concentrations typical for the Pazundaung Creek. Sediment concentrations are calculated by dividing the sediment transport rates by the corresponding discharge rates, see Figure 2.1. To do this, a manual digitalisation was needed, resulting in some errors. Around points of zero discharge and sediment transport small errors can occur which result in some anomalies in calculated concentrations. It appears that typical values vary roughly between $0.3 - 1.0$ kgm^{-3} (or gL^{-1}) during the Monsoon, and Post-Monsoon period and can reach up to about 5.0 gL^{-1} in the Pre-Monsoon period, disregarding anomalies (concentrations higher than 6 gL^{-1} in Pre-Monsoon spring).

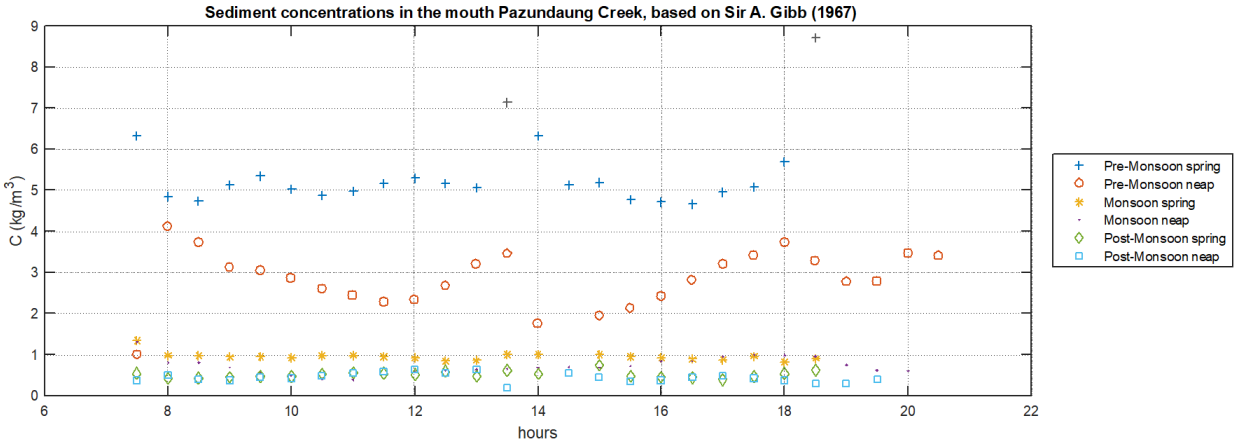

Figure 2.1: Sediment concentrations based on discharge and sediment transport measurements, see Figure A.1

2.4.2 Google Earth satellite imagery

First order estimates of morphological changes can be observed in Google Earth images. In the wet season, the Nga Moe Yeik Sluice Gates are opened roughly between 15 May and 15 November. Figure 2.2 shows Google satellite images of most the upper part of the Nga Moe Yeik Creek with closed sluice gates. The difference in color between the fresh water at the upstream side of the sluice and brown water at the downstream side of the sluice indicate high sediment concentrations downstream of the sluice. The images are taken during different moments in the dry season between 2015 and 2016. Early in the dry season (December 2015) no vegetation is visible on the mud deposits. Halfway through the dry season (February 2016) the mud deposits show some green areas. At the end of the dry season (April 2016) vegetated areas are clearly observed. During the dry season the mud deposits have time to consolidate and dry out while vegetation starts to develop. Dried-out or vegetated mud areas will erode less easily in subsequent wet season.

Figure 2.2: Google satellite images of the upper part of the creek near the Nga Moe Yeik Sluice Gates in the dry season.

2.4.3 Field visits and personal communication with DWIR and Irrigation Department

In the beginning of May 2017 several field visits to the Nga Moe Yeik Creek and its sluice gates were organised, accompanied by staff from DWIR or Irrigation Department. During these field visits the local siltation related problems were discussed. From this it is known that the siltation is most severe upstream from the Industrial Bridge, which is about 30 km from the creek mouth. It was said by an unknown DWIR staff member that at a certain point in this stretch the creek can fall dry in some parts during low water. The bed level downstream of the Nga Moe Yeik Sluice Gates has reached MSL +8 ft (U Toe Nyein, Construction 6 Assistant Director, personal communication May 2017). The sill level, downstream of the sluice, is designed on MSL - 4 ft, see Figure 2.3. This indicates that the occurring siltation near the sluice is in the order of 12 feet (about 4 meters). This is confirmed by the picture in Figure 2.4. This picture is taken from the Nga Moe Yeik Sluice Gates in May 2016 and shows a significant amount of mud deposits. It takes up the mayor part of the cross-section of the creek leaving only a shallow channel.

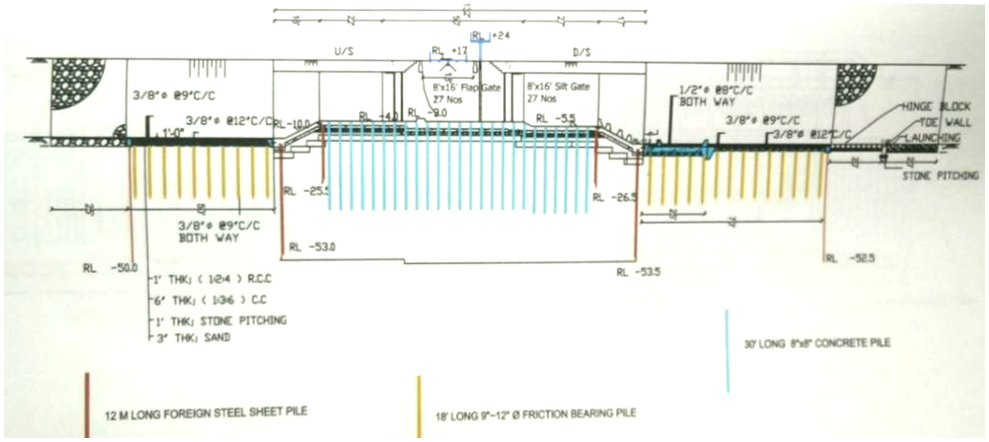

Figure 2.3: Nga Moe Yeik Sluice Gates construction drawing, longitudinal section. Acquired from Irrigation department after a field visit to the sluice site. Dimensions are given in feet compared to the reference level, RL (= MSL).

Figure 2.4: Mud deposits in the Nga Moe Yeik Creek as seen from the Nga Moe Yeik Sluice Gates. This picture was taken in May 2016 (with closed gates) and is acquired from Irrigation department after a field visit to the sluice site.

Chapter 3

Materials and Methods

Fieldwork (section 3.1) has been conducted to gather information relating to the bottom profile of the creek, water levels and sediment concentrations which has not previously or recently been obtained. The collected data is used to build a Delft3D-FLOW model (Section 3.3) to assess the siltation dynamics in the creek.

3.1 Fieldwork methodology

In the Pre-Monsoon season, between May and July 2017, several measurements were conducted. Three phases are discerned: water level monitoring, bathymetric surveying and OBS profiling & sampling.

3.1.1 Phase 1: Monitoring water level

Water level data along the creek is required for the calibration process of the model to simulate the tidal propagation in the creek. In the period between 9 and 30 May 2017 the water level in the Nga Moe Yeik Creek was monitored. Two types of water level data loggers are used to collect data at four stations along the creek; one CTD-Diver and three Cera-Divers. Both types measure pressure and temperature. Additionally, the CTD-Diver measures conductivity, which is a measure for salinity. Below water, these Divers measure absolute pressure. This means that the sensor not only measures the hydrostatic pressure, but also the air pressure pushing on the water surface (Van Essen Instruments, 2016). To correct for variations in atmospheric pressure as part of absolute pressure, a barometer is installed above water. All Divers and barometer were set to measure pressure at a 3-minute interval. The CTD-Diver is installed in a monitoring station in the mouth of the creek. The three Cera-Divers, Diver 1, Diver 2 and Diver 3, are installed at respectively 15, 30 and 45 km upstream from the mouth, see Figure 3.2. The four Divers, used to monitor the water levels along the creek, are installed roughly 0.6 m below the water surface inside a metal measuring well attached to a stationary object, often a pole, see Figure 3.1. It was aimed to install the Divers below the lowest water line (LWL). Unfortunately, the sensor depth with respect to MSL $d_{D,MSL}$ could not be measured in the field. Based on estimates from DWIR $d_{D,MSL}$ is obtained. The most upstream Diver, Diver3, was installed in a measuring well attached to a railing at the downstream side of the sluice gates. A week after instalment this Diver had to be replaced a few meters. The relative height difference was measured for a correction in the data processing. The relative heights as shown in Figure 3.1 are based on estimates from DWIR and notes taken during the instalment of the Divers.

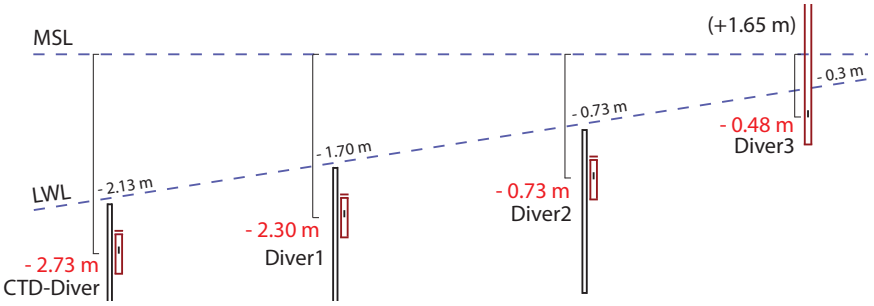

Figure 3.1: Relative heights of the Divers compared to mean sea level (MSL). Assumed values for the low water line (LWL) are depicted in black. MSL + 1.65 indicates the relative height before relocating Diver 3. The estimates for the respective sensor heights w.r.t. MSL, as used in the data processing, are given in red.

3.1.2 Phase 2: Bathymetric surveying

Depth measurements in the creek are required to capture the varying bed level in the creek. Hydrodynamics and sediment transport are influenced by the varying depths in a creek. For a good representation of these processes in the model it is therefore required to have data that describes the submarine topography or bathymetry. A Garmin echo sounder set-up is used to capture the bathymetry. The set-up consists of a display instrument (Garmin echoMAP 42dv) and a transducer (Garmin GT20-TM). The transducer is mounted on a survey boat, 30 cm under the water line, at the transom as suggested by Garmin International, Inc. (2017) and sends out sonic pulses, with a 455 kHz frequency, which reflect on the consolidated bottom. The set-up simultaneously measures the absolute distance between transducer to bottom and tracks GPS coordinates with a sampling rate of 1 second. In a zigzag trajectory, with bends roughly every 100 m, the 45 km stretch between the sluice gates and mouth was covered in four days. The goal was to measure only around high water (HW) to cover the widest possible bathymetry. The tidal variability in water level varied in the order of 2 meters. The measured water depths need to be converted to an absolute datum through post processing (Section 3.2.2).

3.1.3 Phase 3: Measuring turbidity & sampling

To gain insight in sediment dynamics throughout a tidal cycle in the Pazundaung Creek, turbidity profiles are measured with an optical backscatter (OBS) sensor over a tidal period. An OBS sensor is a turbidity sensor which measures the amount of light that is scattered by suspended solids in the water. Based on this signal, suspended sediment concentrations can be estimated. Using the OBS, turbidity is measured with a sampling rate of 1 second. Every 15 min the instrument is lowered manually to the creek bed. In this way turbidity profiles are measured at two locations approximately 2 and 17 km upstream from the mouth. The used OBS-3A combines the OBS probe with pressure, temperature and conductivity sensors (Campbell Scientific, Inc., 2016), so additional profiles of temperature and salinity are measured. To determine the concentration of the suspended particles water samples were taken with a Van Dorn water sampler. By filtering the water sample through filter paper and after drying it in an oven at 105 °C the sediment concentration in the sample is determined.

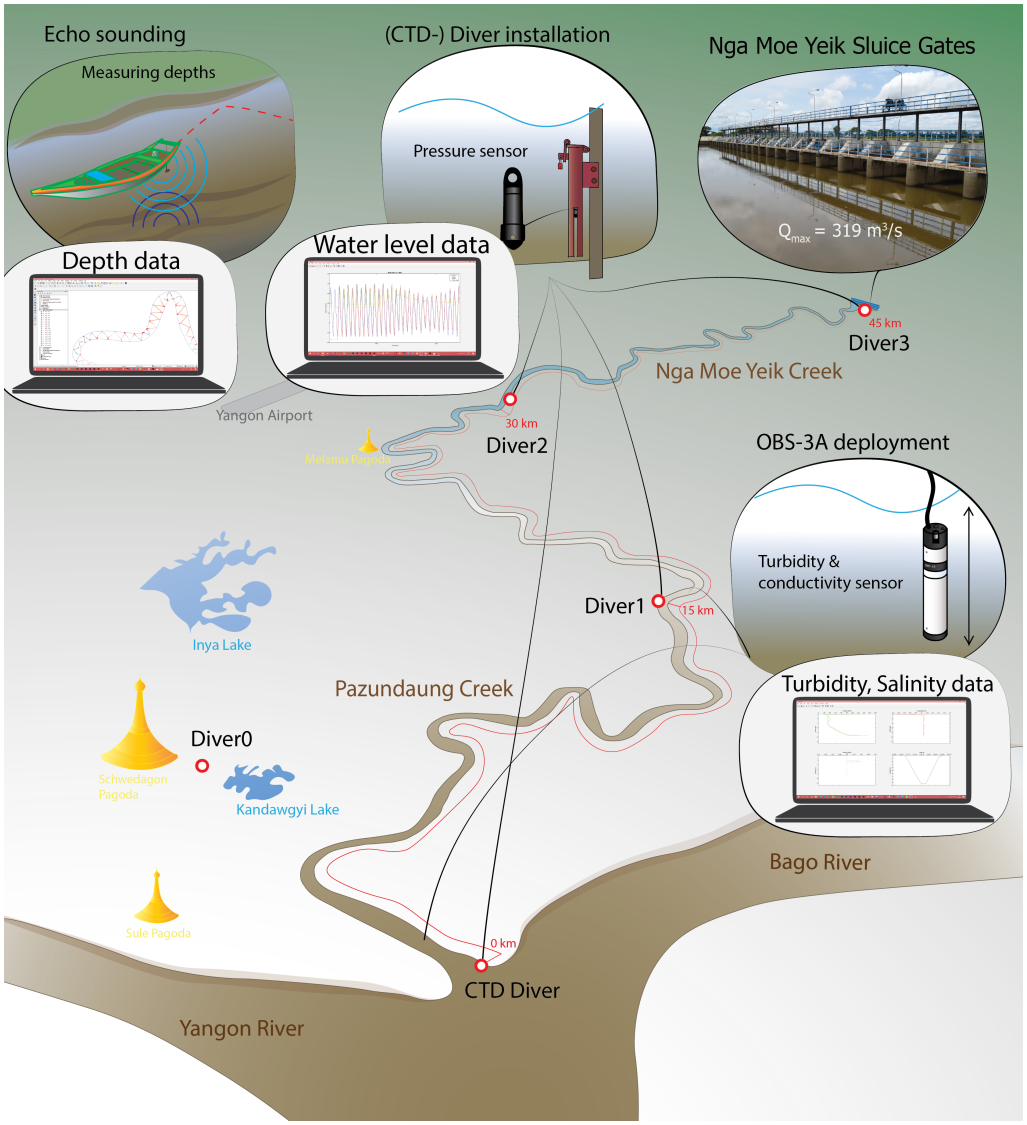

Figure 3.2: Overview of the conducted fieldwork in the Nga Moe Yeik Creek/Pazundaung Creek; Depths are measured with an echo sounder along the whole stretch of 45 km. Water level time series at several locations along the creek are acquired. The locations of the installed divers and barometer (pressure sensors) are indicated with a red circle. Using the OBS-3A sensor turbidity and salinity profiles are acquired during a complete tidal cycle on two locations

3.2 Data processing

3.2.1 Converting pressure to water levels

As discussed in subsection 3.1.1 the Divers measure the absolute pressure at 4 locations along the creek. The pressure (P) is measured in cmH2O. To calculate the corresponding water levels with respect to a horizontal reference datum (MSL), the following steps are taken.
First the measured atmospheric pressure (P_{atm}) is subtracted from the measured absolute pressure (P_{abs}) to obtain the hydrostatic pressure (P_{hyd}).

$$P_{hyd} = P_{abs} - P_{atm} \tag{3.1}$$

Although the Divers measure at the same sample rate of 3 min, they do not measure at exactly the same moments in time. Therefore the data is interpolated to a higher sample rate to be able to subtract corresponding pressure values.

Secondly, the water column above the sensor (WC) can be described by the following equation (Van Essen Instruments, 2016):

$$WC = 9806.65 * \frac{P_{hyd}}{\rho * g} \tag{3.2}$$

In which g is the gravitational constant (9.81 m/s^2) and ρ is the density of water, for which a value of 1000 kg/m^3 was chosen. This indicates fresh water, as was measured during the OBS profiling. In reality the density of water will vary as the salinity varies over time. The density of seawater can reach a maximum of 1030 kg/m^3. It is unlikely that the density in the Nga Moe Yeik Creek will reach this value, but if this happens the chosen value of 1000 kg/m^3 will result in an error of max 3% lower water levels. This error is considered negligible in the scope of this work.
Finally the water level with respect to the horizontal reference MSL ($\zeta_{D,MSL}$) can be calculated by adding the sensor depth with respect to MSL ($d_{D,MSL}$) to the water column above the sensor (WC).

$$\zeta_{D,MSL} = WC + d_{D,MSL} \tag{3.3}$$

3.2.2 Correcting depth measurements

The depth measurements are required to create a bathymetry for the model. As mentioned in Subsection 3.1.2, the observed depth (d_{obs}) includes an unwanted offset due to the varying water level as the tidal wave progresses while the depth is measured in four days along the creek, see Figure 3.3. This signal should be filtered out in order to relate the bed level to MSL ($d_{b,MSL}$). For this correction water levels are needed at the same time and location where the survey boat measured the depths. Using a combination of model and the measured water level data, the tidal water level (ζ_{calc}) can be calculated. $d_{b,MSL}$ is then calculated by subtracting ζ_{calc} from d_{obs}:

$$d_{b,MSL} = d_{obs} - \zeta_{calc} \tag{3.4}$$

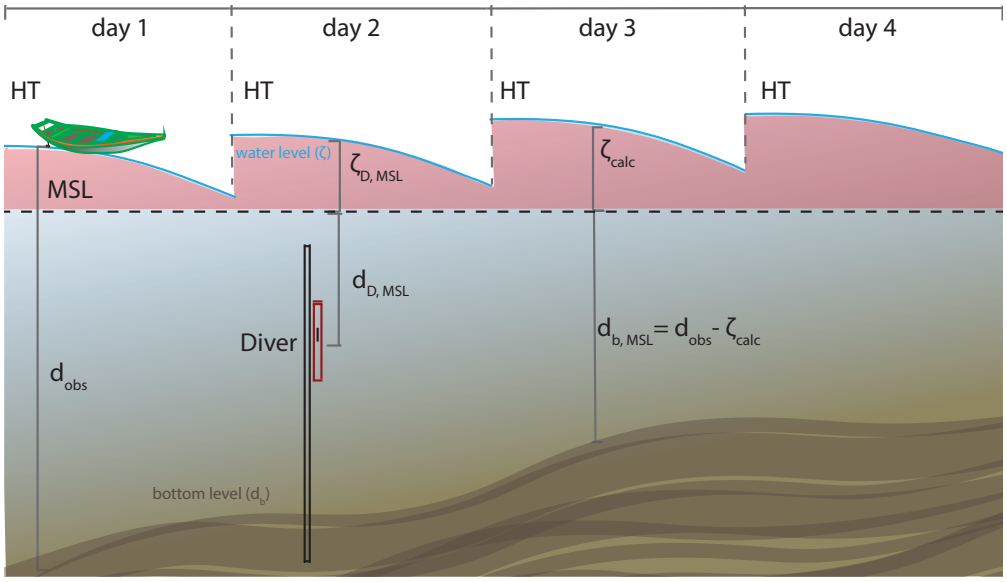

Figure 3.3: The observed depth (d_{obs}) includes an unwanted offset (red area) due to the varying water level in the system. It was aimed to measure around high tide (HT) to capture most of the bathymetry. The locally observed water level ($\zeta_{D,MSL}$) is used to calibrate the model to compute the water level in the whole domain (ζ_{calc}). The bottom depth w.r.t. MSL ($d_{b,MSL}$) can be calculated by subtracting ζ_{calc} from d_{obs}. The sensor depth ($d_{D,MSL}$) is based on estimates and includes uncertainties.

A simple Delft3D-Flow model can be used for calculating water levels in the temporal and spatial domain, but its output (ζ_{calc}) depends on the used bathymetry and measured depth. To solve this paradox some iterations are needed to correct the depth measurements, see Figure 3.4. Starting with the observed depth (d_{obs}),

containing the offset, as a basis for a first bathymetry which is used as input in the model. The output from this model (ζ_{calc}) is then used to correct the observed depth (d_{obs}) using equation 3.4. With the corrected depth ($d_{b,MSL}$) a second bathymetry is created and used as input in the model. The output from this second iteration (ζ_{calc}) is then used to correct the depth from the last iteration ($d_{b,MSL}$) again using equation 3.4. This process is repeated until the difference between two subsequent model outputs (ζ_{calc}) can be neglected.

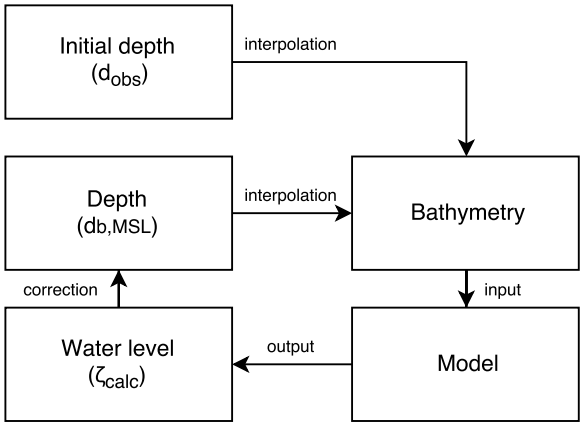

Figure 3.4: Bed level iteration.

The locally observed water level ($\zeta_{D,MSL}$) is based on estimates for the sensor depth ($d_{D,MSL}$). Because it is used to calibrate the model to compute the water level in the whole domain (ζ_{calc}), it introduces uncertainties in the bathymetry. In the scope of this research these are considered negligible.

3.3 Model set-up

A depth-averaged (2DH) Delft-3D FLOW model is set up to simulate the main hydrodynamic and sediment processes in the Nga Moe Yeik Creek. The model is built in order to serve as a starting point in understanding the interaction between siltation rates and fresh water flushing.

3.3.1 Model domain

The model domain covers a creek stretch of 45 km, from the Nga Moe Yeik SLuice Gates to the mouth of the Pazundaung Creek. It is assumed that the effect of various tributaries found along this stretch can be neglected. A computational grid, with 6 grid cells in width and 840 grid cells in length, is created based on Google Earth satellite imagery, see Figure 3.5. The width of the domain is 120 meters at the upstream boundary (at the sluice gates) and gradually increases to 600 meters at downstream the boundary (at the outflow in the Yangon River).

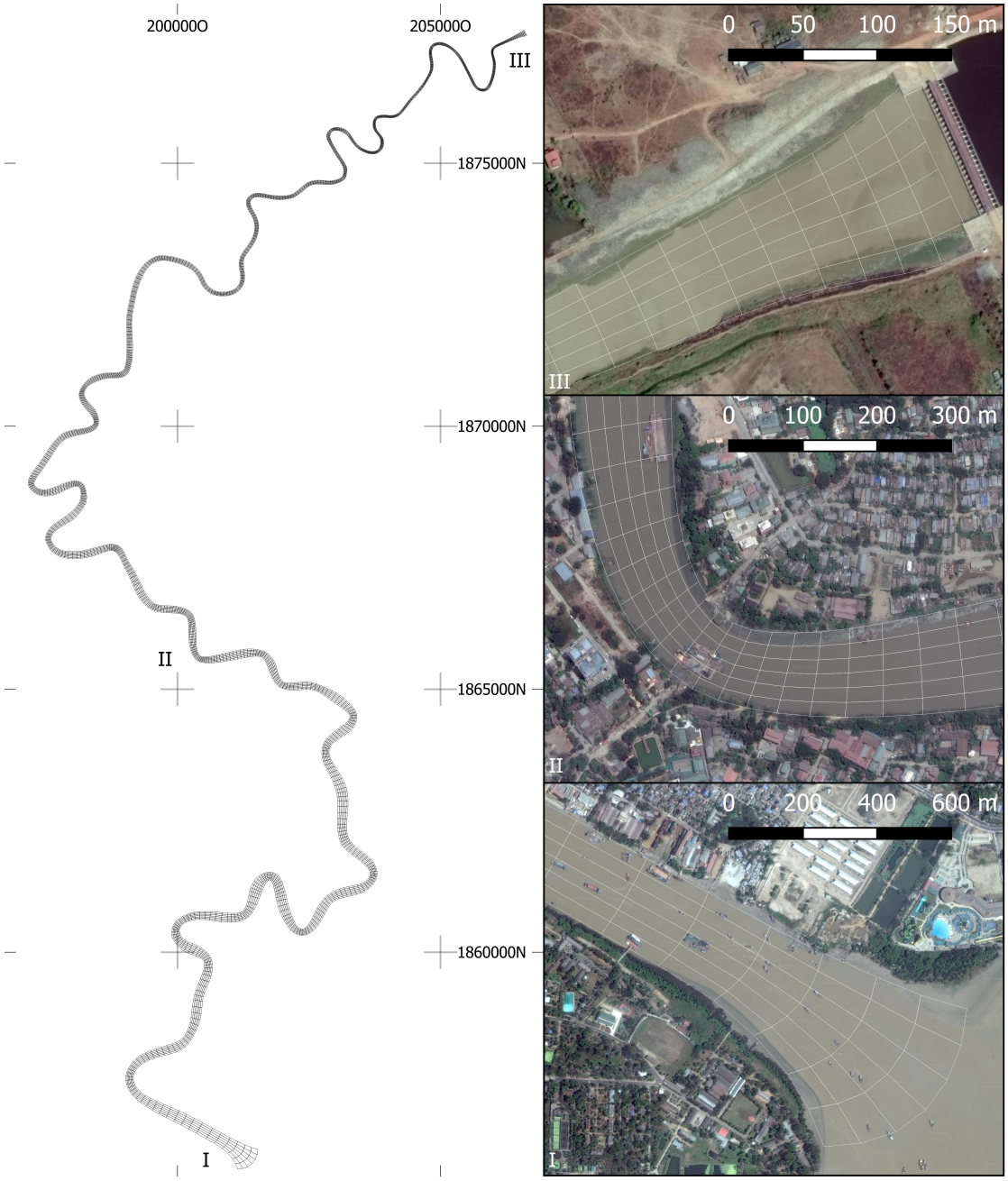

Figure 3.5: The computational grid is generated based on Google Earth satellite imagery and consists of 6 by 840 grid cells

3.3.2 Phase 1: Hydrodynamics

At first, the upstream boundary is set to be a closed boundary ($Q_{fl} = 0$ m^3 s^{-1}), representing the closed sluice gates in the dry season. The downstream boundary is forced by varying water levels that reproduce the tide. These water levels are generated by harmonic constants of tidal constituents (see Table A.1), as calculated from observations at Monkey Point (near the mouth of the Pazundaung Creek) between October 2011 to July 2011 (JICA, 2015). The model runs with a time step of 1 minute for a period of 40 days, which was chosen such that it overlaps the period of water level monitoring and includes a few days of spin-up time. The model is calibrated against water levels observed at the three monitoring stations along the creek by varying inclination (i) and the bed roughness by varying Manning's coefficient (n in $s/m^{-1/3}$). Both parameters (i and n) are set constant over model domain and time. The slope of the Nga Moe Yeik Creek is unknown, but was estimated in Subsection 1.1.4 to be less then 1/15000 ($i < 6.67 \times 10^{-5}$). Therefore three inclinations are modelled; $i_a = 1 \times 10^{-5}$, $i_b = 3 \times 10^{-5}$ and $i_c = 5 \times 10^{-5}$. Manning's bed roughness coefficient (n) is a function of

the Chèzy bed friction coefficient (C in $m^{1/2}/s$) and the waterdepth (h); $n = h^{\frac{1}{6}}/C$ (Te Chow, 1959). The Nga Moe Yeik Creek is assumed to be hydraulically smooth because of the high amounts of mud in the system. Manning's n is therefore varied representing low hydraulic roughness values (n_1 = 0.010, n_2 = 0.012 and n_3 = 0.013 $s/m^{-1/3}$). Table 3.1 shows 9 model runs with different settings for the calibration process in for the hydrodynamic model in phase 1. Based on the calculated water levels from these model runs, the parameters of the run with the best fit to the observed water levels is chosen for the following phase.

Table 3.1: Model parameter settings calibration phase 1: Hydrodynamics

n \ i	$1 * 10^{-5}$	$3 * 10^{-5}$	$5 * 10^{-5}$
0.010	run 1a	run 1b	run 1c
0.012	run 2a	run 2b	run 2c
0.013	run 3a	run 3b	run 3c

3.3.3 Phase 2: Sediment transport

In the second phase of the model, sediment transport processes are also included. In the used approach, all sediment in the domain originates from the downstream boundary. Initially, no sediment is present in the model (starved bed conditions), only sediment entering the model domain through the downstream boundary condition becomes available for erosion and siltation. The upstream boundary condition is still closed (Q_{fl} = 0 $m^3 s^{-1}$). The downstream boundary is forced with a cohesive sediment load. Cohesive sediment particles do not have a constant settling velocity (due to the dynamic processes of flocculation and break up). It is common practise to use two fractions to model the behaviour of cohesive sediments; a bigger fraction representing flocculated sediment with a higher settling velocity and a smaller fraction representing poorly flocculated sediments (van Maren et al., 2015). Sir Alexander Gibb & Partners (1976) showed that typical sediment concentration values at the lower boundary vary between $0.3 - 5.0$ gL^{-1} in a complete seasonal cycle (Section 2.4). For a first approximation concentrations of 1.0 gL^{-1} per fraction, so 2 gL^{-1} in total is forced at the downstream boundary. This is considered a typical yearly averaged concentration. The time step is set to 15 seconds. The run time of the model is set to 2 years to make sure there is enough time for the sediment to deposit in the orders of meters. Two important parameters are the settling velocity (w_s) and the erosion parameter (M). Both are unknown, therefore a wide range in w_s and M are simulated. The bigger fraction ($w_{s1,a}$ = 1, $w_{s1,b}$ = 0.1 and $w_{s1,c}$ = 0.01 $mm s^{-1}$). The settling velocities of the smaller fraction are set at 2 percent of the bigger fraction ($w_{s2,a}$ = 0.2, $w_{s2,b}$ = 0.02 and $w_{s2,c}$ = 0.002 $mm s^{-1}$). The critical bed shear stress for erosion $\tau_{cr,e}$ determines the erosion flux in the model. If the bed shear stress is smaller than the critical value, no erosion takes place. If the bed shear stress is larger than the critical value, erosion is calculated following Partheniades-Krone (Formula 2.4). Typically the peak bed shear stress is 1-2 Pa (van Maren et al., 2015). Typical for non-consolidating to loosely consolidated clay are values in the range of 0.01 - 0.2 Pa (Van Maren & Winterwerp, 2013). As a first estimate the critical bed shear stress is set to $\tau_{cr,e}$ = 0.5 $kg m^{-1} s^{-2}$. This value represents weakly consolidated sediments which is reached during most tidal conditions. Three values for the erosion parameter are considered (M = 0.01, 0.001 and 0.0001 $kg m^{-2}$. Table 3.2 shows the 9 model runs with different settings in phase 2. After a qualitative analysis, based on Section 2.4.1, the best fitting sediment parameters for the final model are chosen.

Table 3.2: Model parameter settings in calibration phase 2: Sediment transport

M \ w_s	1 & 0.2	0.1 & 0.02	0.01 & 0.002
0.01	run 4a	run 4b	run 4c
0.001	run 5a	run 5b	run 5c
0.0001	run 6a	run 6b	run 6c

Chapter 4

Results

First the main field observations concerning water levels and sediment concentrations are discussed (Section 4.1). Next are the results of the model calibration (Section 4.2), which elaborates on the iterative bed level correction, model performance in terms of tidal constituents, a sensitivity analysis of the model parameters of the hydrodynamic model and a qualitative analysis of the sediment model.

4.1 Field observations

The following section elaborates on the fieldwork observations consisting of water level monitoring, a bathymetric survey and OBS profiling.

4.1.1 Water level monitoring

Raw Diver data

Figure 4.1 shows the pressure (in cmH_2O) and temperature (in °C) signal as measured by Diver 1 to 3 at the three stations at respectively 15, 30 and 45 km from the creek mouth. Unfortunately, the CTD Diver installed in the creek mouth was lost (together with its pressure and salinity data) one week after installation. Hereby, it appeared that the pressure sensor of Diver 3 failed on May 23 for an unknown reason. No usable pressure data was recorded hereafter with Diver 3 at the Nga Moe Yeik Sluice Gates. Between 9 and 30 May 2017, the remaining Divers and barometer measured the varying pressure and temperature.

Water levels

As explained in subsection 3.2.1 the measured pressure data of Diver 1 to 3 is converted in corresponding water levels, see Figure 4.2. The resulting water levels clearly show high and low waters twice a day and a tidal range in spring and neap tides in the order of respectively 6 and 4 meters. The observed low water levels at Diver 2 start to show an increasing trend in the order of 1.5 m from the 27th of May. An explanation for this phenomenon could be that the sensor slowly disappeared in the consolidating bottom. This specific Diver was hard to retrieve since it appeared to be covered in sediment. The consolidating soil could explain the occurring increase in measured pressure. The data of Diver 3 seems odd compared to the data of Diver 1 and 2. The observed water levels show a nearly constant value at various low water periods. This phenomenon can be explained by the presence of a shoal in the creek bed around 5 km downstream of the sluice which blocks ebbing water (Aung Kyaw Hmuu, Director DWIR, personal communication May 2017). The exact location of this shoal is unknown. On May 17, the measured signal loses its tidal character for several days. This observation can be explained by the coincidence of neap tide and the opening of the Nga Moe Yeik Sluice Gates. In this period the river discharge seems dominant over the incoming tide. The red line in Figure 4.2 shows a plot of a second data source. These water levels are observed at a location 100 meters downstream of the Nga Moe Yeik Sluice Gates every hour between between 06:00 and 21:00, using a measuring rod (U Toe Nyein, Assistant Director Construction 6 Irrigation Department Yangon, personal communication June 2017), see Figure A.2 and A.3 in Appendix A.2.1. This second data set shows the same trend and is a close match with the Diver 3 data. It confirms the estimated sensor depth with respect to MSL ($d_{b,MSL}$). The difference in low waters (between the two data sets) may be explained by a wider cross section 100 m downstream of the sluice.

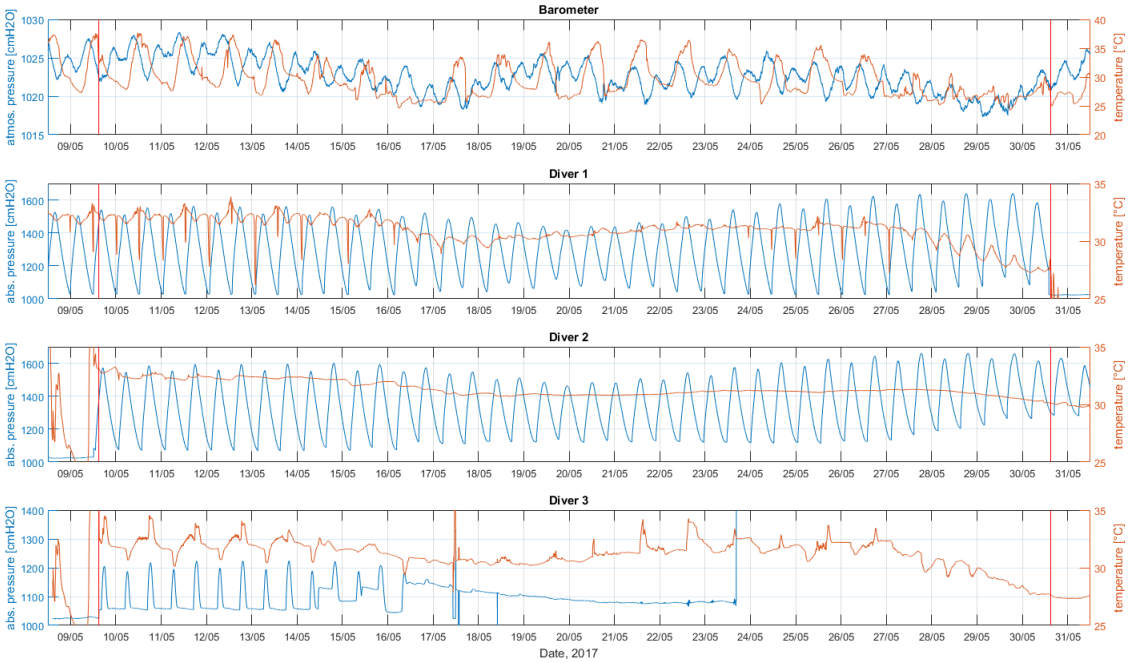

Figure 4.1: In blue: observed atmospheric pressure variations (Barometer) and absolute (= hydrostatic + atmospheric) pressure variations (Diver 1 to 3). In red observed temperatures. For sensor locations in the study area see Figure 3.2

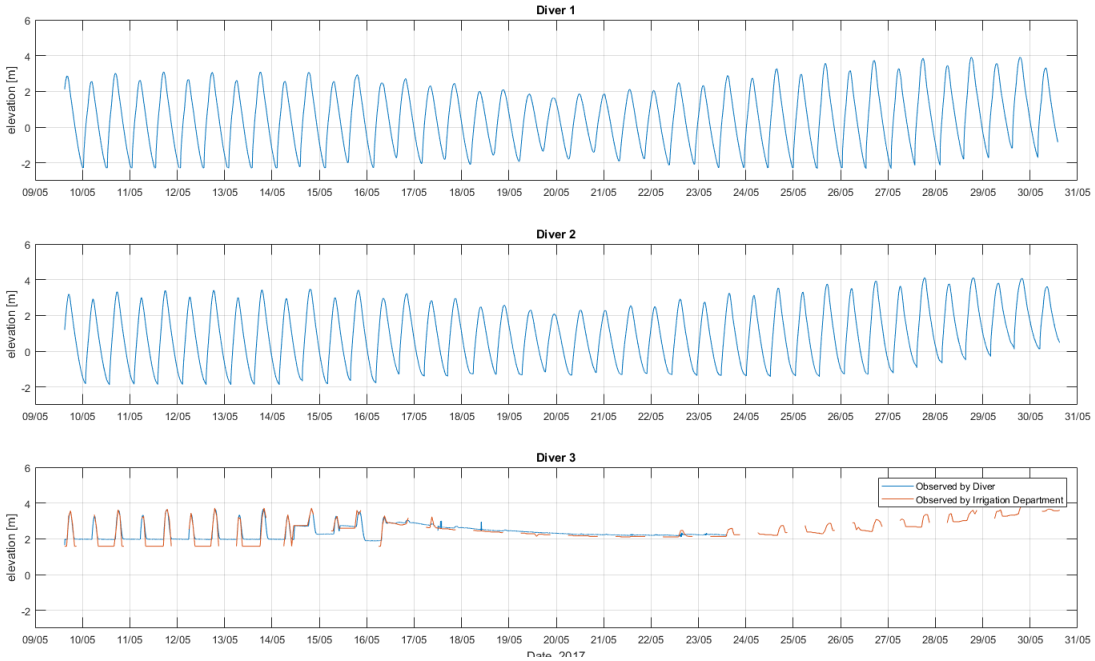

Figure 4.2: In blue: observed water level elevation (Diver 1 to 3). In red: the observed water level elevation near the Nga Moe Yeik Sluice Gates (source: Construction 6, Irrigation Department Yangon). For sensor locations in the study area see Figure. 3.2

Tidal asymmetry

The measured tidal wave shows a flood-dominant character; a short rising period followed by a relatively long falling period, see Figure 4.16a. Because the CTD diver is lost, no measured water level data is available in the mouth. In Section 3.3.2 it was discussed that harmonic constants as calculated from observations at Monkey Point are used to reproduce the tidal forcing at the lower boundary in the model. This reproduced tidal signal is used to replace the missing data in the mouth (see 'lower BC' in Figure 4.16a). Considering the three locations (lower BC = 0 km, Diver 1 = 15 km and Diver 2 = 30 km) a distortion of the propagating tidal wave is observed. The tidal wave develops an increasing asymmetry as it propagates into the Nga Moe Yeik Creek.

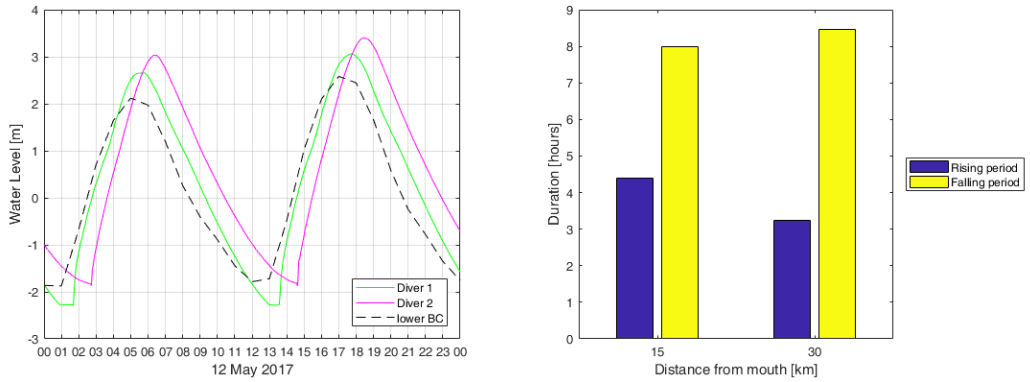

(a) Water levels on 12 May 2017

(b) Mean rising and falling periods

Figure 4.3: Observed flood-dominance

The duration of rising and falling tides are calculated based on differences in peaks and troughs of the water level observations. The periods change with location and time, see Appendix A.2.2. The longest falling period and shortest rising period are observed at 30 km from the mouth and are respectively 9.06 hours (during spring) and 2.74 hours (during neap). Figure 4.16b shows means of the measured rising and falling periods. At 15 km from the mouth, the mean rising and falling periods are respectively 4.4 hours and 7.9 hours, as calculated from Diver 1 measurements. At 30 km from the mouth, the mean rising period shortens to 3.2 hours, while the mean falling period increases to 8.4 hours. This indicates that the tidal wave becomes more flood-dominant while propagating into the creek.

4.1.2 Bathymetric survey

Observed depths

As discussed in Section 3.1.2 the whole stretch between the Pazundaung mouth and Nga Moe Yeik Sluice Gates is measured using an echo sounder. The results of the bathymetric survey give insight in the bed topography. In the mouth, a shallow area is observed with a bottom level between MSL + 0 m and MSL - 2.5 m. Depths between MSL - 7.5 and MSL - 15 m were observed in the next 15 km from the mouth. Typical depths in the middle part are MSL - 10 m to MSL -5 m. The upper 15 km of the Nga Moe Yeik Creek is relatively shallow with typical depths around MSL - 2.5 m. Figure 4.4a shows the zigzag trajectory of depth measurements in the lower part of the Nga Moe Yeik Creek. The deepest parts of the Nga Moe Yeik Creek are observed in the outer bends.

Bathymetry file

Together with the computational grid (Figure 3.5) the depth measurements are used to create the bathymetry file for the model. Triangular interpolation is best suited for data sets that is smaller than the grid resolution (Deltares, 2018). Using this interpolation method depth values in-between the depth measurements are calculated on the grid. Grid points that did not have depths values after the interpolation step, were given values based on internal diffusion. In this way empty cells are given depth values with a smooth transition

with existing values. The result of the bathymetry after these steps is given in Figure 4.4b. The thalweg, the line of lowest elevation, follows a path through every outer bend, as expected in a meandering channel.

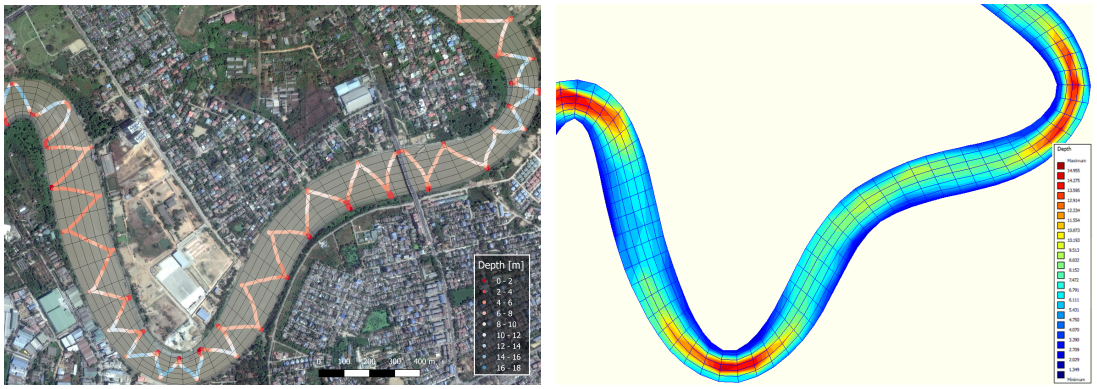

(a) Measured depths along the zigzag trajectory in the lower reach of the Nga Moe Yeik Creek

(b) Bathymetry as a result of triangular interpolated depth values and internal smoothing

Figure 4.4: Main steps in creating the bathymetry

4.1.3 OBS profiling and water sampling

Raw OBS data

The OBS-3A measures temperature, salinity and turbidity as discussed in Section 3.1.3. All results of the measurements of July 16 and 21 are shown in Appendix A.3. The profiles are taken in a complete tidal cycle during neap tide at respectively 2 and 17 km from the mouth. Temperatures varied between 27.2 °C and 27.7 °C. The highest temperatures are observed during rising tide and lowest temperatures during falling tide. The salinity profiles resulted in very low values (in the order of 0.05 PSU) indicating fresh water in all conducted measurements. The turbidity measurements show more variation over the tidal cycle. Figure 4.5 gives the main results of the OBS measurement for different phases in the tidal cycle. Single representative measurements during HW slack, falling tide, LW slack and rising tide are presented. In some measurements two distinct lines are visible. This is due to small differences in the turbidity between measurements taken while the sensor is ascending and descending.

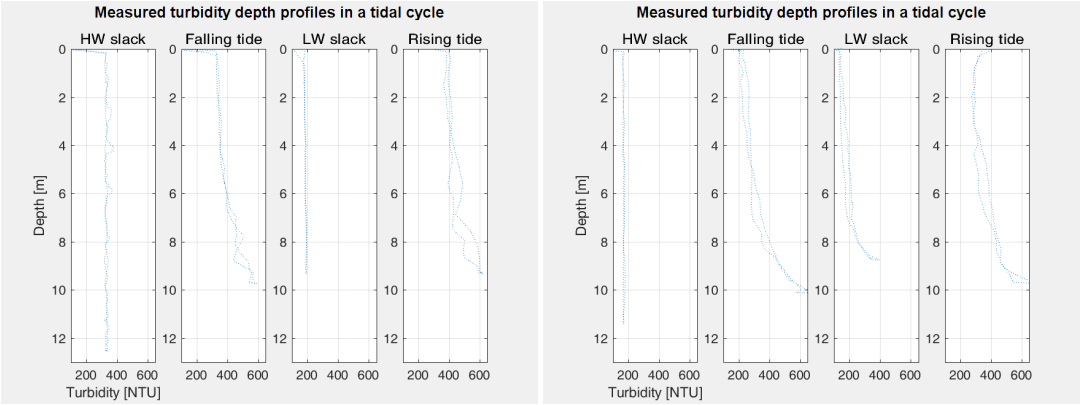

(a) Measured turbidity [NTU] profiles, 2 km from mouth

(b) Measured turbidity [NTU] profiles, 17 km from mouth

Figure 4.5: Measured turbidity profiles of sediment concentrations. The turbidity profiles were measured in the beginning of the Monsoon season, at 1.5 km from the mouth of the Pazundaung Creek.

Estimated sediment concentrations

As discussed in Section 3.1.3 a water sampler is used to find a relation between turbidity in NTU and concentration in gL^{-1}. Unfortunately, the water sampler broke after first use and only one sample could be taken

while measuring the corresponding turbidity. This sample was taken at 10 m depth with a corresponding turbidity value of 390 NTU. In the lab, a sediment concentration of 0.66 gL^{-1} was determined from the water sample. Based on this, a factor of 1.5×10^{-3} is applied, as a rough estimation, to relate the measured turbidity in NTU to gL^{-1}. Besides this, it was noted that the sediment concentration in the water sample remained well-mixed after a several hours, indicating the sample contained particles with a low settling velocity. Figure 4.6 shows the estimated concentrations from the turbidity measurements which vary between 0.3 gL^{-1} and 1.0 gL^{-1}. The estimated sediment concentrations match observations from Sir Alexander Gibb & Partners (1976) during neap tide in the Monsoon period.

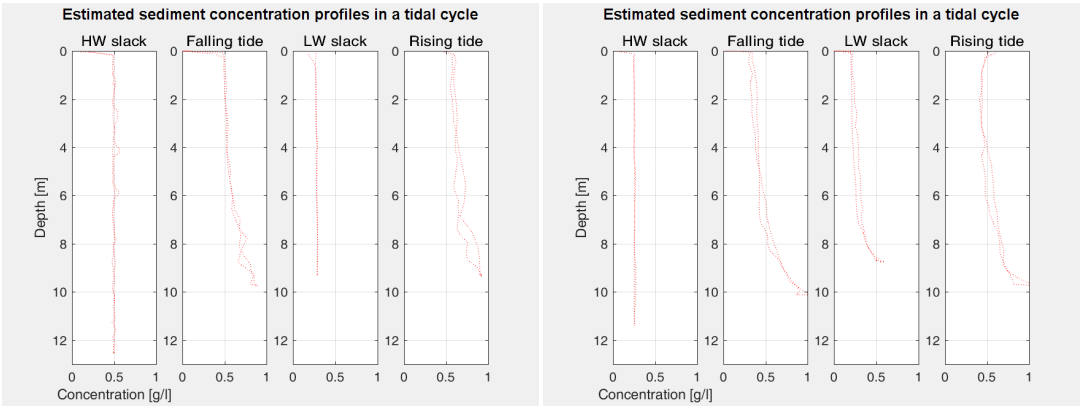

(a) Estimated sediment concentration profiles, 2 km from mouth

(b) Estimated sediment concentration profiles, 17 km from mouth

Figure 4.6: Estimated sediment concentrations based on the turbidity profiles measured during the Monsoon season, at 1.5 km from the mouth of the Pazundaung Creek. A factor of 1.5×10^{-3} is applied to relate the measured turbidity in NTU to gL^{-1})

For both locations, the measurements show a background concentration, which is well-mixed over depth and visible in all measurement during the complete tidal cycle. During rising and falling tides, an additional near-bed concentration is observed. The measured profiles resemble typical Rouse profiles. Because the sediment concentration is well-mixed over the vertical, it is assumed that a 2DH model can generate reliable results. Further analyses is done with depth averaged values, which can be found in Table 4.1.

Table 4.1: Measured depth averaged concentrations [gL^{-1}] of different tidal phases and their mean at two distances from the mouth.

	2 km	17 km
HW slack	0.49	0.25
Falling tide	0.61	0.52
LW slack	0.28	0.40
Rising tide	0.69	0.57
Tidally averaged	0.52	0.44

Both locations show highest sediment concentrations for rising tide, followed by a small decrease during HW slack period. During falling tide, concentrations are increased again, followed by a drop in concentration during LW slack. This drop in concentration during LW slack could indicate that sediment particles are deposited on the bed. Although measured profiles at both locations give similar results, there are some differences. LW slack concentrations at 17 km do not show a well-mixed depth profile as is observed at 2 km. In the field, measurements were conducted roughly every 15 min. The local tidal water level variation was not known and is based on local observations. It is therefore uncertain if the moment of measurement is exactly at moment of flow reversal (LW slack). The depth averaged concentration of 0.4 gL^{-1} in Table 4.1 is therefore believed to be an overestimation for LW slack concentration. Based on concentrations higher in the water column, it should be in the order of 0.25 gL^{-1}. Considering this, it can be noticed that during all phases of the tidal cycle, highest concentrations are observed near the mouth. This can also be seen from the tidally averaged concentrations.

4.2 Model calibration

4.2.1 Introduction

In an iterative process different model simulations with varying settings (such as bathymetries, inclinations, bottom roughness, erosion parameters and settling velocities) have been analysed to find the best set of parameters for the model. Only the main results from this process are discussed. The most appropriate set of parameters, m = 0.013 together with $i_c = 5 \times 10^{-5}$ are used in Section 4.2.2 describing the bed level iteration, and Section 4.2.3 describing the model performance in terms of tidal constituents. Subsequently, the uncertainties in inclination and bottom roughness (discussed in Section 3.3.2) are assessed with a sensitivity analysis in Section 4.2.4. Finally, the uncertainties of the model parameters for erosion and settling (discussed in Section 3.3.3) velocities are assessed in a qualitative analysis in Section 4.2.5.

4.2.2 Bathymetry

Figure 4.7 shows the result for the depth correction as discussed in Section 3.2.2. The depth and water level data is plotted against the number of measurement points. The observed depth (d_{obs}) shows a strongly fluctuating signal. This is due to the differing depth values per diagonal from the zig-zag trajectory of the survey boat, see Figure 4.4a. The time and place-corresponding water levels (ζ_{calc}) are calculated with the model. Using these water levels the offset is iteratively corrected (see Figure 3.4) to relate the bottom level ($d_{b,MSL}$) to a horizontal reference datum. It appeared that no more than two iteration steps were needed as the calculated water levels converged (not shown here). The corrected depth is used to recreate the bathymetry for the model. The thalweg of this bathymetry is plotted in Figure 4.8. Note that around n=240 a sudden bed level change occurs, which is believed to be an unavoidable artefact from the data processing.

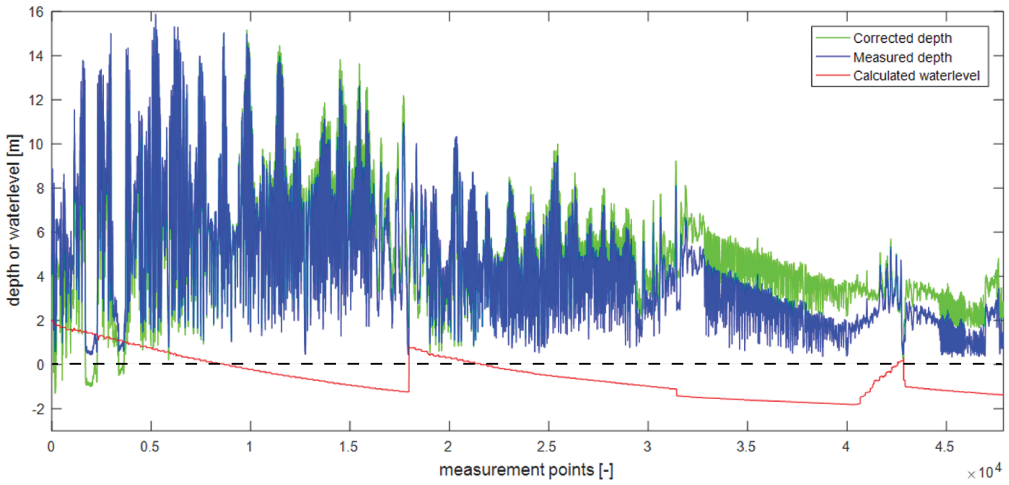

Figure 4.7: Depth correction after two iterations. The observed depth (d_{obs} in blue), the corresponding calculated water level (ζ_{calc} in red) and the corrected depth ($d_{b,MSL}$ in green). The strongly fluctuating signal is due to the zig-zag trajectory while constantly crossing the thalweg

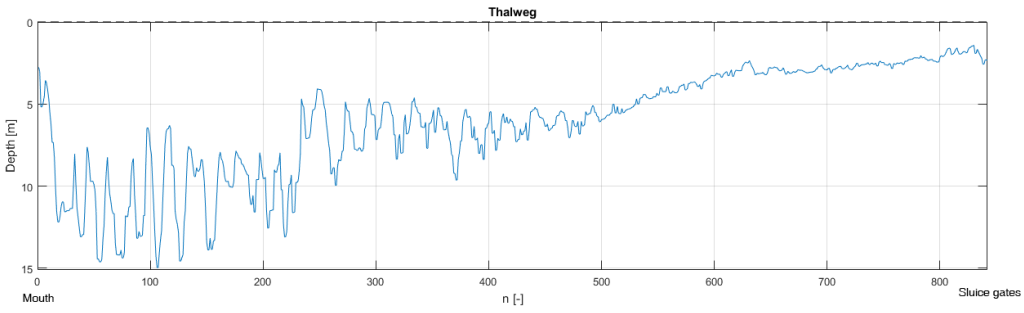

Figure 4.8: Bed levels in the thalweg from the bathymetry.

4.2.3 Tidal constituents

Decomposition of the tidal harmonics gives insight in the observed tidal asymmetry. Depending on the relative phase relationships between M4 and M2 ($2\phi_{m2} - \phi_{m4}$), tidal channel will show flood- or ebb-dominance. For each diver location, respectively 15, 30 and 45 km upstream from the mouth, the measured and calculated water levels are decomposed into the main harmonic constituents using a classical tidal harmonic analysis (T-tide, Pawlowicz et al. (2002)). It appeared that no clear tidal signal could be extracted from the data of Diver 3. The decomposition of the measured water levels from this data gave unreliable results because of the odd data (as discussed in Subsection 4.1.1). Therefore, only the results of the tidal harmonic analysis of Diver 1 and 2 are considered, see Figure 4.9. The measured water level data from Diver 3 is only used to compare with the calculated water levels for calibration.

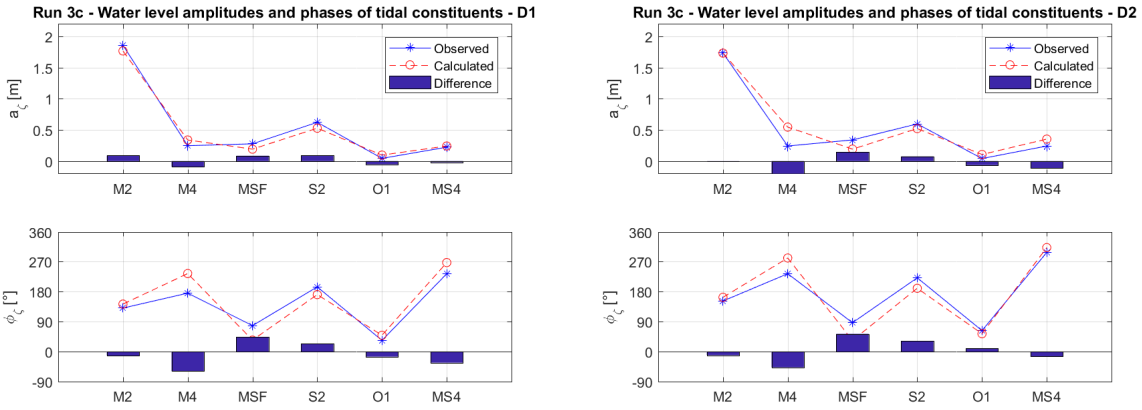

(a) Diver 1 location (15 km upstream from creek mouth)

(b) Diver 2 location (30 km upstream from creek mouth)

Figure 4.9: Calculated (blue) and observed (red) water level amplitudes and phases of tidal constituents at the Diver 1 and 2 locations, as well as the difference between calculated and observed. Calculated using a the parameters in Run 3c, see Table. 3.1

The computed amplitudes of all considered constituents at the location of Diver 1 are within 10 cm of observed amplitudes. At the location of Diver 2 the difference between calculated and observed amplitudes increases. In all the runs the model overestimates the phase of M4 with at least 45°. The phase relationship between M4 and M2 ($2\phi_{m2} - \phi_{m4}$) at the two Diver locations are respectively 90° and 89° for the observed phases, indicating a max flood flow asymmetry, with a longer falling than rising period. The phase relation of the calculated phases give values of respectively 45° and 42°, indicating a less pronounced max flood flow asymmetry. This difference between observed and calculated phase differences could result in underestimation of the modelled residual transport in the flood direction. However, the calculated phase difference still suggests a flood-dominant system.

4.2.4 Sensitivity analysis

The model set-up in the first phase is discussed in Section 3.3.2. Figure 4.10 shows the results of the simulations with varying inclinations ($i_a = 1 \times 10^{-5}$(red), $i_b = 3 \times 10^{-5}$ (green) and $i_c = 5 \times 10^{-5}$ (blue)) using a Manning coefficient of 0.010 (Figure 5.1a), 0.012 (Figure 5.1b) and 0.013 (Figure 5.1c). The solid and dashed lines represent calculated water level phases (upper figure) and amplitudes (lower figure) of respectively M2 and M4 constituents. Corresponding observations of water level phases (upper figure) and amplitudes (lower figure) M2 (squares) and M4 (diamonds) are computed from the Diver 1 and 2 measurements. Figure 4.10d gives an overview of the all results and their differences.

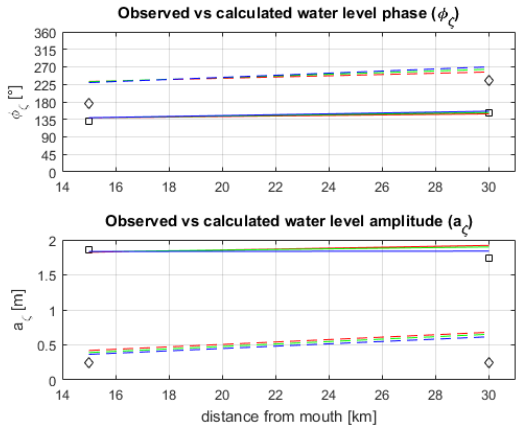

(a) Run 1a to 1c (with varying inclinations). Calculated with Manning's coefficient of 0.010

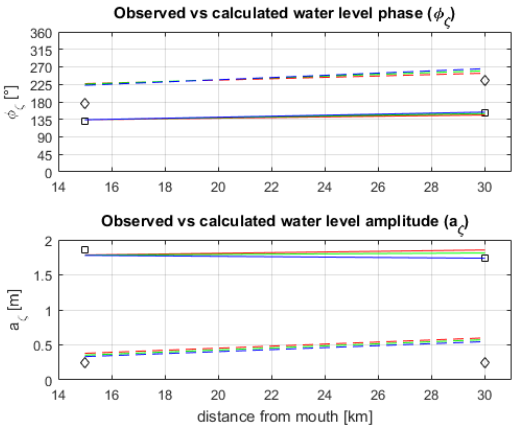

(b) Run 2a to 2c (with varying inclinations). Calculated with Manning's coefficient of 0.012

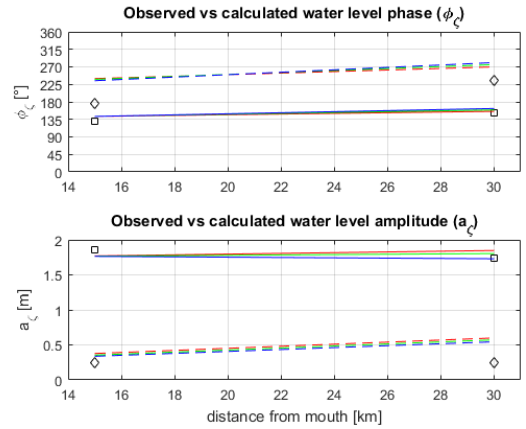

(c) Run 3a to 3c (with varying inclinations). Calculated with Manning's coefficient of 0.013

	Amplitude [m]			Phase [°]		
M2	D1 (15 km)	D2 (30 km)	D1-D2	D1 (15 km)	D2 (30 km)	D1-D2
obs	*1.86*	*1.73*	*-0.12*	*130.65*	*151.90*	*21.25*
1a	1.82	1.92	0.10	138.87	149.22	10.35
1b	1.83	1.90	0.07	139.21	152.43	13.22
1c	1.83	1.84	0.01	139.31	155.96	16.65
2a	1.78	1.86	0.07	133.95	146.34	12.38
2b	1.78	1.81	0.03	134.19	149.91	15.72
2c	1.78	1.74	-0.04	134.09	153.65	19.57
3a	1.77	1.85	0.08	142.61	155.65	13.05
3b	1.77	1.80	0.04	142.80	159.21	16.41
3c	1.76	1.73	-0.03	142.64	162.94	20.30

M4	D1 (15 km)	D2 (30 km)	D1-D2	D1 (15 km)	D2 (30 km)	D1-D2
obs	*0.25*	*0.24*	*0.01*	*175.48*	*233.82*	*58.34*
1a	0.42	0.68	0.26	232.53	256.85	24.33
1b	0.39	0.65	0.26	231.73	263.73	32.00
1c	0.37	0.62	0.25	229.57	270.00	40.44
2a	0.38	0.60	0.22	227.01	253.75	26.73
2b	0.35	0.57	0.22	225.69	259.93	34.24
2c	0.33	0.55	0.21	222.71	265.40	42.69
3a	0.38	0.60	0.22	239.90	269.95	30.05
3b	0.35	0.57	0.22	237.91	275.81	37.90
3c	0.34	0.54	0.21	234.39	281.09	46.69

(d) Overview of all results (run 1a-3c) and differences between locations (Diver 1 and Diver 2).

Figure 4.10: Observed water level phase θ_ζ (upper figure) and amplitude a_ζ (lower figure) of M2 (squares) and M4 (diamonds) and calculated M2 (solid lines) and M4 (dashed lines) water level phases (upper figure) and amplitudes (lower figure) using $i_a = 1 \times 10^{-5}$ (red), $i_b = 3 \times 10^{-5}$ (green) and $i_c = 5 \times 10^{-5}$ (blue).

The computed water levels only vary marginally with roughness and inclination within the parameter space experimented with. At first glance the results from the sensitivity analysis hardly differ. Apparently, the used set of parameters do not give a clear preference for a specific Manning's coefficient and inclination as the differences between the runs are in the order of 0.01 m and 10 °. In the scope of this work such small differences are considered insignificant. However, based on the difference between the observed amplitudes and phases in Figure 4.10d, it can be seen that inclination $i_c = 5 \times 10^{-5}$ in combination with Manning's coefficient of m = 0.012 or 0.013 show slightly better results. Run 2c and 3c show a decrease in amplitude for M2 as was observed by Diver 1 and 2. The observed increase in the phase of M2 is best estimated by $i_c = 5 \times 10^{-5}$ and Manning's coefficient m = 0.013 in run 3c. Although the amplitude of M4 is overestimated in the order of 0.2 m and its phase is underestimated within the order of 30 °, run 3c predicts the observed amplitude and phase the best. It is therefore assumed that a Manning's coefficient m = 0.013 together with $i_c = 5 \times 10^{-5}$ are reasonable parameters for the model.

4.2.5 Sediment transport model

The model set-up in the second phase is discussed in Section 3.3.3. Figures 4.11 to 4.13 summarize the results of the simulations with varying erosion parameter (M) and settling velocity (w_s) for two sediment fractions, as given in Table 4.2, repeated here for convenience. For all simulations, the location of the thalweg (deepest point of cross-section) is determined on the start time of the simulation (t0). At the end of the simulation (t1) the difference in bed level is compared to initial bed level in the thalweg and plotted as siltation. Figures 4.11

to 4.13 show bed profiles over the creek stretch between mouth (left) and sluice (right) and their difference. As discussed before, using a qualitative analysis, the best parameters are chosen for the final model. Based on field observations and personal communication with local authorities, an important characteristic of the model is that there should be a significant bed level change in the orders of meters in primarily the upper part of the thalweg near the sluice.

Table 4.2: Model parameter settings in calibration phase 2: Sediment transport.

M \ w_s	1 & 0.2	0.1 & 0.02	0.01 & 0.002
0.01	run 4a	run 4b	run 4c
0.001	run 5a	run 5b	run 5c
0.0001	run 6a	run 6b	run 6c

The 9 model simulations differ in sediment mobility. Very low settling velocities (w_s = 0.01 & 0.002 mm s^{-1}) result in little or no deposition in run 4c, 5c and 6c. High settling velocities (w_s = 1 & 0.2 mm s^{-1}) lead to intermediate siltation near the sluice in run 4a (M = 0.01 kg m^{-2} s), excessive siltation in the whole thalweg in run 5a (M = 0.001 kg m^{-2} s) and excessive siltation in the mouth in run 6a (M = 0.0001 kg m^{-2} s). Intermediate settling velocities (w_s = 0.1 & 0.02 mm s^{-1}) lead to excess sedimentation of the mouth and little sedimentation in the upper end of the thalweg for a low erosion parameter in run 6b (M = 0.0001 kg m^{-2} s), whereas run 4a and 5b primarily deposit at the upstream end. The observation that both simulations show similar results is logical. The erosion parameter and settling velocity are in balance in 4a and 5b (between 4a and 5b both the erosion parameter and settling velocity are decreased with a factor 10). This should also hold for 6c, but apparently these fractions used in this simulation are easily kept in suspension. Some siltation occurs for run 5b throughout the thalweg. Compared with 4a, more siltation occurs in a larger stretch in the upper domain. Besides, the intermediate settling velocities of 0.1 and 0.02 mm s^{-1} are assumed to be more reliable. Therefore, the settings used in run 5b are chosen to further investigate the effect of the flush scenarios (Section 5.3) on the distribution of siltation.

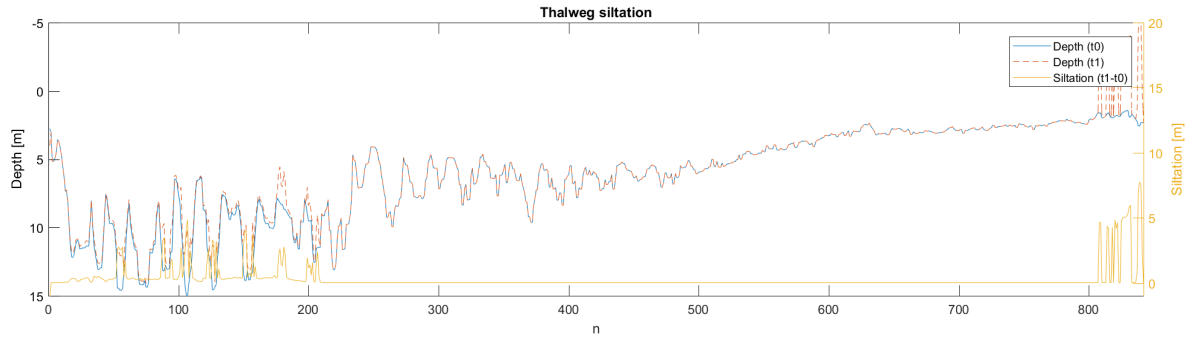

(a) Run 4a, $M = 0.01\ \mathrm{kg\,m^{-2}\,s}$, $w_s = 1\ \mathrm{mm\,s^{-1}}$

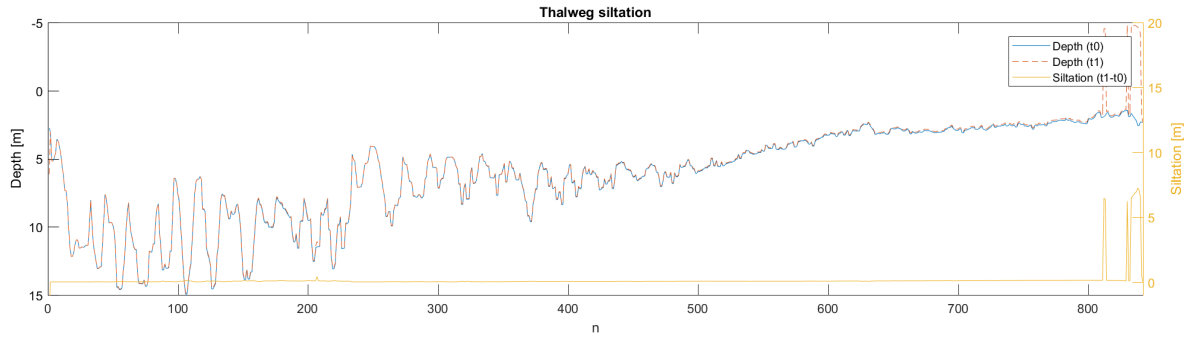

(b) Run 4b, $M = 0.01\ \mathrm{kg\,m^{-2}\,s}$, $w_s = 0.1\ \mathrm{mm\,s^{-1}}$

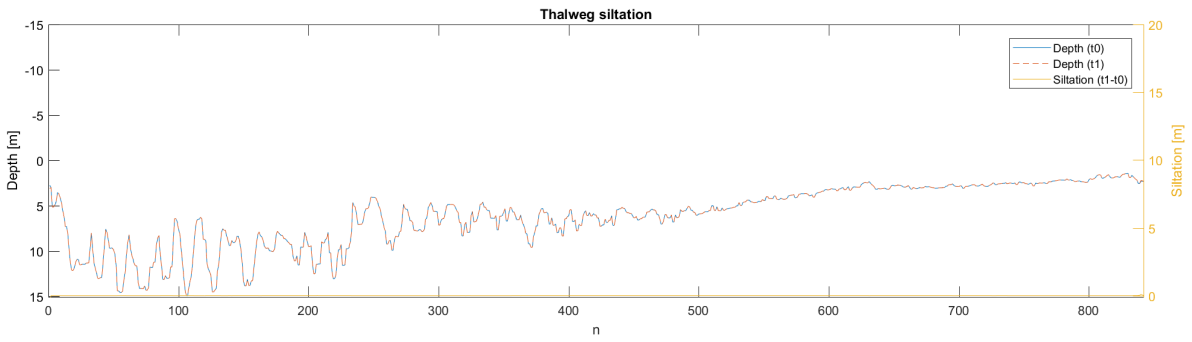

(c) Run 4c, $M = 0.01\ \mathrm{kg\,m^{-2}\,s}$, $w_s = 0.01\ \mathrm{mm\,s^{-1}}$

Figure 4.11: Results runs 4a-c, bottom depth (t0 and t1) and siltation (t1-t0) in the thalweg.

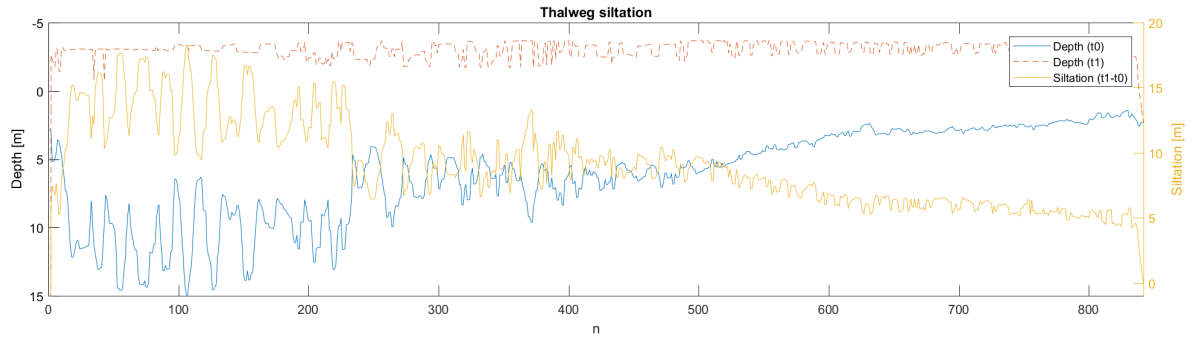

(a) Run 5a, $M = 0.001\ \mathrm{kg\,m^{-2}\,s}$, $w_s = 1\ \mathrm{mm\,s^{-1}}$

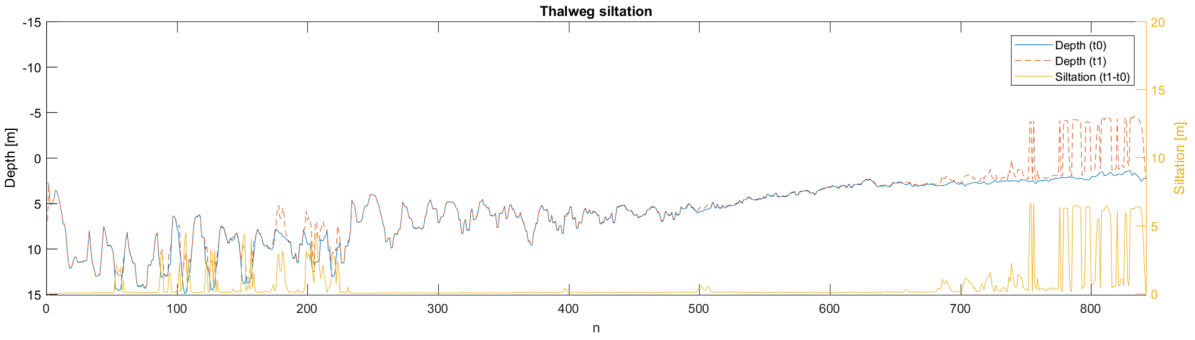

(b) Run 5b, $M = 0.001\ \mathrm{kg\,m^{-2}\,s}$, $w_s = 0.1\ \mathrm{mm\,s^{-1}}$

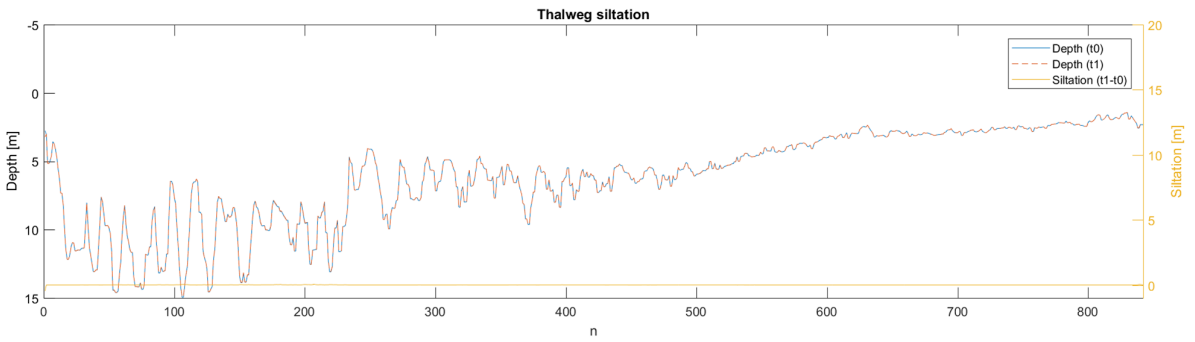

(c) Run 5c, $M = 0.001\ \mathrm{kg\,m^{-2}\,s}$, $w_s = 0.01\ \mathrm{mm\,s^{-1}}$

Figure 4.12: Results runs 5a-c, bottom depth (t0 and t1) and siltation (t1-t0) in the thalweg.

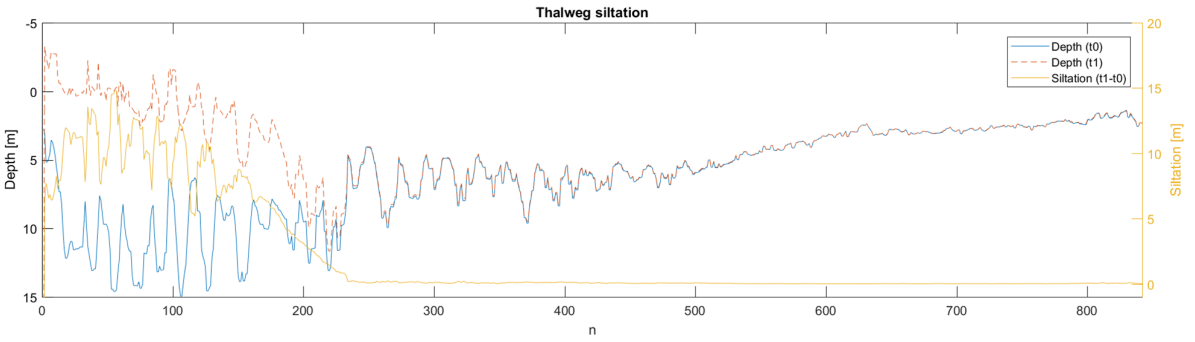

(a) Run 6a, $M = 0.0001\ \mathrm{kg\,m^{-2}\,s}$, $w_s = 1\ \mathrm{mm\,s^{-1}}$

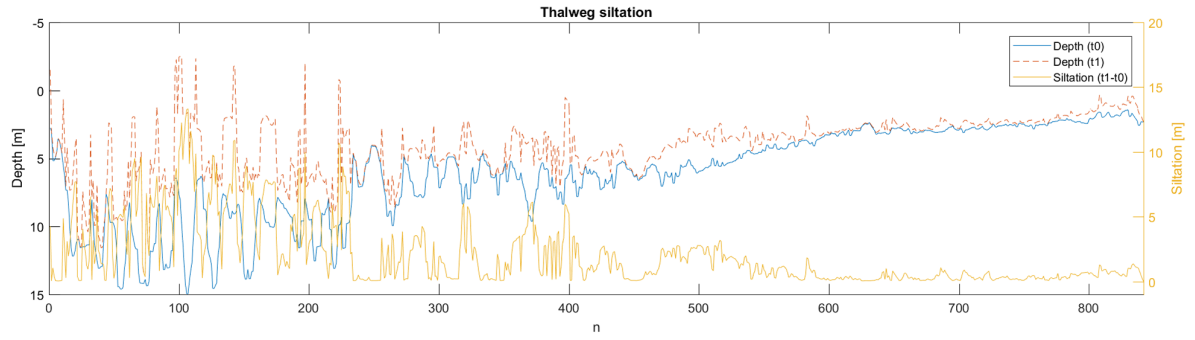

(b) Run 6b, $M = 0.0001\ \mathrm{kg\,m^{-2}\,s}$, $w_s = 0.1\ \mathrm{mm\,s^{-1}}$

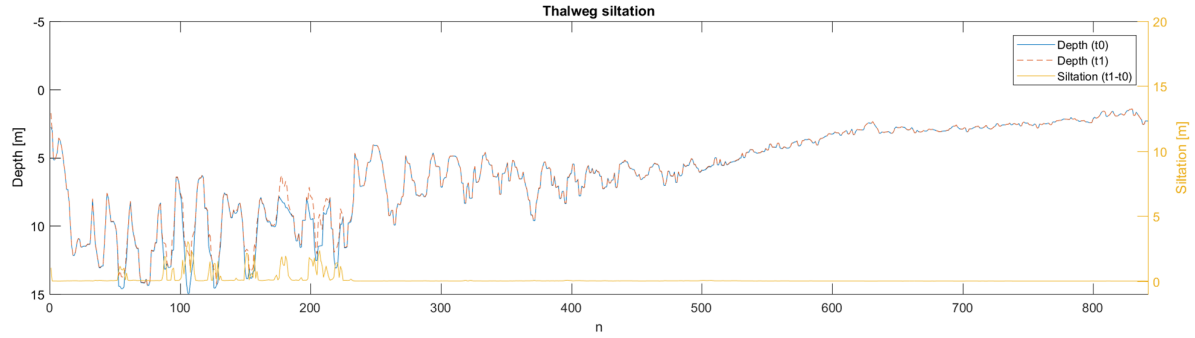

(c) Run 6c, $M = 0.0001\ \mathrm{kg\,m^{-2}\,s}$, $w_s = 0.01\ \mathrm{mm\,s^{-1}}$

Figure 4.13: Results runs 6a-c, bottom depth (t0 and t1) and siltation (t1-t0) in the thalweg.

4.3 Model results

This section elaborates on model results as calculated with the best parameters as found in the model calibration. As hydrodynamic processes, calculated water levels and velocities are assessed. First, the calculated water levels are compared with observations and the asymmetry of the calculated tidal wave is discussed. Then depth averaged velocities, calculated at two mid-domain locations, are assessed. Finally, changes in bottom depths as a result of sediment transport processes are discussed and presented in a rectilinear grid.

4.3.1 Hydrodynamics

Water levels

Figure 4.14 shows the observed and calculated water levels, for the locations of Diver 1 to 3, as calculated using inclination $i_c = 5 \times 10^{-5}$ and Manning's $m = 0.013$. There is a small offset in the calculated values which is larger during spring than neap tides. The water level at Diver 3 is especially hard to predict due to the potential shoal, which blocks ebbing water as discussed before in Section 4.1. The calculated high water matches reasonably with the observed in the first 7 days.

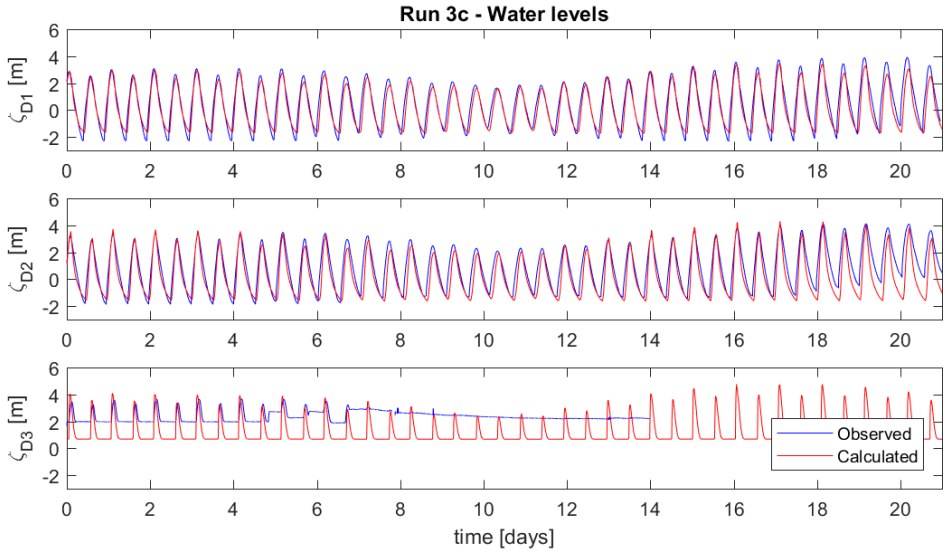

Figure 4.14: Observed vs calculated water levels (using inclination $i_c = 5 \times 10^{-5}$ and Manning's $m = 0.013$)

Tidal asymmetry

The calculated tidal wave shows a distorted signal as it propagates through the domain. The tidal asymmetry has a flood-dominant characteristic (a short rising period followed by a longer falling period), see Figure 4.15a. The tidal wave develops an increasing asymmetry as it propagates into the domain. The duration of rising and falling tides are calculated based on differences in peaks and troughs of the calculated water levels. The longest falling period and the shortest rising period are observed at 30 km from the mouth and are respectively 10 and 3 hours. Figure 4.15b shows the means of the calculated rising and falling periods. At 0 km, mean rising and falling periods are respectively 4.9 and 7.4 hours. At 15 km, the mean rising and falling tides are respectively 4.5 hours and 7.9 hours. And at 30 km, the means are respectively 3.6 and 8.6 hours. This indicates that the calculated tidal wave becomes more flood-dominant as it propagates into the creek.

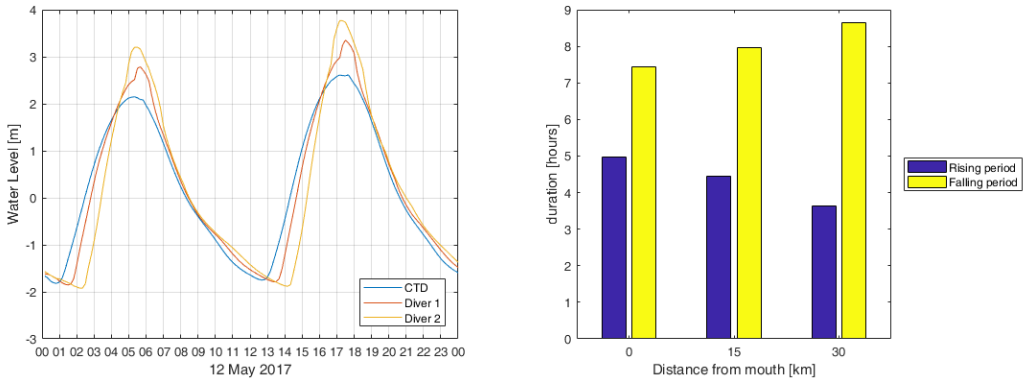

(a) Water levels on 12 May 2017

(b) Mean rising and falling periods

Figure 4.15: Calculated flood-dominance

Velocities

The velocity time series at all 4 observation points for a complete month is discussed in Appendix C.2. Figure 4.16 shows calculated velocities plotted together with water levels at the two mid-domain observation points (15 and 30 km) on 12 May 2017. Positive values for the velocities correspond to flood directed velocities and negative values correspond to ebb directed velocities. The peak flood velocities are larger than the peak ebb velocity, which is referred to as peak flow asymmetry. At 15 km, the maximum flood velocity is in the order of 2 times the maximum ebb velocity. At 30 km, the maximum flood velocity is in the order of 3 times the maximum ebb velocity. This indicates that the effect of the tidal asymmetry on velocity is more pronounced in landward direction. Unfortunately, there are no measurements in the Nga Moe Yeik Creek available for a validation of this phenomenon.

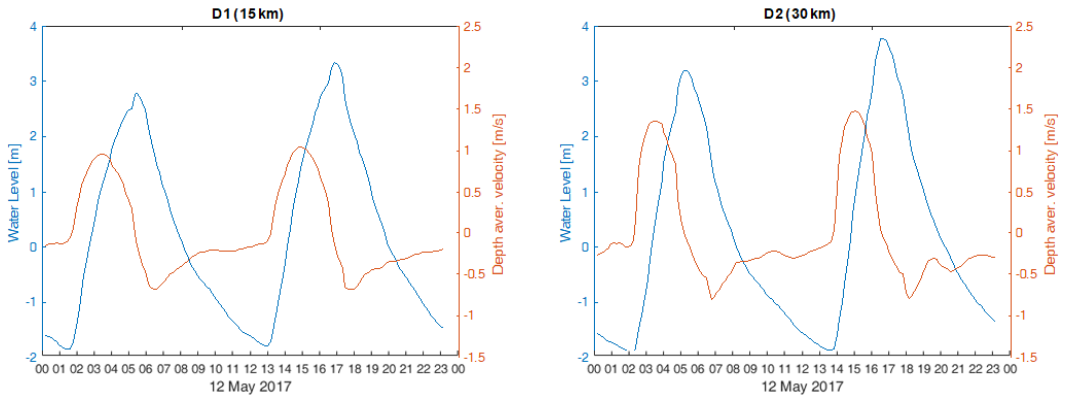

(a) 15 km from mouth

(b) 30 km from mouth

Figure 4.16: Calculated water levels and depth averaged velocities on 12 May 2017

4.3.2 Sediment transport

Similar to the results in Figures 4.11 to 4.13, Figure 4.17 gives the results of run 5b with erosion parameter M = 0.001 kg m^{-2} s and settling velocities w_s = 0.1 and 0.02 mm s^{-1}. The bottom depth at the beginning (t=t0) and end of the simulation (t=t1) are presented in a rectilinear grid, showing the spatial distribution of siltation throughout the domain. It can be seen that most siltation (t1-t0) occurs near the banks in the upper part of the domain. Which matches the observed mud deposits depicted in Figure 2.4.

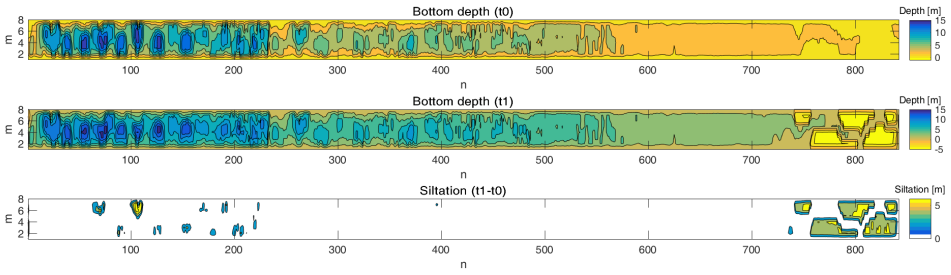

Figure 4.17: Spatial distribution of siltation throughout the domain in run 5b. Contour plots of the bottom depth (t0 and t1) and siltation (t1-t0) in a rectilinear grid.

4.4 Synthesis

Both the model and field data showed similar physical processes, they are compared and combined to increase insight in the main processes that influence the siltation in the Nga Moe Yeik Creek. Hydrodynamic and sediment transport processes are discussed below.

4.4.1 Hydrodynamic processes

The assessed hydrodynamic processes are water level variations (observed and calculated) and corresponding velocities (only calculated). The general shape of the tidal wave matches in both results, see Figure 4.18. The observed and calculated water levels show a flood-dominant tidal asymmetry and a tidal range in the order of 5 m.

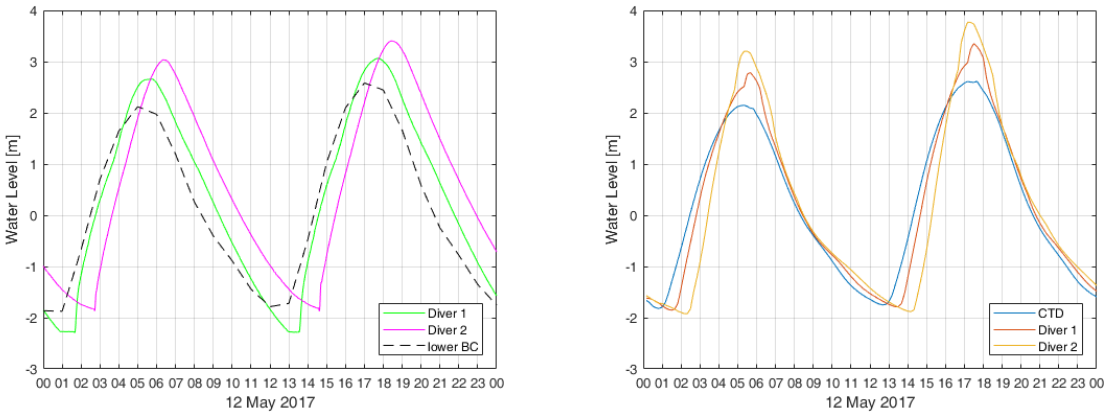

(a) Observed water levels for Diver 1 and 2 on May 2017

(b) Calculated water levels for CTD, Diver 1 and 2

Figure 4.18: Observed and calculated tidal asymmetry

The water level observations in Section 4.1.1 showed that the tidal wave distorts asymmetrically and becomes more flood-dominant as it propagates into the creek. The rising tide shortens and the falling tide enlarges. A similar behaviour is discussed in Section 4.3.1. This phenomenon is also visible in Table 4.3, where the mean rising and falling tides of both observed and calculated are compared.

Table 4.3: Mean rising and falling tides (in hours) as observed and calculated at several locations along the creek

	Observed		Calculated	
	Rising tide	Falling tide	Rising tide	Falling tide
0 km	-	-	4.9	7.4
15 km	4.4	7.9	4.5	7.9
30 km	3.2	8.4	3.6	8.6

It is assumed that the total displaced water volume during flood is equal to the displaced water volume during ebb (with closed sluice gates). Horizontal and vertical tides are related, therefore it is expected that the tidal velocities also become more asymmetric as the tidal wave propagates. In Figure 4.16 a higher flood peak velocity is calculated at 30 km than at 15 km distance from the mouth.

4.4.2 Sediment transport processes

In Section 4.1.3 depth and tidally averaged concentrations are discussed as found from the OBS measurements in a tidal cycle during neap tide. Between model and observations, a phase difference of sediment concentrations within the tidal cycle does exist. However, in the scope of this work it is considered negligible and concentrations are tidally averaged. At 2 and 17 km averaged concentrations of respectively 0.52 and 0.44 are observed gL^{-1} (see Table 4.1). It appeared that the OBS field observation at 2 km from the mouth is too close to the downstream boundary of the model to compare results at the same location in the domain. The constantly forced 2 gL^{-1} at this boundary does not result in physical behaviour in close proximity of the boundary. Therefore, the measurements are compared with depth and tidally averaged concentrations obtained from the inner 2 stations in the model domain. At 15 and 30 km the averaged concentrations are respectively 0.75 and 0.60 gL^{-1}. These concentrations (computed with the constant forcing of 2 gL^{-1}) are in the same order of magnitude as observed in the field. Highest concentrations occur near the mouth similar to the field measurements.

In the previous section, it was discussed that both model and measurements show a similar tidal asymmetry. The peak flood velocity is larger than the peak ebb velocity. Since there is a non-linear relation between sediment transport and velocities, this flood-dominant asymmetry results in a residual inflow of sediment. A small change in velocity leads to a large change in sediment transport. Transport of cohesive sediment is related to U^3. Due to the increased asymmetry further into the creek more siltation is expected here. The siltation results of the model are shown in Figure 4.19. This figure shows the width averaged siltation after a model period of 2 years (without river discharge). It can be noted that most siltation is located at the upper part of the domain. Between 30 and 45 km, 75% of the siltation occurs. As discussed in Section 2.4.3 most severe siltation is observed in the 15 km stretch downstream of the sluice. Significant mud deposits are also visible in a picture taken from the sluice, see Figure 2.4. So, a similar siltation pattern in the Nga Moe Yeik is found in the model results and in field observations. Furthermore, this siltation pattern is in line with the expected siltation based on the peak flow asymmetry.

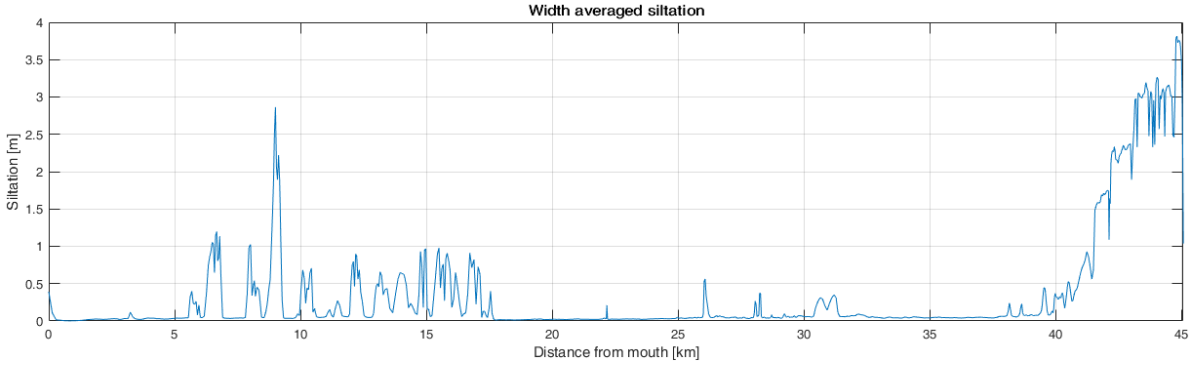

Figure 4.19: Model results of siltation in creek

4.4.3 Main processes

The main process that influences the siltation of the creek is the asymmetry of the tidal wave. The tidal range is in the order of 4-6 meters. The asymmetry in the water level is related to the velocity and therewith the sediment transport. The transported sediment accumulates in front of the sluice. An overview of the conceptual main processes is captured in Figure 4.20. The flood-dominant water level asymmetry shows similar patterns in the model and in the measurements. Calculated velocities in the mid-domain correspond to the observed flood- dominant asymmetry. A higher maximum flood velocity was calculated at 30 km compared to 15 km

from the mouth. The calculated siltation rates near the sluice points towards the observations (based on personal communication with local authorities). In the scope of this work it is therefore assumed that the model gives reliable results on the assessment of water level and siltation.

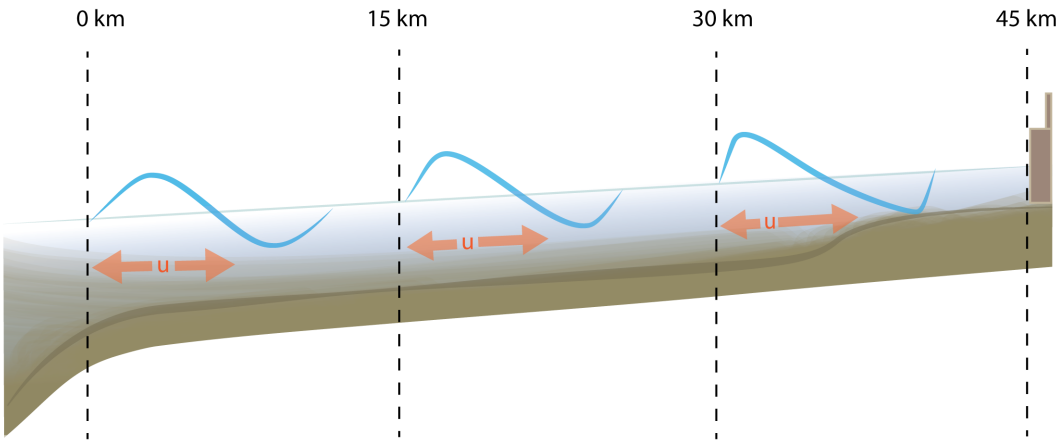

Figure 4.20: Conceptual main processes that influence siltation in the Nga Moe Yeik Creek

Chapter 5

Flushing

5.1 Current situation

In the current situation the Nga Moe Yeik Sluice Gates are opened during the Monsoon season, roughly between 15th of May and 15th of November (U Toe Nyein, Construction 6 Assistant Director, personal communication May 2017). Opening or closing the sluice, which consists of 27 gates, is labour-intensive. A movable engine on a platform directly above the sluice gates lifts the gates one by one after they are manually connected. As a first estimate, the whole process of opening or closing all the sluice gates takes 6 hours approximately.

5.2 Approach flush scenarios

With hydrodynamic and sediment parameters found in Sections 4.2.4 and 4.2.5, 3 flush scenarios (see Figure 5.1) are simulated for a period of 2 years and compared to explore the effects on siltation rates. Potentially, the current operation scheme (continuously flushing between 15 May and 15 November) can be improved. In all flush scenarios a continuous or pulsating discharge is forced at the upstream boundary of the computational domain to simulate the increased discharge during the wet season. There is a limited volume of water to flush with. Per scenario the discharges vary but the total flush volume does not change between scenarios.

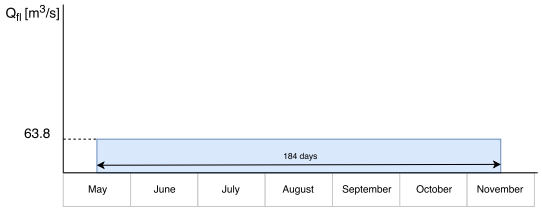

(a) Scenario 0, continuously flushing ($Q_{fl,0} = 63.8$ $m^3\,s^{-1}$))

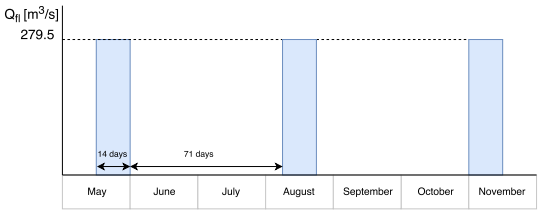

(b) Scenario 1, pulsatile flushing ($Q_{fl,1} = 279.5$ $m^3\,s^{-1}$)

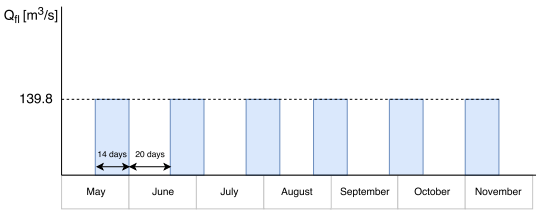

(c) Scenario 2, pulsatile flushing ($Q_{fl,2} = 139.8$ $m^3\,s^{-1}$))

Figure 5.1: Flush scenarios

The first scenario (Scenario 0) acts as a reference scenario. It is based on the current operating scheme of the Nga Moe Yeik Sluice Gates, where the gates are opened roughly every 15th of May and closed every 15th of

November depending on the weather forecast (U Toe Nyein, Construction 6 Assistant Director, personal communication May 2017). Unfortunately, the total flush volume is unknown. It is assumed that the mean flush discharge in the rainy season (Q_m) is 20% of the design discharge ($Q_d = 319\ m^3\ s^{-1}$) of the Nga Moe Yeik Sluice Gates ($Q_m = 0.2 * Q_d = 63.8\ m^3\ s^{-1}$). In Scenario 0 the model is forced continuously with $Q_{fl,0} = Q_m = 63.8\ m^3\ s^{-1}$ for a period of 184 days (between 15 May and 15 November).

In the second scenario (Scenario 1) the creek is flushed 3 times. Starting at 15 May, the model is forced with $Q_{fl,1} = 279.5\ m^3\ s^{-1}$ for a period of 14 days (spring-neap tidal cycle). Then the discharge is set to 0 for the following 71 days. In the middle of the wet season, between 8 and 22 August and at the end between 1 and 15 November the discharge is again set to $Q_{fl,1} = 279.5\ m^3\ s^{-1}$.

In the last scenario (Scenario 2) the model is forced with a pulsating discharge similar to the second scenario, but here the creek is flushed 6 times. Starting at 15 May, $Q_{fl,2}$ is set to $139.8\ m^3\ s^{-1}$ for a period of 14 days, followed by a period of 20 days where the discharge is set to $0\ m^3\ s^{-1}$, then at 18 June $Q_{fl,1}$ is set to $139.8\ m^3\ s^{-1}$ again. This cycle repeats until the 6th pulse between 1 and 15 November.

The flushing scenarios are assessed using the bed shear stress (τ_b), which is a measure for energetic forcing. In this way, the siltation/erosion patterns can be analysed by comparing the bed shear stress, τ_b with the critical bed shear stress, $\tau_{b,cr}$. Where the bed shear stress is greater than the critical value erosion occurs and vice versa siltation. Furthermore, by assessing the bed shear stress insight is gained in the model sensitivity for the parameter choice.

To better see the effect of flushing in the bed shear stress, percentiles are calculated from the model results. The 90th percentile is chosen in analogy to the velocity of tidal current in a tidal cycle, which is a useful scale for evaluating morphodynamics in coastal areas (Hu et al., 2015). It gives the highest bed shear stress that is exceeded in 10 % of the simulated time. The 50th percentile is chosen as a reference and gives the highest bed shear stress that is exceeded in 50% of the time. First, τ_b is maximised in the time domain, then the resulting τ_b is maximised in the cross section (in m-direction) of all 840 grid-cells (in n-direction). Subsequently, the 50th and 90th percentile of the max occurring bed shear stress ($\tau_{b,max}$) are determined in time per cross section and compared with the critical bed shear stress, $\tau_{b,cr}$.

5.3 Results flush scenarios

Based on the results from the two calibration phases ($i_c = 5 \times 10^{-5}$, $m = 0.013$, $M = 0.001\ kg\,m^{-2}\,s$ and $w_s = 0.1$ and $0.02\ mm\,s^{-1}$), the flush scenarios as discussed in Section 5.2 are simulated between 3 May 2015 (t0) and 30 May 2017 (t1). Figure 5.2 shows bed levels (t0 and t1) siltation (t1-t0) in the thalweg for all flushing scenarios. The width averaged siltation, just before the last flush event is plotted in Figure 5.3. Since 75 % of the siltation occurs in the upper 15 km of the creek, the width averaged siltation is only depicted in the upper 15 km of the domain. For the width averaged siltation in the complete domain, one is referred to Appendix C.3. Table 5.1 gives the corresponding percentage of siltation between the start time of the simulation and just before the last flush event. All flushing scenarios reduce siltation significantly. However, pulsatile flushing seems to mitigate siltation better than continuous flushing.

Table 5.1: Siltation in the upper 15 km stretch of the domain (in period 14 May 2017 - 3 May 2015) of different flush scenarios compared to no flushing.

Flushing scenario	Q [$m^3\ s^{-1}$]	Siltated
No flushing	0	100%
Continuously (1 pulse)	63.8	11.7%
Pulsatile (6 pulses)	139.8	9.6%
Pulsatile (3 pulses)	279.5	5.7%

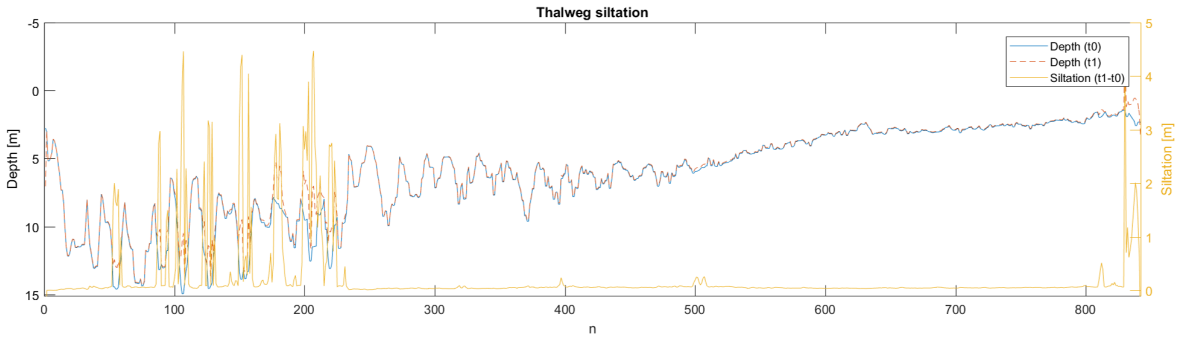

(a) Scenario 0, continuous flushing $Q_{fl,0} = 63.8\ \mathrm{m^3\,s^{-1}}$

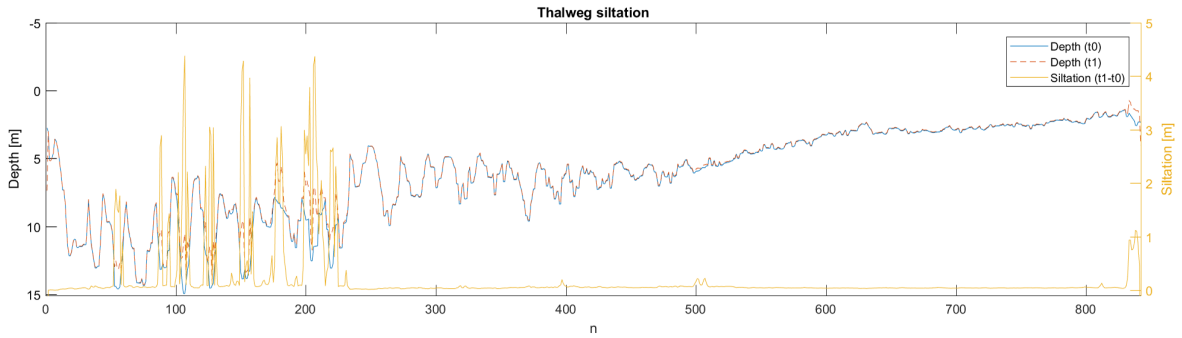

(b) Scenario 1, pulsatile flushing $Q_{fl,1} = 279.5\ \mathrm{m^3\,s^{-1}}$ (3 pulses)

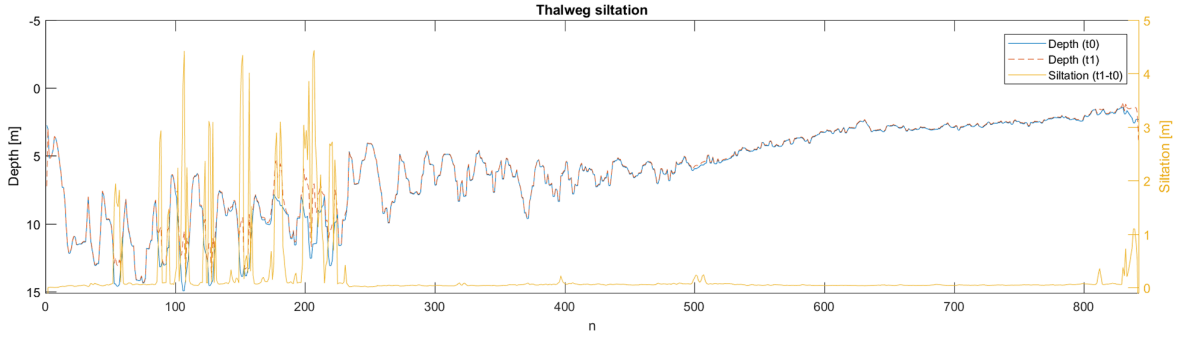

(c) Scenario 2, pulsatile flushing $Q_{fl,2} = 139.8\ \mathrm{m^3\,s^{-1}}$ (6 pulses)

Figure 5.2: Results flush scenarios, thalweg siltation

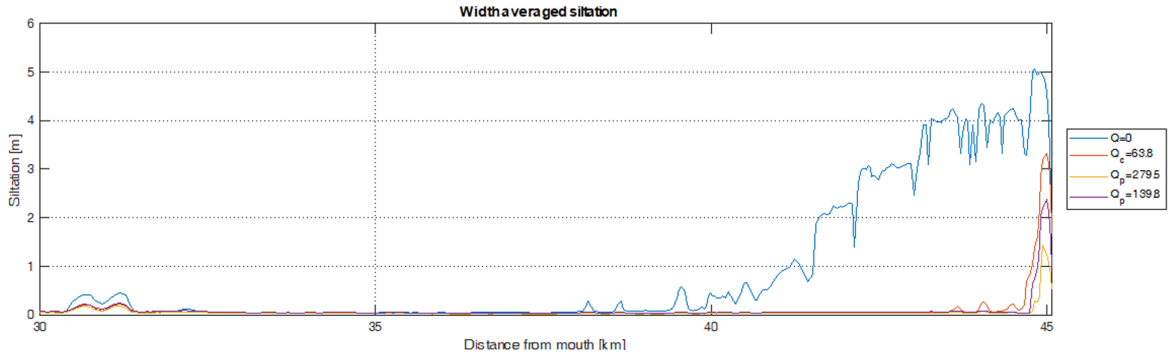

Figure 5.3: Results flush scenarios, width averaged siltation in upper 15 km stretch of the creek

Figures 5.4a and 5.4b show the 50th and 90th percentile of $\tau_{b,max}$ which is exceeded by respectively 50 and 10 % of the time for all considered scenarios. In these figures $\tau_{b,cr}$ is also given, indicating erosion where $\tau_{b,max} > \tau_{b,cr}$. In cases of flushing, the highest values for $\tau_{b,max}$ occur in both ends of the domain (mouth and sluice). Without flushing, $\tau_{b,max}$ is highest at the mouth and lowest at the sluice. $\tau_{b,max}$ suddenly increases around n = 240, which may be explained by the sudden change in bottom depth as can be observed at the same location in Figure 4.17.

Figure 5.4 shows that for 50% of the time erosion does not occur throughout most of the domain ($\tau_{b,max} < \tau_{b,cr}$). For 10% of the time, erosion is dominant throughout the domain ($\tau_{b,max} > \tau_{b,cr}$). This could be explained by the flood-dominance of the tide (short rising periods, with a strong flood current). In the upper end of the domain, $\tau_{b,max}$ differs significantly between the flushing scenarios. No flushing (blue), results in the lowest values for $\tau_{b,max}$ in the upper part of the domain while it shows slightly higher values in the rest of the domain, indicating the order of influence of flushing in the lower part of the domain. Model results, given in Appendix C.1 showed that the maximum flood tidal discharge at the mouth is approximately 10 times the design discharge of the Nga Moe Yeik Sluice Gates. Flushing strengthens the ebb current (increases the $\tau_{b,max}$), but the flood-dominance of the tide remains, resulting in little difference in $\tau_{b,max}$ between scenarios in the downstream end of the domain. Consequently, flushing can only affect siltation in the upper part of the domain. Figure 5.4 shows that higher $\tau_{b,max}$ occur for higher discharges.

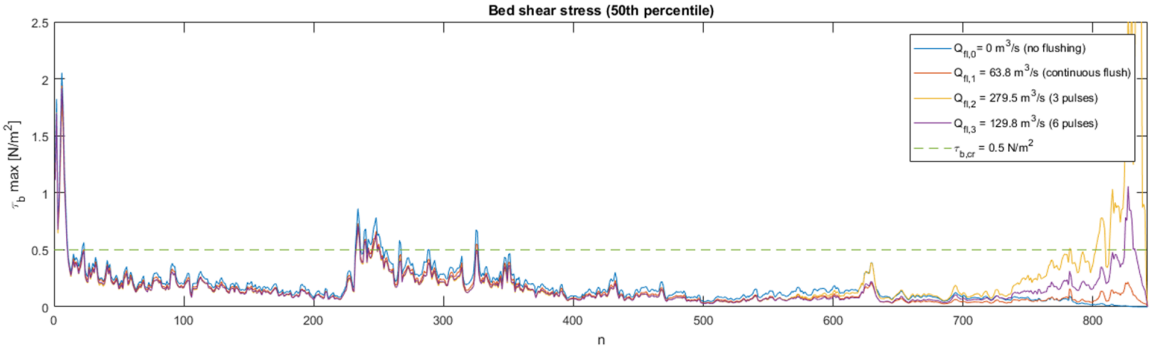

(a) 50th percentile

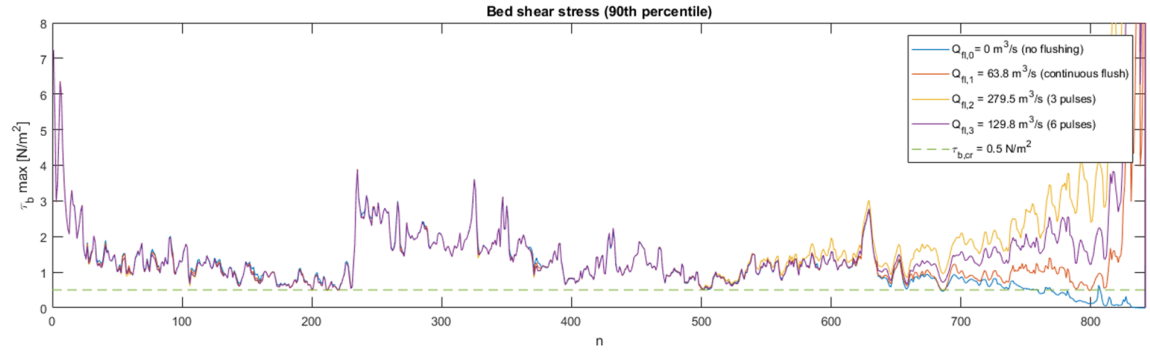

(b) 90th percentile

Figure 5.4: Max bed shear stress $\tau_{b,max}$ over the length of the domain for all flushing scenarios.

Chapter 6

Discussion

In this section, the acquired results are reviewed for their quality and shortcomings with respect to the research questions in analogy to the objectives.

6.1 Insight in processes

Flood-dominant tidal asymmetry

The observed tidal wave has an asymmetrical shape, the rising period is shorter than the falling period. This is typical for a flood-dominant system. This behaviour is caused by the higher water level during flood period. The funnel-shaped creek amplifies the tidal wave. The combination of available sediment and flow velocities cause transport of sediment which could eventually result in siltation. In the Nga Moe Yeik Creek high siltation occurs close to the sluice in both the model results and in field observations (from local authorities). In a flood-dominant system the flood velocities are higher than the ebb velocities which cause residual inflow of sediment. This is in line with the observed siltation in the upper stretch of the creek. Furthermore, the bed inclination and roughness are small in this area (general in muddy coasts) which enables the tidal wave to propagate far into the system. This strengthens the effect of the tidal wave further into the creek. The high amounts of sediment available downstream of the creek in combination with the flood-dominant system results in higher sediment concentrations in the upper stretch of the creek which could lead to severe siltation in areas with low energy. In the bathymetry a sudden bed level change can be observed (around n = 240). This is believed to be an artefact of the data processing. In the calculated bed shear stress this can also be observed. The high bed shear stresses in this area are considered overestimated by the model. With more water level observation stations such errors could be mitigated. However, it is expected that this local bed level change does not effect the general siltation distribution. Using a classical harmonic analysis both observed and calculated water levels for all Diver locations are decomposed to find the main harmonic constants. The model underestimates the M4 phase significantly (in the order of 45°). Therefore, the model could result in underestimation of the residual transport in the flood direction. However, the calculated phase difference between M2 and M4 still suggests a flood-dominant system.

Sediment concentrations

The turbidity measurements in the wet season showed well-mixed depth profiles. During falling and rising tide, the profiles resemble Rouse profiles. During slack tide, they develop into uniform mixed profiles. It is expected that similar measurements in the dry season would result in higher sediment concentrations, as observed by Sir Alexander Gibb & Partners (1976) and Nelson (2001). Since during dry season river discharge is limited and consequently the tidal wave propagates further landward increased sediment transport is expected. Furthermore, in saline water flocculation processes are enhanced so siltation rates could increase. The conversion between turbidity in NTU and concentration in gL^{-1} was based on just one water sample, because the sampler broke after first use. Ideally, sediment concentration are determined from multiple water samples taken over depth per location and related to corresponding NTU values. This would result in a more reliable conversion. However, the used conversion factor (1.5×10^{-3}) resulted in concentrations similar as observations from Sir Alexander Gibb & Partners (1976). It is therefore assumed that the results of the

concentrations profiles are not significantly influenced by the limited conversion. Extreme values are occasionally observed in the raw turbidity profiles. This could be the result of various causes. An extreme value low in the profile could be the result of the sensor measuring in fluid mud. At the water surface the sensor is influenced by the transition between water and air. In the water column the sensor can be temporarily blocked by suspended trash. The most severe disturbances are not considered in the depth averaging. As observed in Section 4.4 the depth and tidal averaged concentrations are in the same order of magnitude in model and measurements. In general the results of both are similar. A higher concentration is observed near the mouth compared to mid-domain concentrations. This is in line with expectations based on research of Ramaswamy et al. (2004). The Gulf of Martaban contains continuously high suspended sediment concentration and is covered with an inner-shelf mud belt. This high amount of available sediment could explain the higher concentrations in the mouth.

Salinity driven processes

The model and field observations showed similar physical processes, see Section 4.4. It was concluded that tidal asymmetry is the main process that drives the siltation. A flood-dominant behaviour is observed based on water levels measurements in the dry season. However, salinity also affects siltation rates. Unfortunately, the CTD diver was lost together with salinity observations in the dry season. Saline processes are expected to occur in the Nga Moe Yeik Creek in the dry season. In the Yangon River, freshwater discharges decreases after mid-September, and saline conditions become fully established by the end of the year (Nelson, 2001). Salinity could effect siltation in two ways. A horizontal salinity gradient could drive another sediment carrying process; gravitational circulation. It is assumed that the effect of the gravitational circulation is restricted because of limited horizontal salinity gradient and river depth. Due to the combination of the occurring tidal range and the relatively low depths, the creek is assumed to be a well-mixed system. Therefore, the effect of gravitational circulation is assumed to be negligible compared to the tidal asymmetry. Furthermore, the process of flocculation is enhanced by salinity. But also this is assumed to have a small effect on siltation compared to the effect of tidal asymmetry. The influence of both gravitational circulation and enhanced flocculation is already reduced because the mouth of the Pazundaung Creek is located 40 km into the Yangon estuary. Here, at 40 km from sea, it is expected that salinity levels are always lower than sea values. It is expected that the combined fresh water discharge of Bago and Yangon rivers decreases salinity values, since only fresh water values were observed with the OBS measurements in the wet season, see Appendix A.3. It is assumed that also during wet season the effect of salinity is inessential relative to tidal asymmetry due to expected lower salinity values. Therefore, it is assumed that salinity is not essential in this research and a 2DH model gives sufficient insight in the problem.

6.2 Effect of flushing

Flush scenarios

The effect of several flushing scenarios on siltation is assessed in Chapter 5.3. The current operating scheme of the Nga Moe Yeik Sluice Gates flushes the creek continuously in the wet season. During dry season, the gates are closed and no river discharge is allowed in the creek. Through flushing it is aimed to counteract the effect of the tidal asymmetry by strengthening the ebb velocities with an increased river discharge. Next to continuously flushing, pulsatile flushing is assessed. The time averaged model results show that all flushing schemes are effective to mitigate siltation, but only in the upper 15 km stretch of the domain. The flushing scheme with 3 pulses appeared to be most effective. However, considering this scenario, the longest period (71 days) occurs where the sediments consolidate between flush periods. The flushing scheme with 6 pulses is more effective than a continuously flushing scheme. In all schemes the total river discharge is the same. In the pulsating schemes a constant flushing period of a spring-neap cycle (14 days) is used. This results in higher discharges in case of lower flush frequency, which explains why the flushing scheme with 3 pulses is more effective than with 6 pulses. The discharge during continuously flushing is the lowest and explains that this is less effective.

Critical bed shear stress

Velocity is related to discharge. A higher river discharge induces increased ebb velocities. Siltation and erosion are related to bed shear stresses which depend on velocity. Higher velocities induce increased bed shear stresses which counteracts siltation and enhances erosion. In the model simulations, the critical bed shear stress is set to a constant value of $\tau_{cr,e} = 0.5\ \mathrm{kg\,m^{-1}\,s^{-2}}$. This value represents weakly consolidated sediments which is reached during most tidal conditions (van Maren et al., 2015). The chosen value for the critical bed shear stress determines siltation and erosion patterns in the whole domain. However in reality, bed properties, including critical bed shear stress (and the erosion parameter), vary over time and place. Because the model does not consider the time and place dependency of the critical bed shear stress, it could give unreliable results for a quantitative siltation assessment. With the chosen value for the critical bed shear stress only weakly consolidated soil is assessed. Therefore, results may not represent earlier siltated and consolidated material. The model is calibrated with reasonably mobile sediments, otherwise no sediment would be imported into the domain. Once accumulated on the bed, the sediment layer starts to consolidate with time. During this development, characteristics of the consolidated bed change. For more consolidated areas, a higher critical bed shear stress is expected (in the order of several Pa). The consolidating soil gains strength. The erosion parameter decreases, which results in less effective flushing events. In the flush scenario study this is not considered, therefore the results may be overestimating the effectiveness of the flushing. In case of a more consolidated bed ($\tau_{cr,e}$ = 1-2 Pa), the 90th percentile of the bed shear stress (see Figure 5.4) indicates significantly less mobilised sediments for all scenarios. Only pulsatile flushing (with higher discharges) would still plead for a mitigating effect on siltation. However, the consolidation time increases with fewer pulses and higher discharges and the bed can gain more strength. Considering this, the model should be used sensibly. Choosing the best scenario is a trade-off between consolidation time and maximal flush discharge.

Flush capacity

The total flush volume in a typical wet season depends on hydrological conditions such as the total precipitation of the catchment area of the Nga Moe Yeik Creek. Information on this could not be acquired so in Section 5.2 an assumption was made based on the design discharge of the Nga Moe Yeik Sluice Gates. The assumption of a total flush volume of 20% of the design discharge may be an underestimation. An increased flushing discharge results in less siltation over a larger part of the creek. So an increased discharge is more effective to mitigate siltation. However, for the relative proportions between the various flushing scenarios no alteration is expected with an increased discharge.

6.3 Data poor environment

Relevance of field data

For this research in a data poor environment, the Nga Moe Yeik Creek in Myanmar field observations measurements and a model simulations are used to increase insight in the local siltation problem. For this siltation problem the following parameters are analysed; water and bed levels, sediment concentrations, bed inclination, bed roughness, erosion parameter, settling velocity and critical bed shear stress. The water levels, bed levels and sediment concentrations are processed based on measurements of absolute pressure, depth and turbidity. The remaining parameters are based on expert judgement. The water level observations showed the propagation of the tidal wave into the creek. This gives some general insight in the siltation problem. A more asymmetric tidal wave is observed further in the creek. From the bathymetry survey lower depths are observed in the upstream part of the creek. Findings from these measurements can be confirmed by field observations. The headroom of certain bridges is so small during high water that barges could not always pass. It is unlikely that these bridges are designed and constructed with this headroom. This suggests that the situation has changed and the bed level near these bridges has increased, see Appendix D. Furthermore, from personal communication with DWIR and Irrigation Department it is known that most siltation occurs in the upper 15 km stretch of the Nga Moe Yeik Creek. With only the measured data a first order analysis of the siltation problem is possible.

Combination of model and data

Using the acquired field data a reliable model could be set up, which is used for analysis of the siltation problem. This model showed a similar flood-dominance in the system. The tidal asymmetry is an important process in the siltation problem. So, the measured water levels are needed to validate the model. The observed depth was measured during high water periods of 4 different days. Due to the tidal range an unwanted offset in the order of 2 m occurs (Section 3.2.2). To get rid of this offset the model was essential. For a first order validation of this model, water levels are required. Observed water levels from three monitoring stations are used to correct the measured depth. It is expected that more stations would improve the process. By the iterative process of bed level correction, both the calculated water levels in the whole computational domain and the bathymetry improved significantly. Observed and calculated water levels after this iteration are closely matched. Using the model the calculated water levels are improved by the corrected bed levels. The depth and water level observations are dependent on each for corrections, which result in more reliable model results. Therefore, the measured bed level is equally essential. Without the bathymetry survey and water levels monitoring, the model would not generate reliable results.

Essential model parameters

For a similar case study in a data poor environment bed level and water level are minimum necessary parameters. Since erosion and siltation processes are important to assess the problem, the erosion parameter (M), settling velocity (w_s) and the critical bed shear stress ($\tau_{b,cr}$) are also relevant. After a qualitative analysis, based on information acquired from field visits and personal communication with DWIR and Irrigation Department (Section 2.4.3), the best fitting sediment parameters for the final model were chosen. With more quantitative data on suspended sediment concentration and deposition rates, the model could be further calibrated by fine-tuning the model parameters w_s and M (narrowing down the wide range in w_s and M). Within the scope of this research this is not realistic because of the lack of data to further validate the model. Further calibration would therefore only marginally decrease the remaining uncertainties. Because the model does not consider the time and place dependency of the critical bed shear stress, erosion parameter and settling velocity, it could give unreliable results for a quantitative siltation assessment. Other imposed parameters are the inclination, Manning parameter for bed roughness and sediment concentration. From the sensitivity analysis in Section 4.2.4 it appeared that the computed water levels only varied marginally with roughness and inclination within the parameter space experimented with. Model results are less sensitive to these parameters. Therefore they are considered to be less essential. The downstream boundary is forced with a sediment concentration which is based on yearly averaged measurements from Sir Alexander Gibb & Partners (1976). The measured turbidity over depth profiles appeared to be less essential for model results because the final 2DH model does not consider vertical gradients.

Chapter 7

Conclusions and recommendations

In Chapter 1 three objectives and corresponding research questions are formulated to quantify and increase insight in processes that determine siltation in the Pazundaung/Nga Moe Yeik Creek. This chapter will give short answers to these research questions in Section 7.1 and finally some recommendations in Section 7.2.

7.1 Conclusions

Fieldwork is conducted and a Delft3D-flow model is set up. A combination of both model and acquired data has been used to achieve the following objectives:

- To quantify and increase insight in processes that determine siltation in the Pazundaung/Nga Moe Yeik Creek.
- To evaluate the effect of flushing the Nga Moe Yeik Creek in order to minimise siltation rates.
- To provide generic guidance for the use of limited data in combination with a model in data poor environments

The research questions are answered in analogy with these objectives.

Insight in processes

- What are the main processes that influence siltation in the Nga Moe Yeik Creek?

  The main driving force behind the siltation problem is the tidal asymmetry. Due to its flood-dominant character, the tidal wave transports sediments into the creek. Both the model and field data confirm this.

- How does the tidal wave propagate and deform in the Nga Moe Yeik Creek ?

  Water levels at three locations along the creek have been monitored for a period between 9 and 30 May 2017. From the measurements, a tidal range in the order of 4-6 m was observed. All stations showed a shorter rising period and longer falling period, which is typical for flood-dominance. The effect of shorter rising period and longer falling period increases in landward direction.

- What are typical suspended sediment concentrations in the Nga Moe Yeik Creek?

  In the beginning of the Monsoon period, sediment concentrations between 0.3 and 1.0 gL^{-1} have been measured over depth during a complete tidal cycle. Depth and tidally averaged concentrations are in the order of 0.5 gL^{-1} and observed in field and model results. These values are similar to observations by Sir Alexander Gibb & Partners (1976).

- When and where do highest concentrations occur?

  In the Nga Moe Yeik Creek highest depth averaged sediment concentrations occur during rising tide followed by falling tide. During rising tide a maximum depth averaged concentration of 0.7 gL^{-1} is observed near the mouth and a concentration of 0.6 gL^{-1} at 17 km landward of the mouth. During falling tide, depth averaged concentrations of respectively 0.6 gL^{-1} and 0.5 gL^{-1} are observed. Averaged over depth and tidal cycle sediment concentrations are respectively 0.5 gL^{-1} and 0.4 gL^{-1}. The model is not calibrated on the tidal phasing of sediment concentrations. However, results are in the same order of magnitude and show a similar decreasing trend between mouth and mid-domain as the observations.

- What is the distribution of siltation in the Nga Moe Yeik Creek?

  Most severe siltation occurs in the upper 15 km of the creek. Here, some parts of the creek bed fall dry during low water and low headroom of bridges form a risk for vessels during high water. According to the model, in almost the whole domain siltation occurs during 50% of the simulated period (2 years). Most siltation occurs in the upper part of the domain and especially on the banks.

Effect of flushing

- What is the effect of fresh water discharge (flushing) on siltation?

  Fresh water discharge results in higher erosion rates in the upper 15 km of the creek. All considered flush scenarios reduced siltation in the upstream thalweg significantly, however there are some calculated differences in bed shear stress between the various scenarios.

- To what extent can an improved operating scheme of the Nga Moe Yeik Sluice Gates mitigate siltation?

  The mitigating result of the considered flushing scenarios on siltation is only effective in the most upstream 15 km of the creek. Higher bed shear stresses occur for flushing scenarios with higher discharges. The scenario with 3 pulses gives best results followed by the scenario with 6 pulses. Less effective is the current flushing scheme with a continuous discharge. However, to be able to give a quantitative answer on the extend of mitigation, exact values of imposed river discharge and critical bed shear stress are necessary.

Data poor environment

- What are the minimum necessary parameters to assess siltation rates in a data poor environment?

  To assess a siltation problem in a data poor environment, it is important to identify the main processes that could influence siltation. Personal communication with local actors and field observations help to get a first order insight in the problem. In macro-tidal muddy coasts the asymmetry of the tidal wave could be a dominant feature in the system. In that case, water levels and bed levels are most essential parameters. Less essential are erosion parameter (M), settling velocity (w_s) and the critical bed shear stress ($\tau_{b,cr}$). With expert judgement for these parameters a qualitative siltation assessment could be done. However, for a quantitative assessment more specific values for these parameters are required.

- To what extent are model and field data dependent on each other in a data poor environment?

  First of all, in a data poor environment it is important to use a model that consistently simulates the required physics to explore the processes that influence the problem. It is recommended to start with a simple model (2DH). If for example well-mixed sediment concentrations are observed, a simple 2DH model could already give valuable insights. In a data poor environment limited data is available, but by an combination of rough field data and a simple hydrodynamic model, both can be improved by each other. Without the use of a model, field observations and measurements could only give first order insight in the significant processes. In this case, an elaborative analysis is not possible. Without data for input and validation, a model could also only give first order insight with the use of estimations.

7.2 Recommendations

In this section, recommendations for future research are discussed. A division is made for recommendations on data collection and model improvements, the siltation problem in the Nga Moe Yeik Creek and more general in a data poor environment. The recommendations on data collection and model improvements could contribute to a more quantitative analysis of the problem. To make a distinction in requirements, these are prioritised (labelled as 'must have' and 'nice to have').

7.2.1 Data collection

Must have

- Bathymetric change study

  Conduct a full-scale flush scenario experiment with the Nga Moe Yeik Sluice Gates and assess bathymetric changes. A bathymetric change study could contribute to an increased insight in the effects of flushing on siltation rates in the creek. By monitoring the bed level changes in the Nga Moe Yeik Creek before and after a flush event, the model could be improved on morphodynamic predictions by calibrating it on the measured bathymetric changes.

- Flow measurements

  Gather field data on flow velocities in the creek. Based on flow velocity measurements close to the Nga Moe Yeik Sluice Gates during wet season would, the available flush volume can be better estimated. With this data more realistic flush scenarios could be assessed.

Nice to have

- Relative heights

  Measure relative vertical distances between multiple water level stations. Water levels observations are important for the model and bed level correction. It is recommended to use a device that precisely measures the relative height of the sensors to a horizontal datum.

7.2.2 Model improvements

Must have

- Initial sediment layer simulation

  Run the model with initial sediment in the domain. An initial sediment layer at the beginning of a simulation could improve the bathymetry. In this way the simulation starts with sediment in the domain, which results after some simulation time in a smoother bathymetry. Consequently, the influences of abrupt bed level errors are mitigated. This bathymetry can than be used for further simulation.

Nice to have

- Sediment parameters $\tau_{b,cr}$, M and w_s

  Improve the model with specific data on the critical bed shear stress $\tau_{b,cr}$, erosion parameter M and settling velocities w_s. Extensive field- and lab work is required to determine parameters that represent time and place dependent bed features and conditions in the Nga Moe Yeik Creek.

- Effect salinity

  Evaluate the effect of salinity on siltation rates. Higher salinity values in the dry season could enhance siltation rates.

- Boundary condition

  Evaluate the effect of the upper (closed) boundary in the model domain. A longer computational domain landward of the sluice, through which the tidal wave can propagate might be important in future studies.

7.2.3 Siltation problem

As a potential mitigating solution for the siltation problem in the Nga Moe Yeik Creek, flushing is assessed in this study. A flush scenario with 3 pulses appeared to be the best among the tested scenarios, but could only influence the most upper 15 km of the creek. The model showed that the incoming tidal discharge is a factor 10 greater than the design discharge of the Nga Moe Yeik Sluice Gates. Upgrading the sluice gate facilities in order to store and flush more water could be interesting to evaluate. It is also relevant to explore other potential solutions for the siltation problem. For example, since the tidal asymmetry is the main driving force in this case, siltation rates could be mitigated if the tidal wave propagation is diminished or even completely blocked in the creek.

7.2.4 Data poor environment

In data poor environments data is limited. In order to do research, measurements are required. Not every parameter can be measured, so some relevant parameters need estimations. In some cases, estimating these parameters a in data poor environments can be hard because reference cases may be data poor as well. Not only collecting and sharing data are essential, but also storing and organising the data in a database is relevant to make better estimations in the future. A data poor environment is often a feature of a developing countries. It is therefore relevant to help each other in simple and cheap solutions. Individual projects and studies could achieve a higher goal by openly publishing data. By sharing data, a better picture is obtained of what is already done and what attempts are made to increase insight in specific processes. In this way problems could be solved in a more effective way. Furthermore, increasing local knowledge is relevant for these countries in order to tackle future challenges independent of western companies or knowledge institutes.

Bibliography

Aung, L. L., Zin, E. E., Theingi, P., Elvera, N., Aung, P. P., Han, T. T., Oo, Y. & Gangstø Skaland, R. (2017), 'Myanmar climate report', *METreport* .

Aung, T. T., Shimozono, T. & Okayasu, A. (2013), 'Numerical simulation on sedimentation in yangon river and its navigation channel', *La mer* **51**, 91–104.

Bosboom, J. & Stive, M. J. (2015), *Coastal Dynamics 1 Lecture Notes CIE4305*, Delft Academic Press (VSSD-uitgeverij).

Campbell Scientific, Inc. (2016), 'Obs-3a turbidity and temperature monitoring system', `https://s.campbellsci.com/documents/us/manuals/obs-3a.pdf`.

Deltares (2014), 'Delft3d-flow user manual', *Delft, the Netherlands* .

Deltares (2018), 'Delft3d-quickin user manual', *Delft, the Netherlands* .

Doodson, A. T. (1921), The harmonic development of the tide-generating potential, *in* 'Proc. R. Soc. Lond. A', Vol. 100, The Royal Society, pp. 305–329.

Garmin International, Inc. (2017), 'Transom/trolling motor mount transducer installation instructions', `http://static.garmin.com/pumac/Trolling_Transom_Transducer_GT22-52_Install_EN.pdf`.

Gatto, V. M., van Prooijen, B. C. & Wang, Z. B. (2017), 'Net sediment transport in tidal basins: quantifying the tidal barotropic mechanisms in a unified framework', *Ocean Dynamics* **67**(11), 1385–1406.

Haurwitz, B. (1964), 'Atmospheric tides', *Science* **144**(3625), 1415–1422.

Hu, Z., Wang, Z. B., Zitman, T. J., Stive, M. J. & Bouma, T. J. (2015), 'Predicting long-term and short-term tidal flat morphodynamics using a dynamic equilibrium theory', *Journal of Geophysical Research: Earth Surface* **120**(9), 1803–1823.

JICA (2014), 'Data collection survey on water resources potential for thilawa special economic zone and adjoining areas final report : main report', `http://open_jicareport.jica.go.jp/617/617/617_104_12183752.html`.

JICA (2015), 'The urgent project for rehabilitation of yangon port and main inland water transport in the republic of the union of myanmar', `http://open_jicareport.jica.go.jp/pdf/12230660.pdf`.

Kitnan, R. B. (2012), 'In hailing the peasant's day, ngamoe yeik sluice gate was commissioned into service in yangon region', `http://www.ssig.gov.my/blog/2012/03/15/in-hailing-the-peasants-day-ngamoe-yeik-sluice-gate-was-commissioned-into-service-in-yangon-region/`.

Meade, R. H. (1996), River-sediment inputs to major deltas, *in* 'Sea-level rise and coastal subsidence', Springer, pp. 63–85.

Nelson, B. W. (2001), 'Sediment dynamics in rangoon river, myanmar', *Science of the total environment* **266**(1), 15–21.

OBG (2017), 'The report: Myanmar 2017', *Oxford Business Group* .

Pawlowicz, R., Beardsley, B. & Lentz, S. (2002), 'Classical tidal harmonic analysis including error estimates in matlab using t_tide', *Computers & Geosciences* **28**(8), 929–937.

Postma, H. (1954), 'Hydrography of the dutch wadden sea', *Arch. Neerl. Zool* **10**(4), 405–511.

Pugh, D. T. (1996), *Tides, surges and mean sea-level (reprinted with corrections)*, John Wiley & Sons Ltd.

Ramaswamy, V., Rao, P., Rao, K., Thwin, S., Rao, N. S. & Raiker, V. (2004), 'Tidal influence on suspended sediment distribution and dispersal in the northern andaman sea and gulf of martaban', *Marine Geology* **208**(1), 33–42.

Rao, P., Ramaswamy, V. & Thwin, S. (2005), 'Sediment texture, distribution and transport on the ayeyarwady continental shelf, andaman sea', *Marine Geology* **216**(4), 239–247.

Richardson, J. & Zaki, W. (1954), 'The sedimentation of a suspension of uniform spheres under conditions of viscous flow', *Chemical Engineering Science* **3**(2), 65–73.

Sir Alexander Gibb & Partners (1976), *Rangoon Sea Access Channel and Associated Port Improvement Study: Final Report*, Vol. IV, United Nations Development Programme.

Te Chow, V. (1959), *Open channel hydraulics*, McGraw-Hill Book Company, Inc; New York.

The Lake of Missouri Volunteer Program (n.d.), 'Diy van dorn sampler (grab sampler)', `http://www.lmvp.org/kayakswarm/LMVP/Equipment/VanDorn.xhtml`.

Thonnya, K.-M. (2013), 'Ngamoeyeik creek needs re-dredging', `http://www.burmalibrary.org/docs15/NLM-2013-06-16-red.pdf`.

Van Essen Instruments (2016), 'Product manual diver', `https://www.vanessen.com/images/PDFs/Diver-ProductManual-en.pdf`.

van Maren, D. S., Winterwerp, J. C. & Vroom, J. (2015), 'Fine sediment transport into the hyper-turbid lower ems river: the role of channel deepening and sediment-induced drag reduction', *Ocean Dynamics* **65**(4), 589–605.

Van Maren, D. & Winterwerp, J. (2013), 'The role of flow asymmetry and mud properties on tidal flat sedimentation', *Continental Shelf Research* **60**, S71–S84.

van Rijn, L. (2012), 'Field survey for sediment parameters in muddy environments'.

Wilson, W. T. (2014), 'Beating the middle-income trap in southeast asia', *The Heritage Foundation, August* **27**(1).

Winterwerp, J. C. & Van Kesteren, W. G. (2004), *Introduction to the physics of cohesive sediment dynamics in the marine environment*, Vol. 56, Elsevier.

Appendix A

Measurements in the Nga Moe Yeik Creek

A.1 Digitalised measurements from Sir Alexander Gibb & Partners (1976)

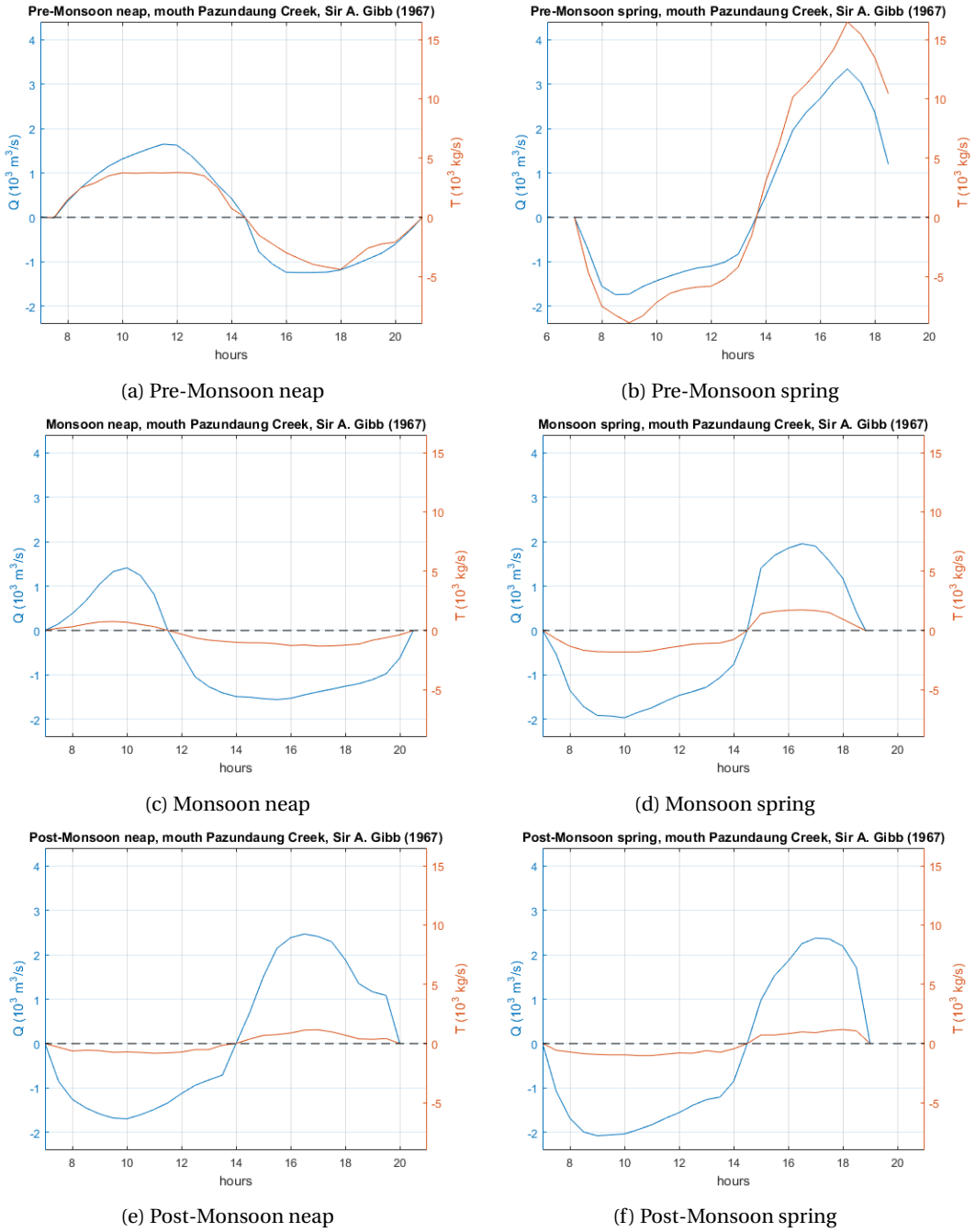

(a) Pre-Monsoon neap

(b) Pre-Monsoon spring

(c) Monsoon neap

(d) Monsoon spring

(e) Post-Monsoon neap

(f) Post-Monsoon spring

Figure A.1: Discharge and sediment transport measurements in the mouth Pazundaung Creek (Nga Moe Yeik Creek) digitalised from Sir Alexander Gibb & Partners (1976)

A.2 Water levels

A.2.1 Water level observations at the sluice

Water levels Nga Moe Yeik Sluice Gates
source: Construction 6, Irrigation Department
US = upstream, DS = downstream (100 m)

		06:00	07:00	08:00	09:00	10:00	11:00	12:00	13:00	14:00	15:00	16:00	17:00	18:00	19:00	20:00	21:00
1-5-2017	US	10.3	10.3	10.3	10.3	10.3	10.3	10.3	10.3	10.3	10.3	10.3	10.2	10.2	10.2	10.2	10.2
	DS	5.2	5.2	10.6	11.4	8.1	5.2	6	6	6	6	6	8	8	8	8	11.2
2-5-2017	US	10.3	10.3	10.3	10.3	10.3	10.3	10.3	10.3	10.3	10.3	10.3	10.3	10.3	10.3	10.3	10.3
	DS	5.2	5.2	5.2	5.2	5.2	10.4	8.3	5.2	5.2	5.2	5.2	5.2	5.2	5.2	5.2	5.2
3-5-2017	US	10.3	10.3	10.3	10.3	10.3	10.3	10.3	10.3	10.3	10.3	10.3	10.3	10.3	10.3	10.3	10.3
	DS	5.2	5.2	5.2	5.2	5.2	5.2	5.2	5.2	5.2	5.2	5.2	5.2	5.2	5.2	5.2	5.2
4-5-2017	US	10.3	10.3	10.3	10.3	10.3	10.3	10.3	10.3	10.3	10.3	10.3	10.3	10.3	10.3	10.3	10.3
	DS	5.2	5.2	5.2	5.2	5.2	5.2	5.2	5.2	5.2	5.2	5.2	5.2	5.2	5.2	5.2	5.2
5-5-2017	US	10.3	10.3	10.3	10.3	10.3	10.3	10.3	10.3	10.3	10.3	10.3	10.3	10.3	10.3	10.3	10.3
	DS	5.2	5.2	5.2	5.2	5.2	5.2	5.2	5.2	5.2	5.2	5.2	5.2	5.2	5.2	5.2	5.2
6-5-2017	US	10.4	10.4	10.4	10.4	10.4	10.4	10.4	10.4	10.4	10.4	10.4	10.4	10.4	10.4	10.4	10.4
	DS	5.2	5.2	5.2	5.2	5.2	5.2	5.2	5.2	5.2	5.2	5.2	5.2	5.2	5.2	5.2	5.2
7-5-2017	US	10.4	10.4	10.4	10.4	10.4	10.4	10.4	10.4	10.4	10.4	10.4	10.4	10.4	10.4	10.4	10.4
	DS	5.2	5.2	5.2	5.2	5.2	5.2	5.2	5.2	5.2	5.2	10.7	11.3	5.2	5.2	5.2	5.2
8-5-2017	US	10.4	10.4	10.4	10.4	10.4	10.4	10.4	10.4	10.4	10.4	10.4	10.4	10.4	10.4	10.4	10.4
	DS	5.2	5.2	5.2	5.2	5.2	5.2	5.2	5.2	5.2	5.2	5.2	11.1	10	5.2	5.2	5.2
9-5-2017	US	10.5	10.5	10.5	10.5	10.5	10.5	10.5	10.5	10.5	10.5	10.5	10.5	10.5	10.5	10.5	10.5
	DS	10.6	5.2	5.2	5.2	5.2	5.2	5.2	5.2	5.2	5.2	5.2	10.7	11.7	9.2	5.2	5.2
10-5-2017	US	10.5	10.5	10.5	10.5	10.5	10.5	10.5	10.5	10.5	10.5	10.5	10.5	10.5	10.5	10.5	10.5
	DS	11	9	5.2	5.2	5.2	5.2	5.2	5.2	5.2	5.2	5.2	8.1	11.9	10.8	5.2	5.2
11-5-2017	US	10.5	10.5	10.5	10.5	10.5	10.5	10.5	10.5	10.5	10.5	10.5	10.5	10.5	10.5	10.5	10.5
	DS	10.3	10.7	5.2	5.2	5.2	5.2	5.2	5.2	5.2	5.2	5.2	5.2	11.4	12	10.1	5.2
12-5-2017	US	10.5	10.5	10.5	10.5	10.5	10.5	10.5	10.5	10.5	10.5	10.5	10.5	10.5	10.5	10.5	10.5
	DS	8.3	11.3	9	5.2	5.2	5.2	5.2	5.2	5.2	5.2	5.2	5.2	9.1	12.2	10.7	5.2
13-5-2017	US	10.5	10.5	10.5	10.5	10.5	10.5	10.5	10.5	10.5	10.5	10.5	10.5	10.5	10.5	10.5	10.5
	DS	5.2	10.5	10.2	5.2	5.2	5.2	5.2	5.2	5.2	5.2	5.2	5.2	5.2	10.5	12.2	10.4
14-5-2017	US	10.6	10.6	10.6	10.6	10.6	10.6	10.6	10.5	10.5	10.4	10.4	10.3	10.3	10.3	10.3	10.3
	DS	5.2	8.6	11	9	5.2	9	9	9	9	9	9	9	9	10.7	12.2	11
15-5-2017	US	10.3	10.3	10.3	10.3	10.3	10.3	10.2	10.2	10.1	10.1	10	10	9.9	9.9	10	10.3
	DS	8	8	10	10.7	8.5	8.5	8.5	8.5	8.5	8.5	8.5	8.5	8.5	11.8	11	11.8
16-5-2017	US	10.1	10.1	10.2	10.2	10.1	10	10	9.9	9.9	9.8	9.7	9.6	9.6	9.7	9.8	9.9
	DS	5.2	5.2	9.1	10.8	9.6	9.5	9.5	9.4	9.4	9.3	9.2	9.1	9.1	9.2	9.3	10.4
17-5-2017	US	9.2	9.1	9.1	9.2	9.2	9.1	9	9	8.9	8.9	8.9	8.9	8.8	8.8	8.7	8.7
	DS	8.7	8.6	8.6	10.6	9	8.6	8.5	8.5	8.4	8.4	8.4	8.4	8.3	8.3	8.2	8.2
18-5-2017	US	8.6	8.6	8.5	8.5	8.5	8.5	8.4	8.4	8.4	8.3	8.3	8.3	8.3	8.3	8.2	8.2
	DS	8.1	8.1	8	8	8	8	7.9	7.9	7.9	7.8	7.8	7.8	7.8	7.8	7.7	7.7
19-5-2017	US	8.1	8.1	8.1	8	8	8	8	8	7.9	7.9	7.9	7.9	7.8	7.8	7.8	7.8
	DS	7.6	7.6	7.6	7.5	7.5	7.5	7.5	7.5	7	7.4	7.4	7.4	7.3	7.3	7.3	7.3
20-5-2017	US	7.7	7.7	7.7	7.6	7.6	7.6	7.6	7.6	7.6	7.6	7.6	7.5	7.5	7.5	7.5	7.5
	DS	7.2	7.2	7.2	7.1	7.1	7.1	7.1	7.1	7.1	7.1	7.1	7	7	7	7	7
21-5-2017	US	7.5	7.5	7.5	7.4	7.4	7.4	7.4	7.4	7.5	7.5	7.5	7.5	7.5	7.5	7.5	7.5
	DS	7	7	7	6.9	6.9	6.9	6.9	6.9	7	7	7	7	7	7	7	7
22-5-2017	US	7.4	7.4	7.4	7.4	7.4	7.4	7.4	7.4	7.4	7.6	7.6	7.6	7.6	7.5	7.5	7.5
	DS	6.9	6.9	6.9	6.9	6.9	6.9	6.9	6.9	6.9	8.1	8.1	7.4	7.1	7	7	7
23-5-2017	US	7.5	7.5	7.5	7.5	7.5	7.5	7.5	7.5	7.5	7.7	7.9	8	7.8	7.8	7.8	7.8
	DS	7	7	7	7	7	7	7	7	7	8.2	8.4	8.5	7.3	7.3	7.3	7.3
24-5-2017	US	7.9	7.9	7.9	7.9	7.8	7.8	7.8	7.8	7.7	7.7	7.7	8	8.5	8.5	8.2	8.2
	DS	7.7	7.4	7.4	7.4	7.3	7.3	7.3	7.3	7.2	7.2	7.2	8.5	9	9	7.7	7.7
25-5-2017	US	8.5	8.3	8.3	8.3	8.2	8.2	8.1	8.1	8	8	8.1	8.5	8.9	8.9	8.6	8.6
	DS	9	7.8	7.8	7.8	7.7	7.7	7.6	7.6	7.5	7.5	8	9	9.4	9.4	8.1	8.1
26-5-2017	US	9	9	8.7	8.7	8.7	8.6	8.6	8.5	8.5	8.4	8.4	8.3	9.2	9.6	9.2	9.1
	DS	9.5	9.5	8.2	8.7	8.2	8.1	8.1	8	8	7.9	7.9	9.3	10.1	10	9.7	8.8
27-5-2017	US	9.2	9.5	9.2	9.2	9.2	9.2	9.2	9.2	9.2	9.1	9.1	9.1	9.8	10	10.3	9.9
	DS	9.9	10.2	10	8.8	8.8	8.8	8.8	8.8	8.8	8.7	8.7	8.7	10.7	11	11	9.5
28-5-2017	US	9.7	10.3	10.5	10.1	10.1	10.1	10.1	10.2	10.3	10.3	10.3	10.5	11	11.3	11.3	11.3
	DS	9.5	11	11.2	9.7	9.7	9.7	9.7	9.8	9.9	9.9	9.9	11	11.5	11.8	11.1	11.8
29-5-2017	US	10.7	11.1	11.3	11.9	11.1	11.1	11.1	11.2	11.3	11.3	11.3	11.4	11.5	11.9	12.3	12.3
	DS	10.3	11.6	11.6	11.9	10.7	10.7	10.7	10.8	10.9	10.9	10.9	11	11.1	12.3	12.6	12.7
30-5-2017	US	12	12	12.1	12.2	12.2	12.1	12.1	12.1	12.1	12.2	12.2	12.2	12.2	12.4	12.4	12.4
	DS	11.6	11.6	11.7	12	12	11.9	11.7	11.7	11.7	11.8	11.9	11.9	11.9	12.2	12.2	12.2
31-5-2017	US	12.4	12.4	12.4	12.4	12.5	12.5	12.4	12.4	12.4	12.4	12.3	12.3	12.3	12.3	12.3	12.3
	DS	12.2	12.2	12.2	12.2	12.3	12.3	12.2	12.2	12.2	12.2	12.1	12.1	12.1	12.1	12.1	12.1
1-6-2017	US	12.1	12.1	12.1	12.1	12.1	12.1	12.1	12.1	12	12	12	12	11.9	11.9	11.9	11.9
	DS	11.7	11.7	11.7	11.7	11.7	11.7	11.7	11.7	11.6	11.6	11.6	11.6	11.5	11.5	11.5	11.5
2-6-2017	US	11.7	11.7	11.7	11.6	11.6	11.6	11.5	11.5	11.5	11.4	11.4	11.3	11.3	11.3	11.2	11.2
	DS	11.3	11.3	11.3	11.2	11.2	11.2	11.1	11.1	11.1	11	11	10.9	10.9	10.9	10.8	10.8
3-6-2017	US	11	11	10.9	10.9	10.8	10.8	10.7	10.7	10.7	10.6	10.6	10.6	10.5	10.5	10.4	10.4
	DS	10.6	10.6	10.5	10.5	10.4	10.4	10.3	10.3	10.3	10.2	10.2	10.2	10.1	10.1	10	10
4-6-2017	US	10.1	10	10	9.9	9.9	9.9	9.9	10	10.1	10.2	10.3	10.4	10.4	10.4	10.4	10.4
	DS	9.7	9.6	9.6	9.5	9.5	9.5	9.5	9.6	9.7	9.8	9.9	10	10	10	10	10
5-6-2017	US	10.4	10.3	10.3	10.3	10.3	10.3	10.3	10.3	10.3	10.3	10.4	10.4	10.3	10.3	10.2	10.2
	DS	10	9.9	9.9	9.9	9.9	9.9	9.9	9.9	9.9	9.9	10	10	9.9	9.9	9.8	9.8
6-6-2017	US	10	9.9	9.9	9.9	9.8	9.8	9.7	9.7	9.7	9.8	10.2	10	9.9	9.9	9.8	9.8
	DS	9.6	9.5	9.5	9.5	9.4	9.4	9.3	9.3	9.3	9.4	10.5	9.8	9.5	9.5	9.4	9.4
7-6-2017	US	9.6	9.6	9.5	9.5	9.5	9.4	9.3	9.3	9.3	9.2	9.2	9.9	9.5	9.5	9.5	9.5
	DS	9.2	9.2	9.1	9.1	9.1	9	8.9	8.9	8.9	8.8	8.8	10.6	9.1	9.1	9.1	9.1
8-6-2017	US	9.7	9.4	9.3	9.8	9.2	9.2	9.1	9.1	9	9	9	9.5	9.8	9.6	9.6	9.5
	DS	10.1	9	8.9	8.9	8.8	8.8	8.7	8.7	8.6	8.6	8.6	10.1	10.4	9.2	9.2	9.1
9-6-2017	US	10.1	10.3	9.9	10	10	10	10	10.1	10.1	10.1	10.1	10.5	10.9	11.1	10.9	10.9
	DS	10.7	10.9	9.5	9.6	9.6	9.6	9.6	9.7	9.7	9.7	9.7	11	11.4	11.6	10.7	10.5
10-6-2017	US	10.9	11.2	10.9	10.9	10.8	10.7	10.7	10.7	10.7	10.7	10.7	10.7	11.2	11.4	11.3	10.3
	DS	10.7	11.8	10.7	10.5	10.4	10.3	10.3	10.3	10.3	10.3	10.3	10.5	11.8	12	11.1	10.4
11-6-2017	US	10.7	11.2	11.1	10.9	10.9											
	DS	10.3	11.8	10.9	10.5	10.5											

Figure A.2: Observed water levels between 1-5-2017 and 11-6-2017 up- and downstream near the Nga Moe Yeik Sluice Gates.

The water levels in Figure A.2 are manually recorded (written down) every hour during daylight, after reading a measuring rod (U Toe Nyein, Assistant Director Construction 6 Irrigation Department Yangon, personal communication June 2017). The colors indicate the water levels in feet. The difference between upstream (US) and downstream (DS) is clearly visible in the period before the gates opened on May 17. For a plot of this data see Figure 4.2. The measuring rod is depicted in Figure A.3

Figure A.3: Water level measuring-rod used to observe water levels 100 m downstream of the Nga Moe Yeik Creek

A.2.2 Falling and rising tides

Figure A.4 shows rising and falling period as calculated from the water level measurements between 9 and 30 May 2017. In this period, spring tides are observed around 13 and 27 May and a neap tide around 20 May. Per day two rising and two falling periods occur, so in the 21 days 40 periods are observed. The x-axis shows the number of rising/falling periods. The periods around 20 in the figure correspond to neap tide conditions.

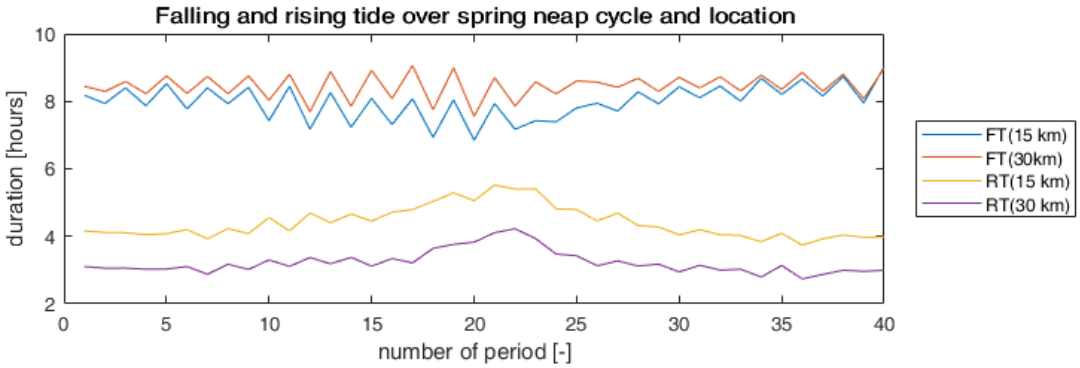

Figure A.4: Observed rising and falling periods

A.3 OBS profiles

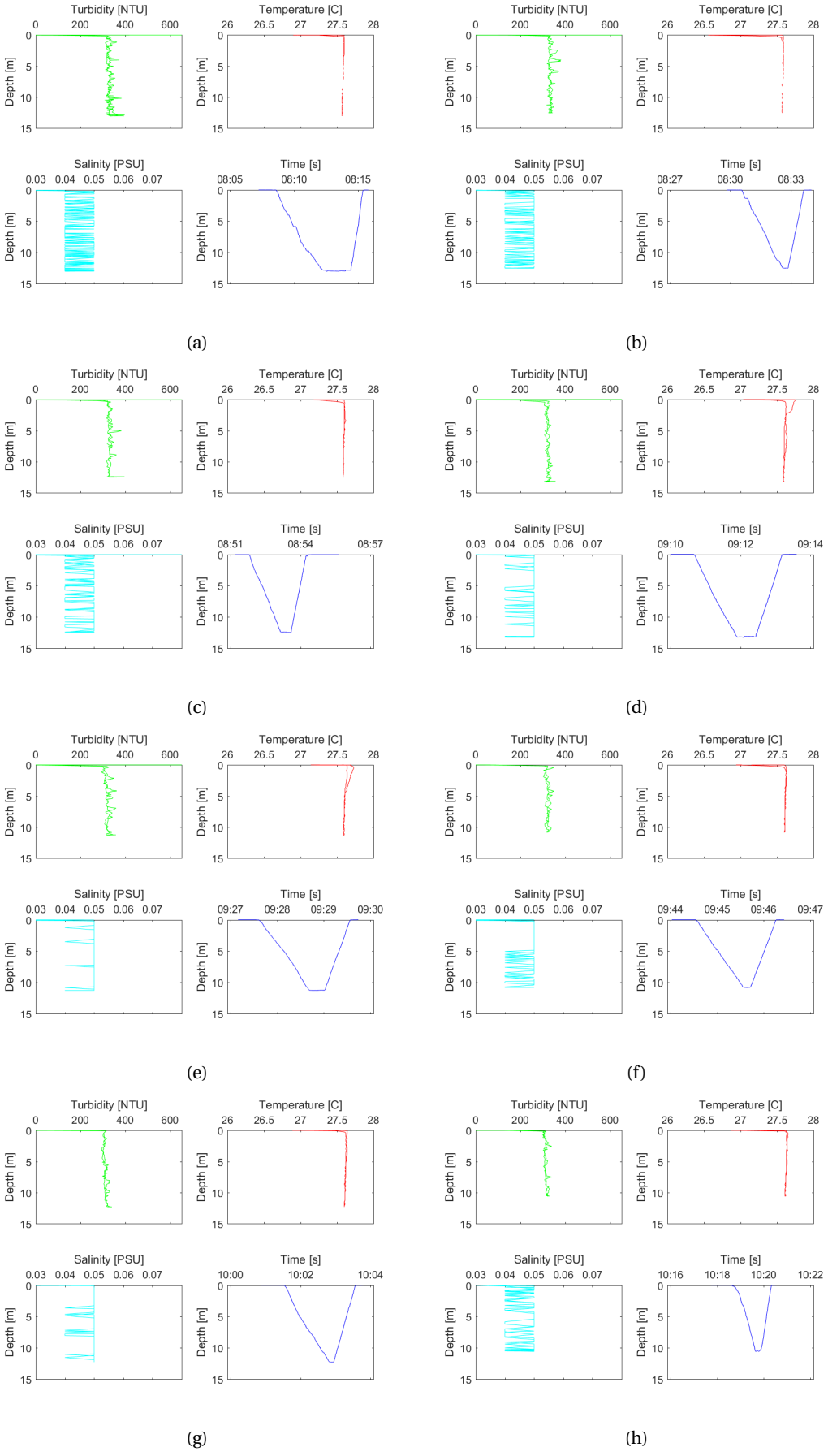

Figure A.5: Measured OBS profiles between 08:00 and 10:30, 2 km from the mouth.

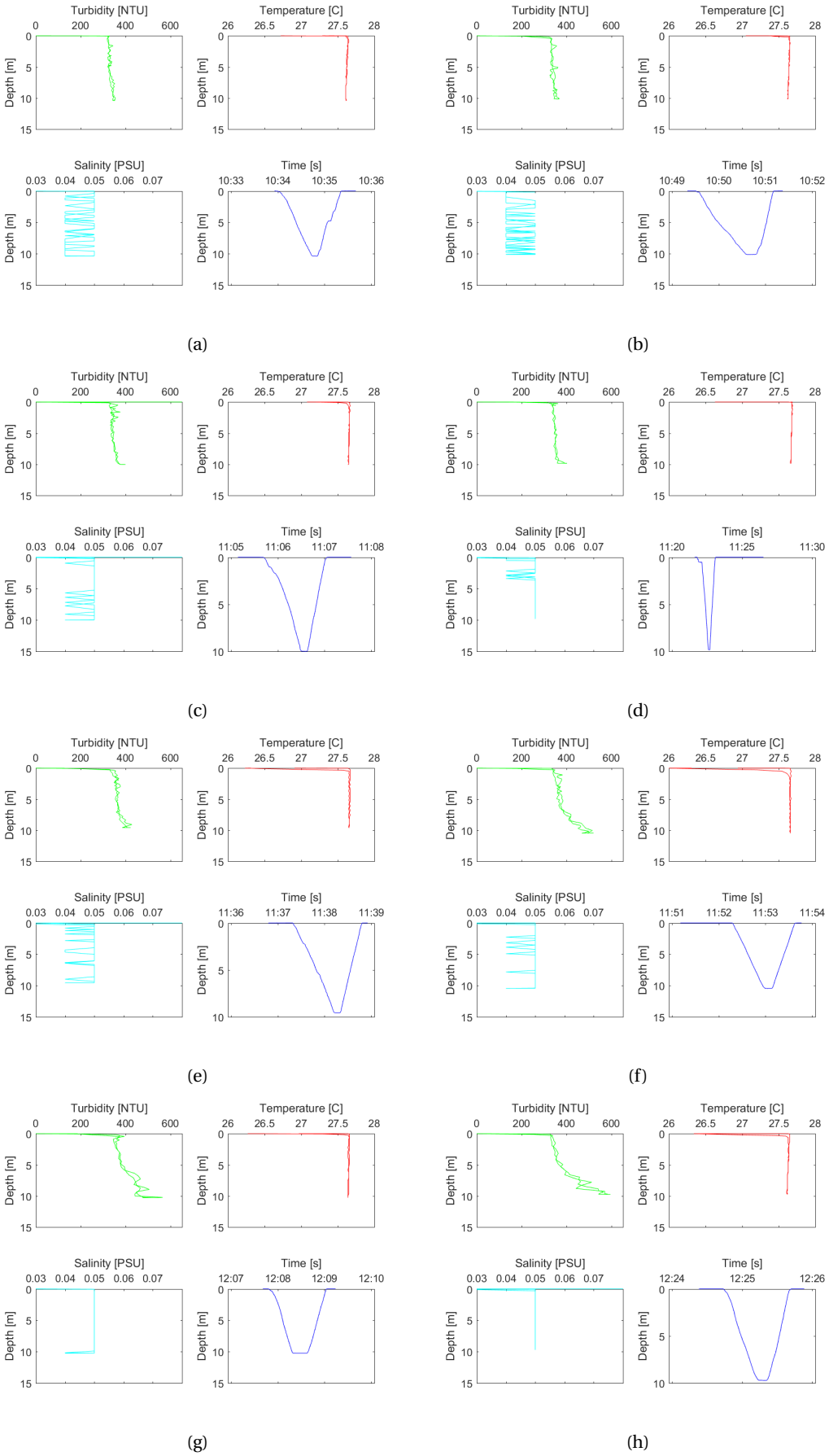

Figure A.6: Measured OBS profiles between 10:30 and 12:30, 2 km from the mouth.

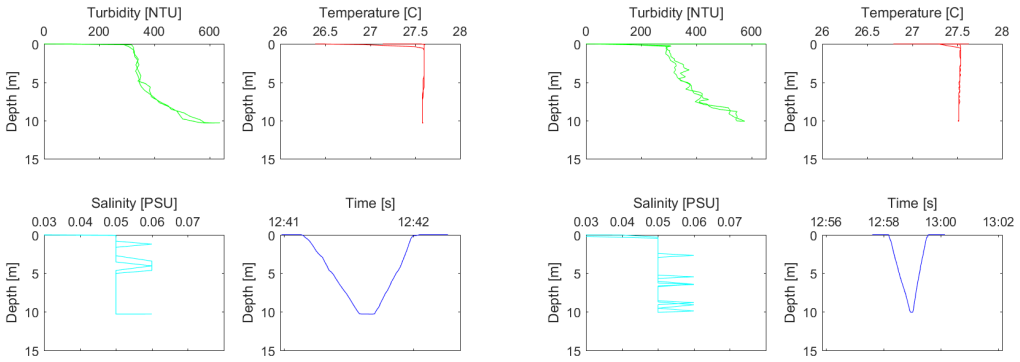

(a)

(b)

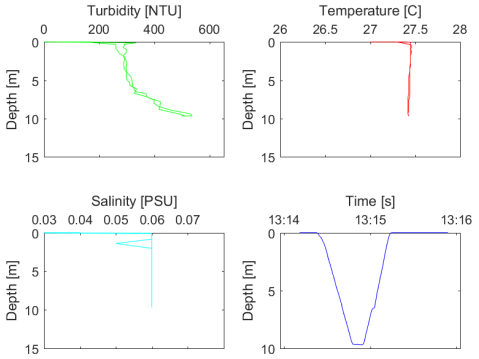

(c)

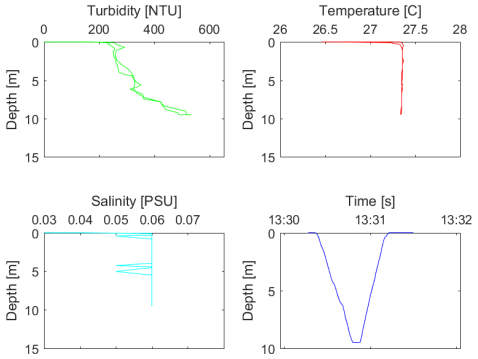

(d)

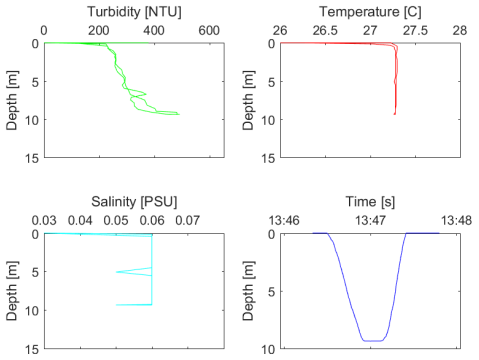

(e)

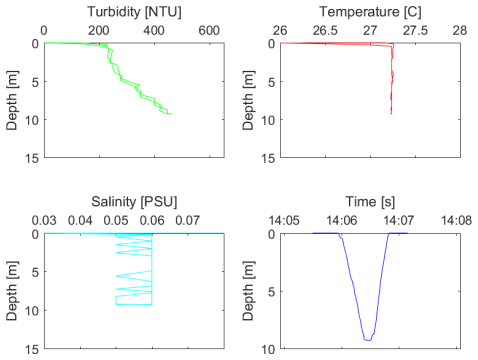

(f)

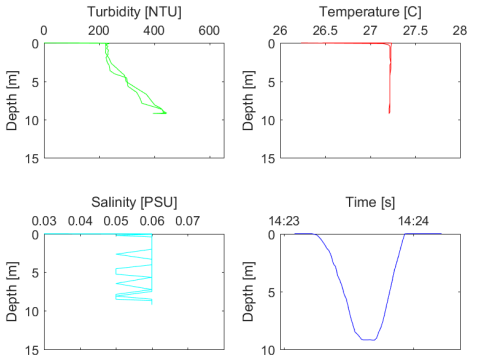

(g)

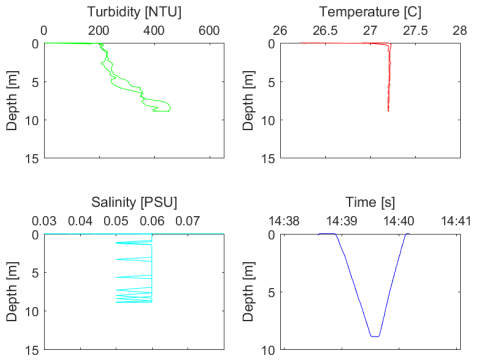

(h)

Figure A.7: Measured OBS profiles between 12:30 and 14:45, 2 km from the mouth.

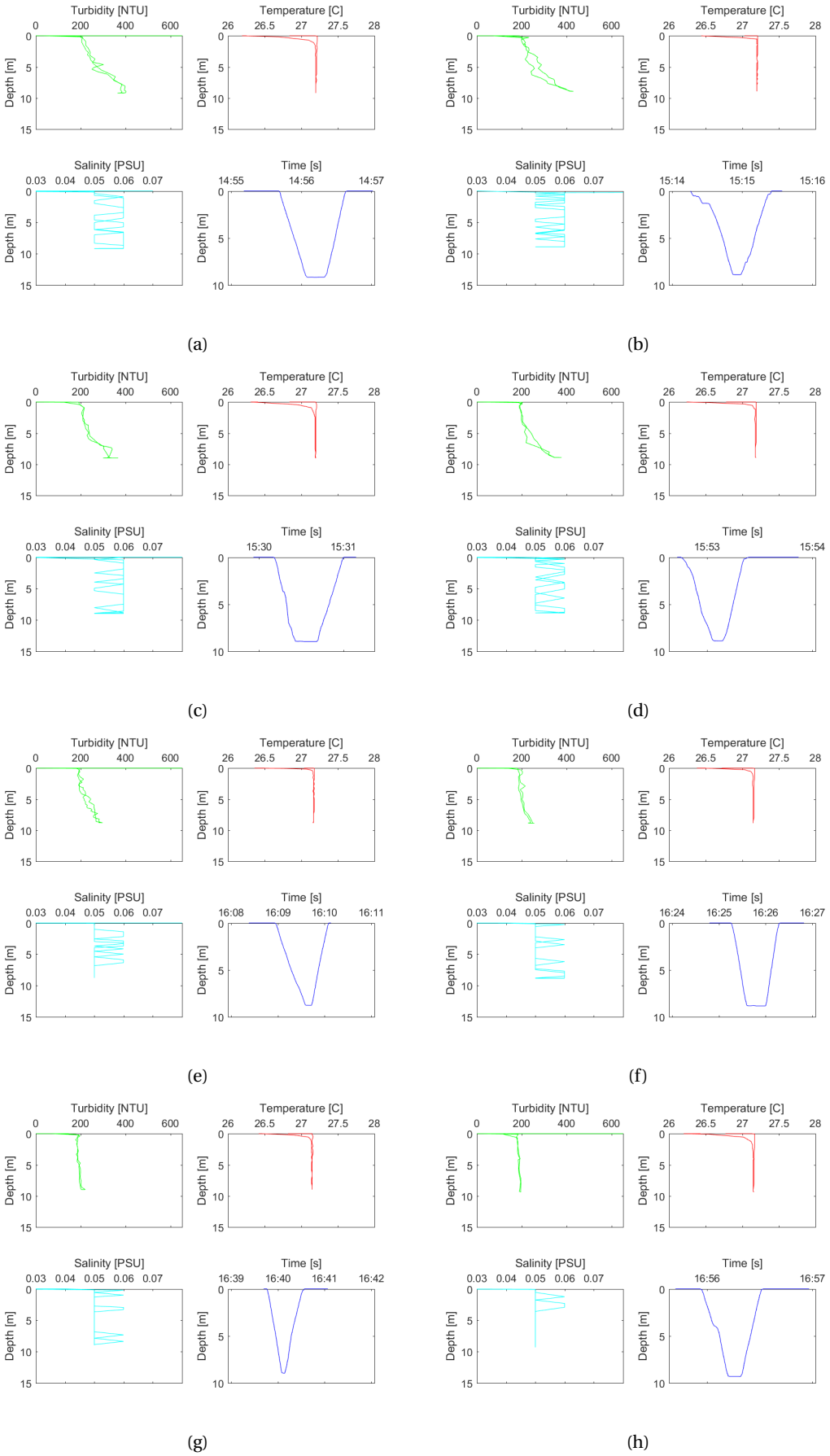

Figure A.8: Measured OBS profiles between 14:45 and 17:00, 2 km from the mouth.

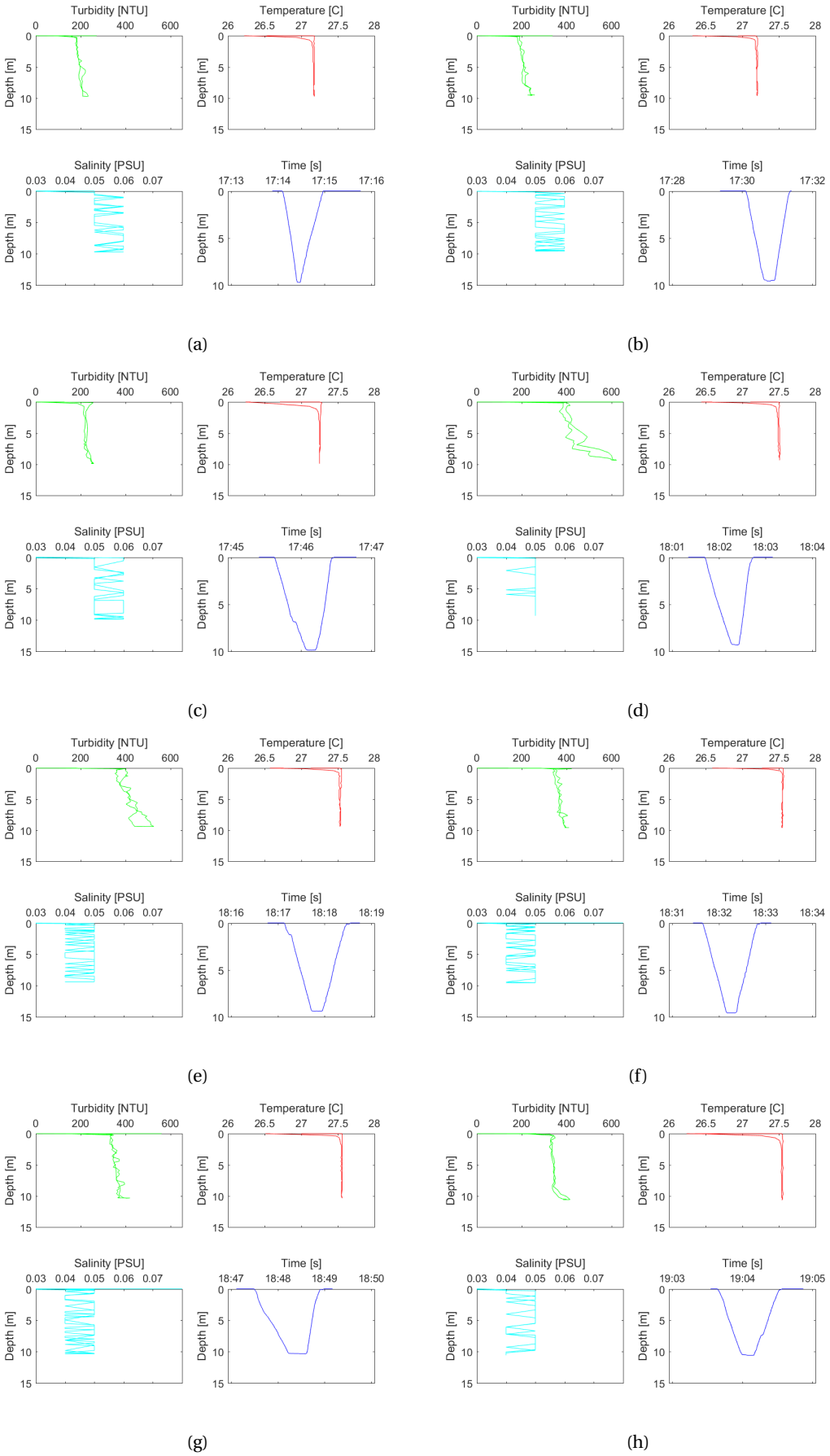

Figure A.9: Measured OBS profiles between 17:00 and 19:15, 2 km from the mouth.

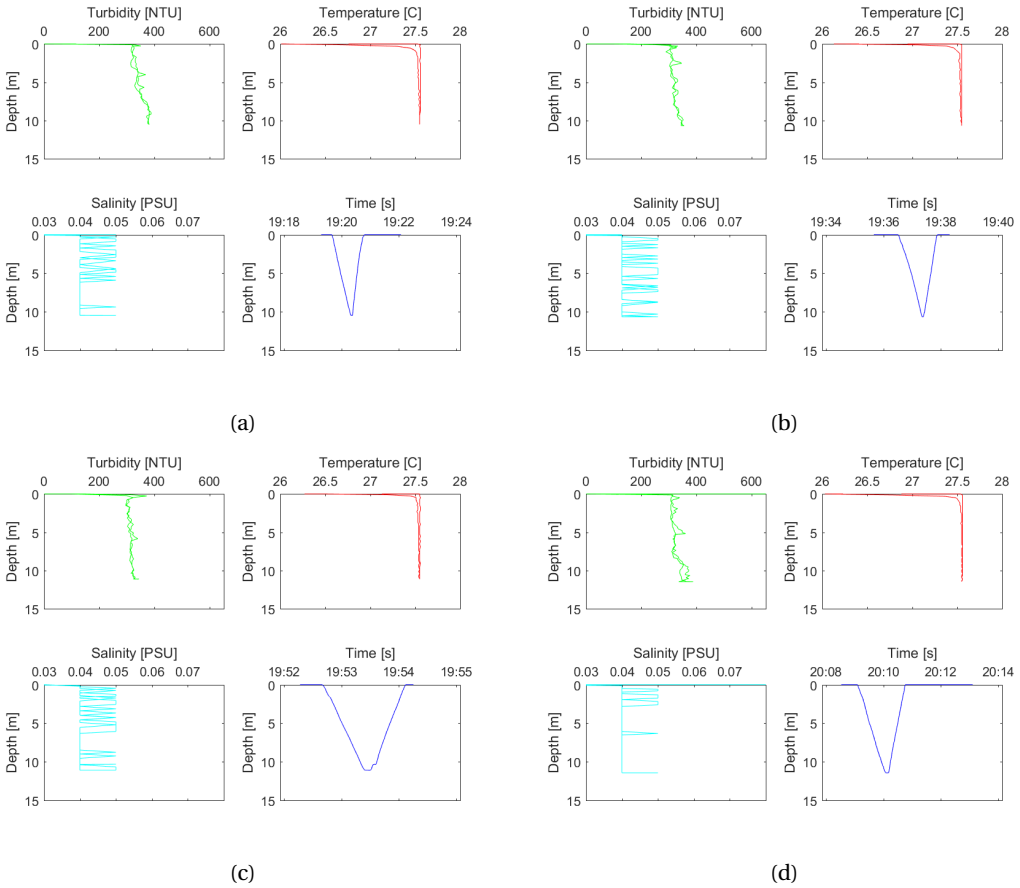

Figure A.10: Measured OBS profiles between 19:15 and 20:15, 2 km from the mouth.

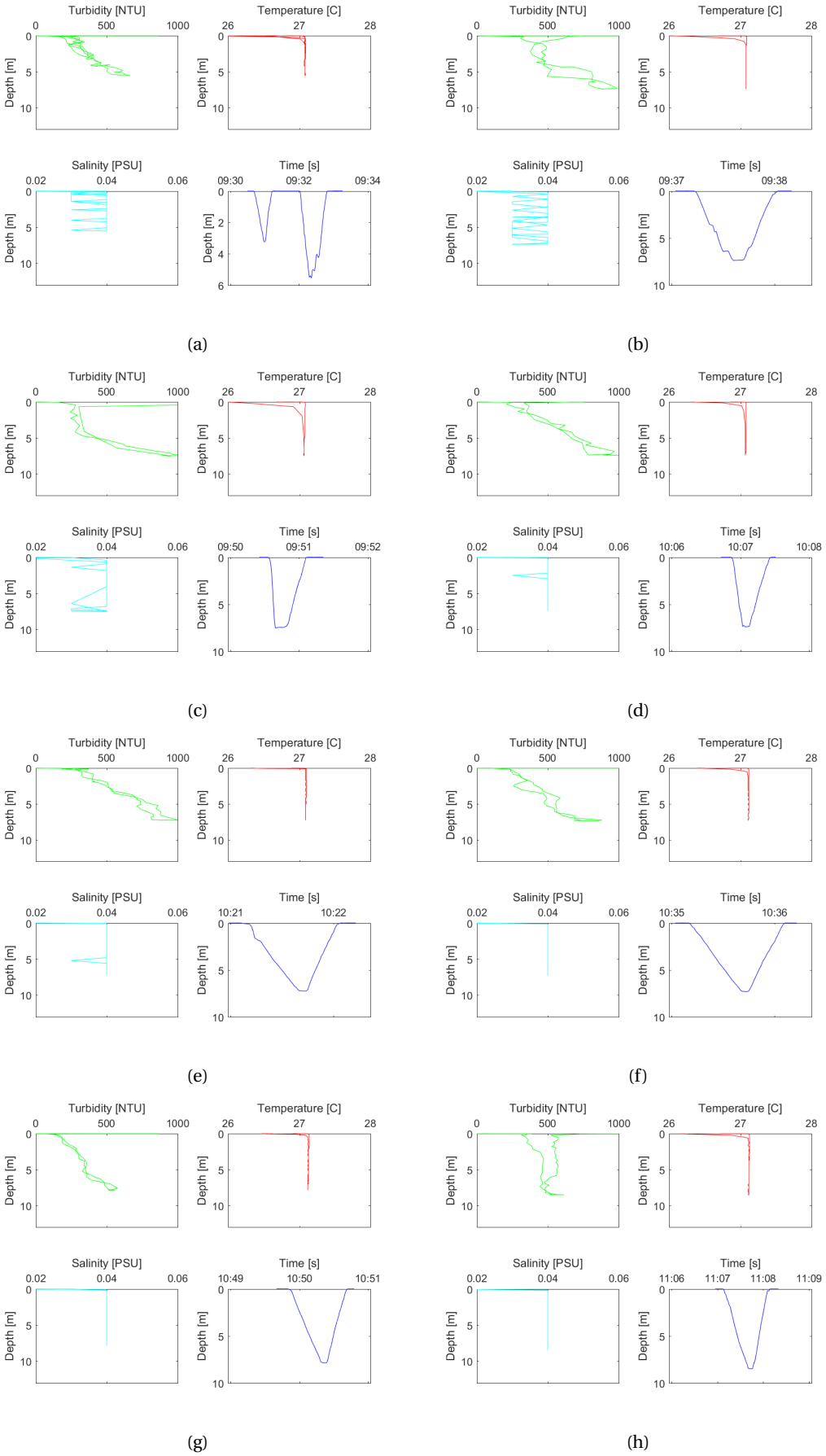

Figure A.11: Measured OBS profiles between 09:30 and 11:15, 17 km from the mouth.

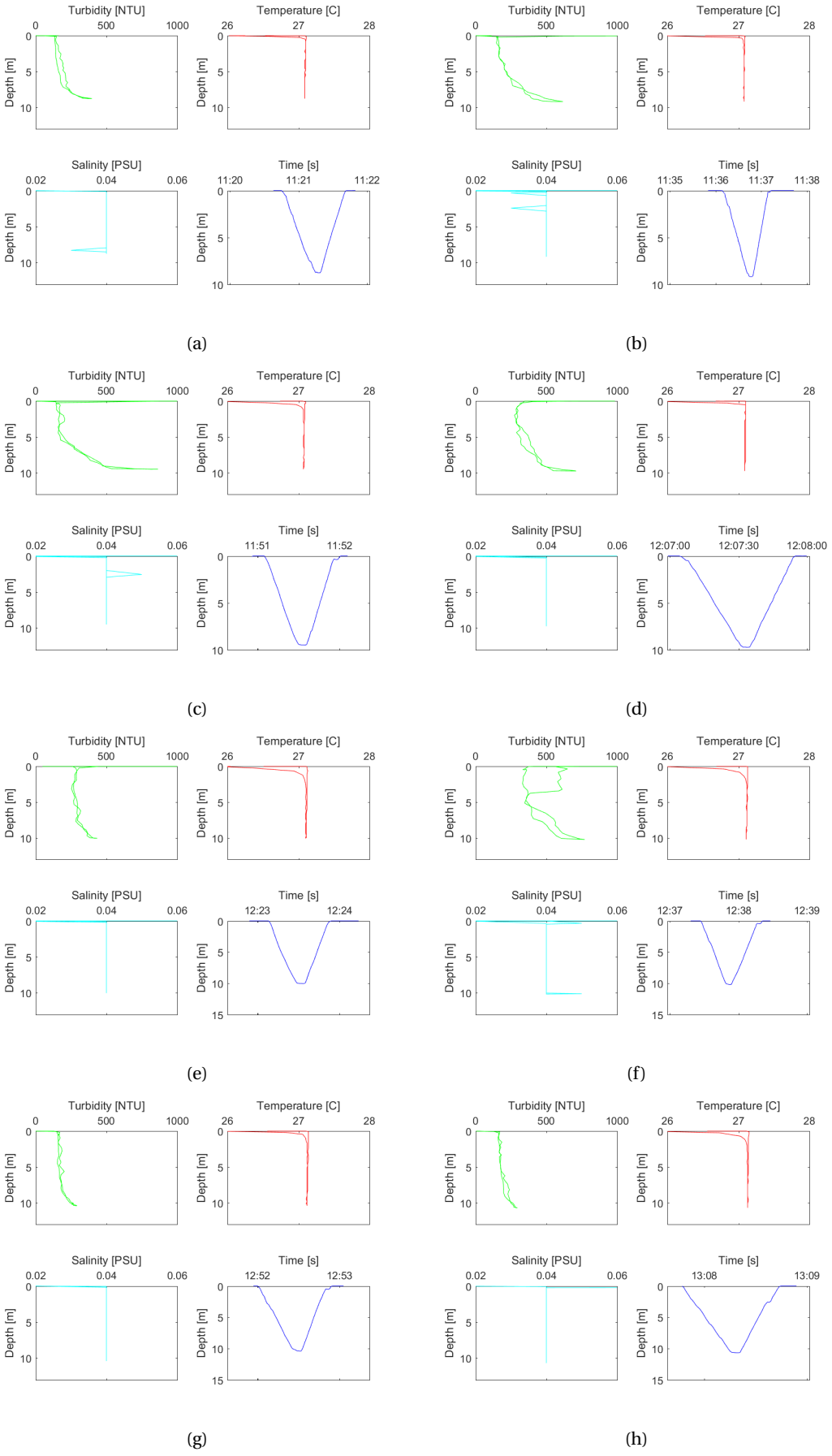

Figure A.12: Measured OBS profiles between 11:15 and 13:15, 17 km from the mouth.

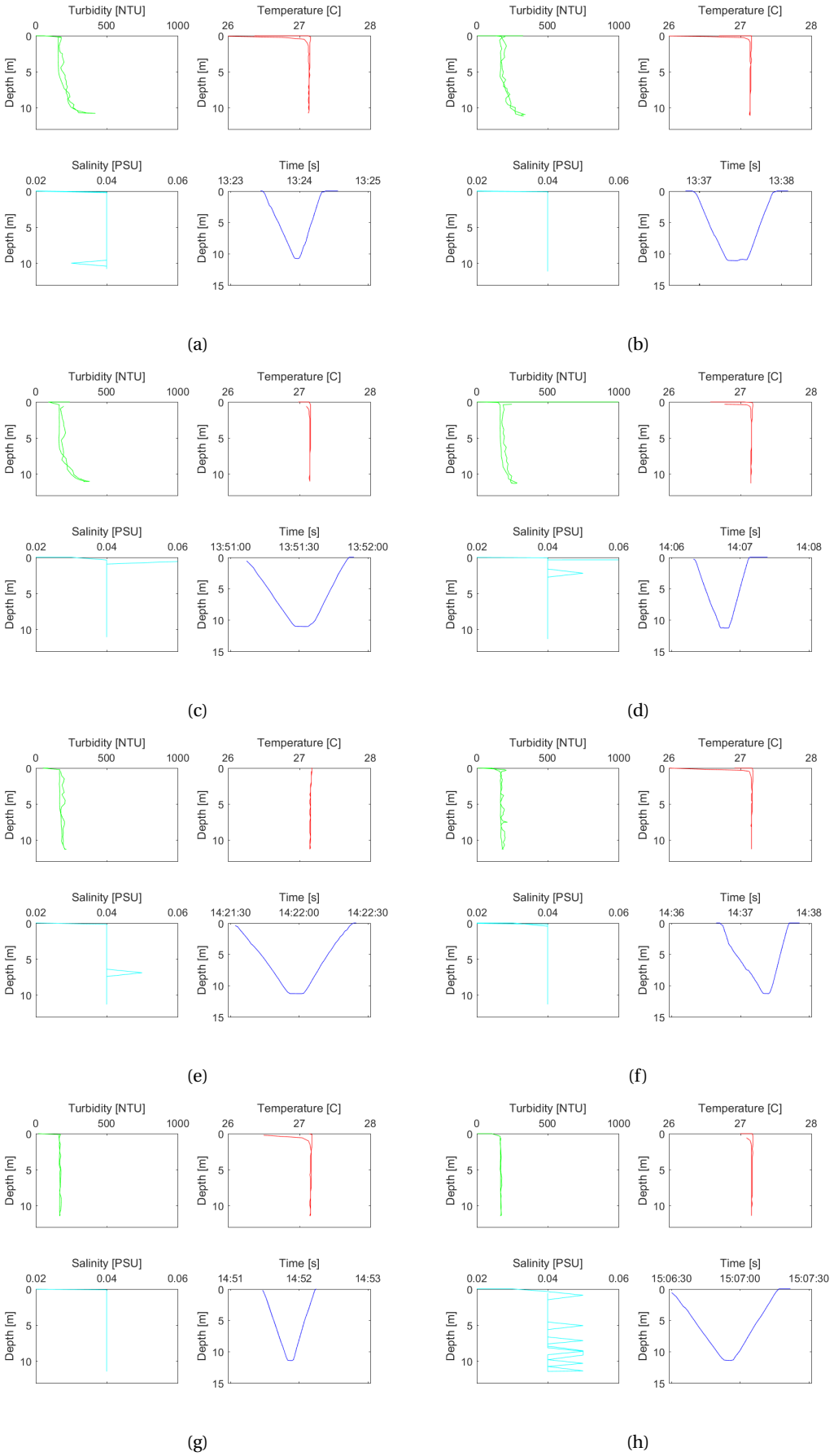

Figure A.13: Measured OBS profiles between 13:15 and 15:15, 17 km from the mouth.

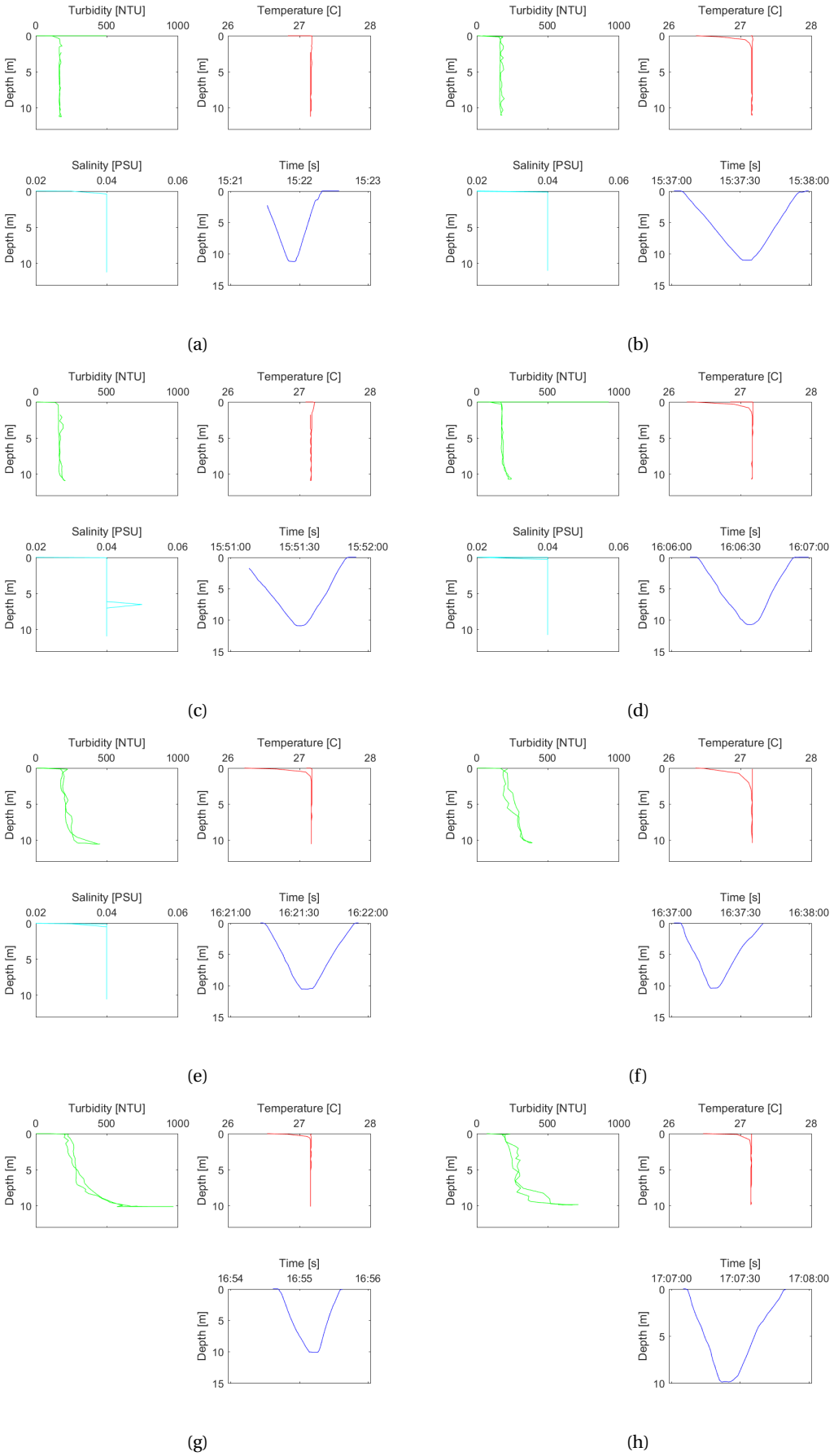

Figure A.14: Measured OBS profiles between 15:15 and 17:15, 17 km from the mouth.

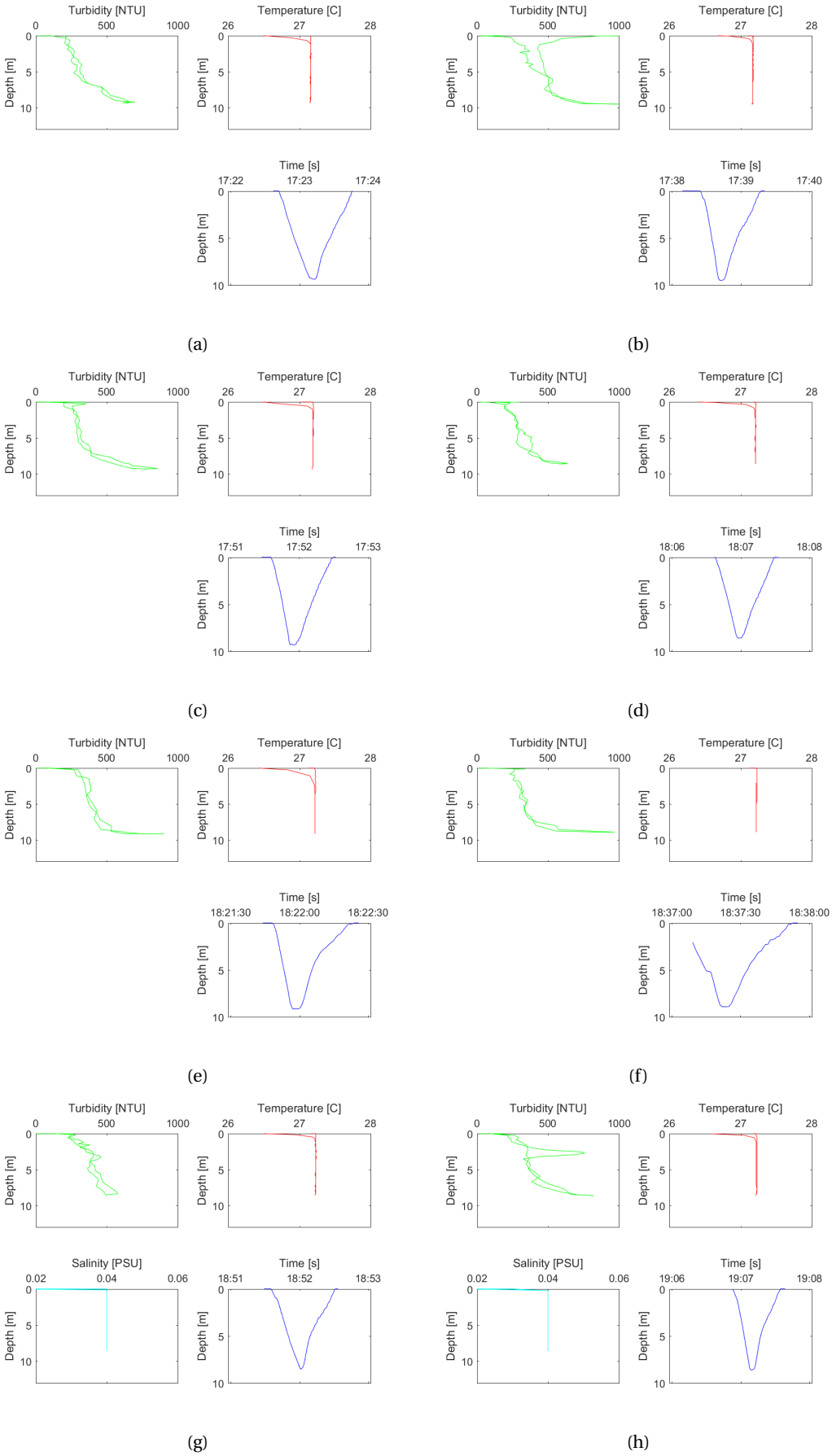

Figure A.15: Measured OBS profiles between 17:15 and 19:15, 17 km from the mouth.

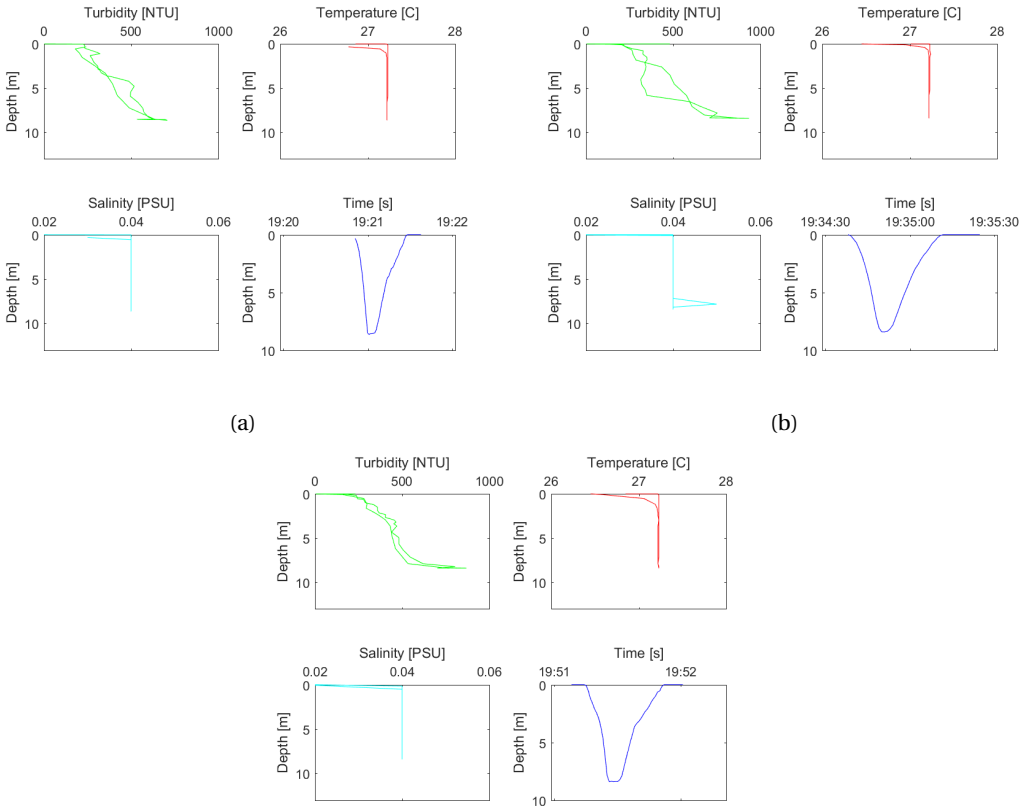

Figure A.16: Measured OBS profiles between 19:15 and 20:00, 17 km from the mouth.

A.4 Tidal constituents

Table A.1: Tidal constituents used at the downstream boundary of the model domain, source: JICA (2015)

Tidal constituent	Amplitude [m]	Phase [°]
2MS6	0.078	135.8
MK4	0.051	207.9
MN4	0.085	155.8
MK3	0.054	74.2
LABDA2	0.075	159.4
MS4	0.206	211.5
2SM2	0.059	39.6
T2	0.064	167.7
L2	0.159	142.7
MKS2	0.057	257.6
NU2	0.099	100.7
MU2	0.151	278.6
MNS2	0.063	271.2
P1	0.050	51.9
MSF	0.148	45.9
M6	0.062	92.2
SA	0.366	151.6
K2	0.186	160.2
K1	0.208	31.1
M2	1.819	124.9
O1	0.098	20.2
N2	0.347	110.5
M4	0.227	168.0
S2	0.679	163.3

Appendix B

Instruments

B.1 Echo sounder

An echo sounder is used for the bathymetric survey. The instrument consists of a display instrument (Garmin echoMAP 42dv) and a transducer (Garmin GT20-TM). The transducer is mounted on a survey boat, under the water line, at the transom or trolling motor (Garmin International, Inc., 2017) and sends out sonic pulses at a certain frequency which reflects on the consolidated bottom.
The set-up simultaneously measures the absolute distance between transducer to bottom and tracks GPS coordinates. During the survey the water level will vary significantly due to the occurring tidal range (of about 5 m). In post processing this tidal signal must be kept in mind in order to relate the depths to a horizontal reference level.

B.2 Pressure sensors

The Divers measure temperature and absolute pressure. This means that the sensor not only measures the hydrostatic pressure, but also the air pressure pushing on the water surface. The hydrostatic pressure is dependent on variations in temperature and salinity.
Both the CTD-Diver and the Divers have a maximum of 48,000 measurements. If the memory is full the Diver stops measuring.
The (CTD-) Divers are mounted on fixed poles in the creek. The Van Essen Instruments (2016) advises to use 3 inch PVC tubes and steel closures with locks to prevent theft. It is important that there is sufficient circulation around the sensor (Van Essen Instruments, 2016). Regular checks are needed to collect data and clean the instrument in case of biofouling.
A fourth Diver measures air pressure (barometer). The output is used to correct the pressure measurements of the Divers and CTD. It is assumed that spatial air pressure differences can be neglected. Therefore, it can be installed at any location in Yangon (for example inside a building).

B.3 Turbidity sensor

An OBS is a turbidity sensor which measures the amount of light that is scattered by suspended solids in the water. Based on this signal, suspended sediment concentrations can be estimated. The OBS-3A combines the OBS probe with pressure, temperature and conductivity sensors. To minimise synchronicity errors during calibration, the OBS-3A and the Van Dorn sampler should take a sample at the same time and at the same point above the bottom (van Rijn, 2012).

B.4 Water sampler

The van Dorn water sampler is a relatively simple device and can be handcrafted using PVC tubes (The Lake of Missouri Volunteer Program, n.d.). It consists of a horizontal tube and a mechanism that remotely closes both open ends. The sampler is lowered with a cable in the water column to a certain depth. There, the

mechanism triggers the closures and the water inside the tube is contained. The samples are labelled and stored in PET bottles. From such a sample the concentration suspended sediment is determined.

B.5 Soil sampler

The Veen Grab sampler is a mechanical instrument that retrieves a soil sample of the bed. When lowered into the water two levers with buckets on their ends are spread like an open scissor and close when hitting the bed. van Rijn (2012) recommends to use a Van Veen Grab to collect a bed sample consisting of firmly deposited mud. The available sampler is small in size, so it can only be used in low flow velocities. The samples will be labelled and stored.

Appendix C

Model results

C.1 Discharge

The lower boundary of the model is forced by tidal constituents (see Appendix A.1). These represent the tidal wave in all simulations. Figure C.1 shows the induced instantaneous discharge in a cross section in the mouth. It can be seen that the maximum tidal discharge (in flood direction) is in the order of 3000 $m^3 s^{-1}$. Sir Alexander Gibb & Partners (1976) observed a similar discharge, see Figure A.1b.

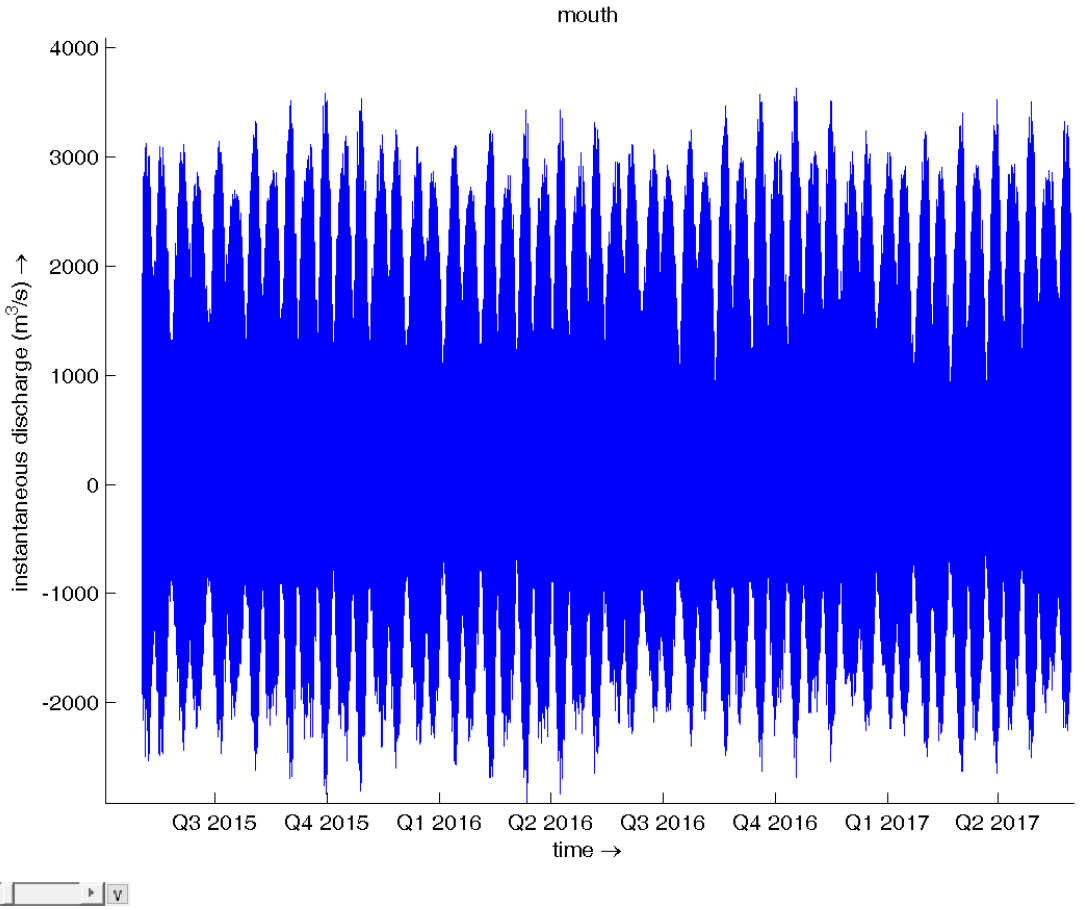

Figure C.1: calculated instantaneous discharge in mouth

C.2 Velocity

Calculated velocities at the observation points CTD, D1, D2 and D3 are given in Figure C.2

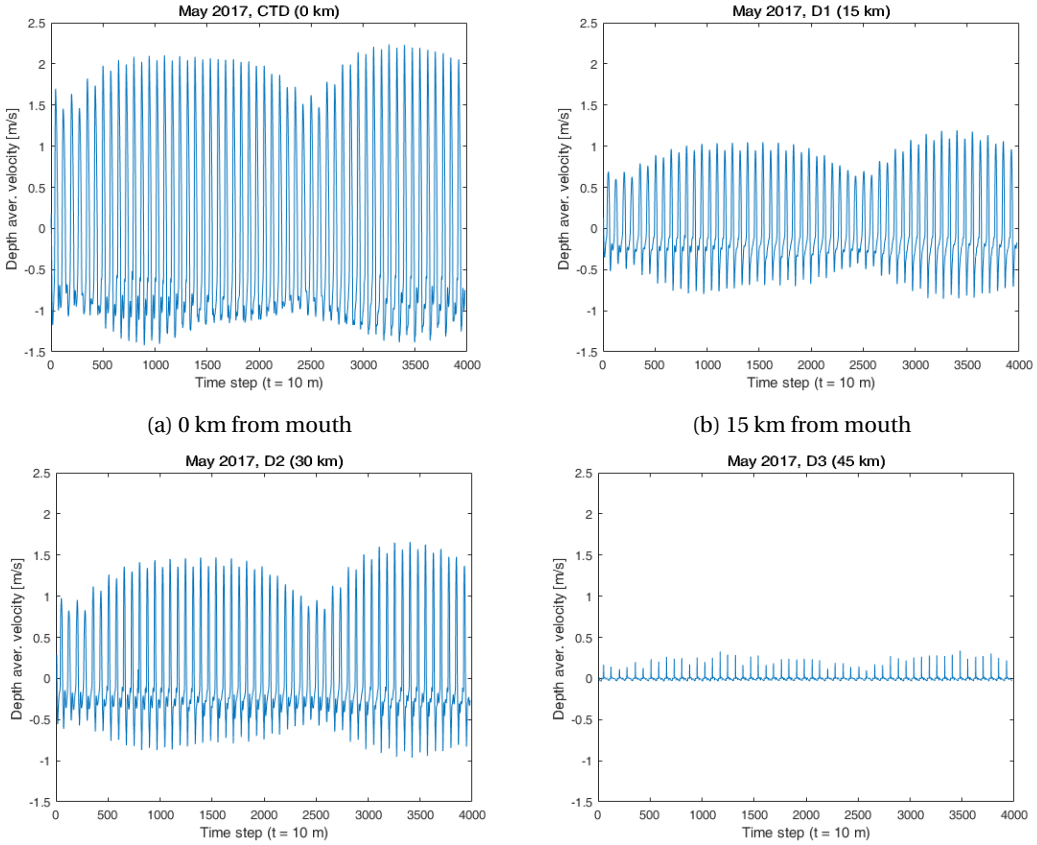

(a) 0 km from mouth

(b) 15 km from mouth

(c) 30 km from mouth

(d) 45 km from mouth

Figure C.2: Calculated depth averaged velocities at four locations, May 2017

Depth averaged velocities are plotted against a time series in the month may 2017. Positive velocities are in flood direction and negative velocities are in ebb direction. For all locations, higher flood directed velocities are found than ebb directed velocities. In the mid-domain (D1 and D2) the flood directed velocities increase in landward direction. The observation point at 45 km is located on the (closed) boundary, therefore only low velocities occur. At the mouth (0 km), the model result are highest, since depths near the mouth are low. But observations on the boundaries are is assumed to be less accurate, due to unknown boundary effects. However, the general shape of the velocity tends to become more asymmetrical as the tidal wave propagates into the domain, see Figure C.3

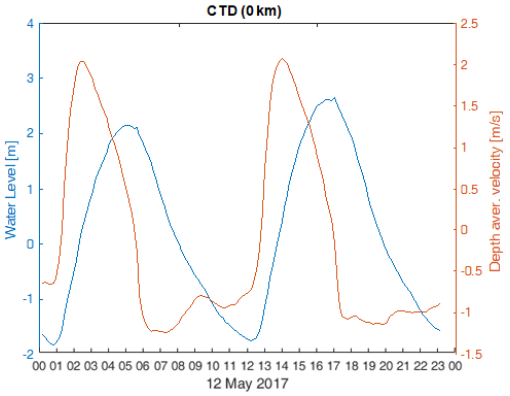

(a) 0 km from mouth

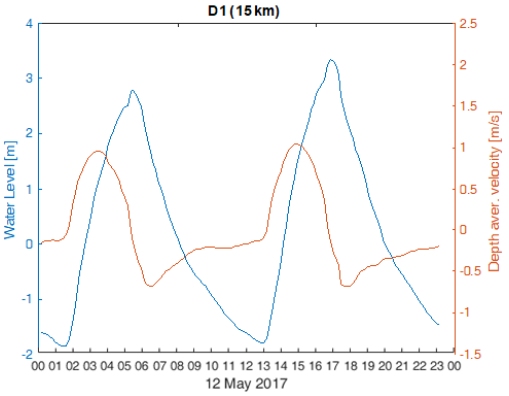

(b) 15 km from mouth

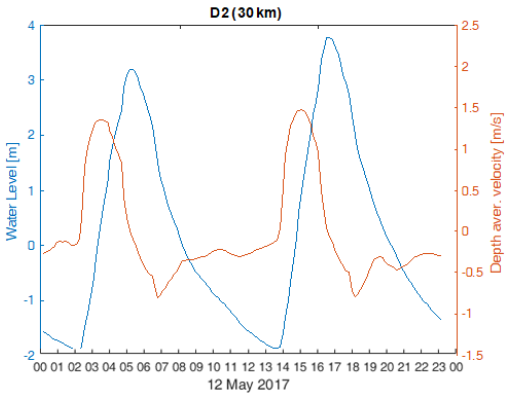

(c) 45 km from mouth

Figure C.3: Calculated water levels and depth averaged velocities on 12 May 2017

C.3 Flushing scenarios

Figure C.4 shows the width averaged siltation of the complete computational domain. Next to the 3 flushing scenarios, a scenario without discharge is plotted. Most siltation (75%) occurs in the upper 15 km of the creek in case of no flushing.

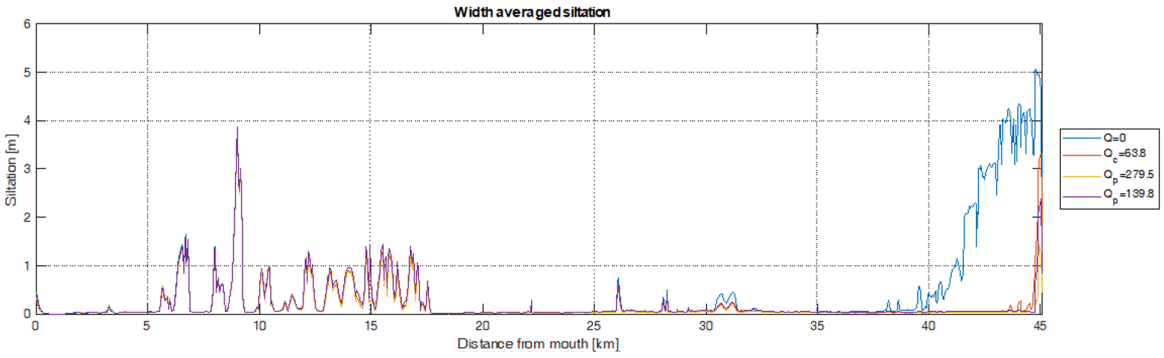

Figure C.4: Results flush scenarios, width averaged siltation

Appendix D

Human induced sediment flux

A lot of time was spent on the water in order to install or retrieve instruments, measure depths or sediment concentrations or sampling water or soil samples. During the field survey, in particular during the OBS measurements covering 13 subsequent hours at one location, a lot of barges carrying a mix of fine sediment and water were observed, see Figure D.1. The operations of these boats might have an long-term influence on the siltation problems in the Nga Moe Yeik Creek. In this section an educated guess is made to calculate the contribution of this human induced sediment flux in the sediment balance on a yearly scale.

D.1 Observed barges

About 50 barges enter the Pazundaung Creek just before high tide every day. It seemed they wait for a certain water level to ensure enough draught before racing upstream in a short tidal window. They race against the upcoming water to reach a dumping site to release the content of their holds on the muddy river bank and then return unloaded with the ebbing tide. At a certain moment during high tide the water level is too high for the barges to make it past certain bridges see Figure D.2.

Figure D.1: During high tide several barges were observed carrying a mixture of fine sediment and water upstream. They raced against the rising water to make it past certain bridges. In the upper picture: a sailing barge just in time to pass under the bridge. Four more barges after this followed, approaching in the lower picture. Both pictures were taken shortly after each other, 17 km upstream of the mouth of the Pazundaung Creek

One of these dumping locations is seen around 1.5 km from the river mouth. Here it was observed how various barges released the content of their holds using a pump and pipes see Figure D.3. The pipes bring the content behind a wooden structure on the bank. It is assumed that this is built to hold back the sediment while water flows back into the creek in order to improve the bank. Because a lot of loaded barges passed a location 17 km upstream of the mouth (Figure D.2), it can be assumed that a similar dumping site is located further upstream.

Figure D.2: The last boat of the day just squeezes under the bridge at a location of roughly 17 km from the mouth. Its predecessor wasn't low enough and damaged its wheelhouse after a collision with the bridge. The remaining ships decided to wait for the next tidal window.

Figure D.3: This dumping site was observed about 1.5 km from the river mouth. During an OBS survey covering 13 hours, several barges have been observed while emptying their holds at this location. To empty the boats hold, use is made of a pump and hose combination to place the sediment behind the wooden structure

D.2 Sediment flux

In this section the contribution of the barges on the yearly sediment balance is calculated and compared with the simulated natural sediment fluxes. All the barges seemed to be the same type and, therefore it is assumed that they have the same hold capacity. The typical type of barge can easily be recognised in satellite imagery from Google Earth, see Figure D.6. From this, the dimensions of the ship and hold are guessed. The difference in draught is guessed using a side view of a stranded barge see Figure D.5 and Figures D.1 and D.4. Using Archimedes' principle and the difference between a loaded and an unloaded barge (compare Figure D.1 and Figure D.4, the difference in weight (representing a full load) can be determined. This weight is used, together with an assumption for the hold capacity, to guess the sediment import by barges during one flood period.

Archimedes' principle reads; The uplifting force (F_A) that is experienced by a body in a fluid or gas is equal to the density of the fluid or gas (ρ) times the volume of the displaced fluid or gas (V_d). In formula; $F_A = \rho * V_d$. Using this principle and the assumption that the difference in uplifting forces of a loaded and unloaded barge is representative for the gravitational force induced by the content of the hold, the mass of a loaded hold is 94 ton (dry soil). With 50 boats, this results in a rough guess of 4700 tons per flood period for the human induced

Figure D.4: An unloaded barge is making its way back downstream, note the difference in draught of about 1 m, compared to a loaded barge.

Figure D.5: A barge on the river bank, during low water. From this and the above pictures assumptions for the draught of a loaded (2 m) and unloaded barge (1 m) are made

sediment flux.
If compared to the natural sediment flux measured by (Sir Alexander Gibb & Partners, 1976) in a cross section in the mouth of the Pazundaung Creek (pre-monsoon period) the human induced sediment flux is 2-3% of the natural sediment flux. It is therefore considered negligible.

Figure D.6: some barges spotted in the Nga Moe Yeik Creek in Google Earth imagery, using the measuring tool the main dimensions of the barges and their hold are guessed

.